

NASA Technical Memorandum 110398

Nonlinear Dynamics & Numerical Uncertainties in CFD

H. C. Yee and P. K. Sweby

April 1996



National Aeronautics and
Space Administration

Nonlinear Dynamics & Numerical Uncertainties in CFD

H. C. Yee and P. K. Sweby, Ames Research Center, Moffett Field, California

April 1996



National Aeronautics and
Space Administration

Ames Research Center
Moffett Field, California 94035-1000

Table of Contents

Abstract

I. Introduction

II. Background & Motivations

2.1. Nonlinear Dynamics & Fluid Dynamics

2.2. Nonlinear Dynamics & CFD

2.3. Dynamics of Numerical Approximations of ODEs vs. Time-Dependent PDEs

2.4. Nonlinear Dynamics & Time-Marching Approaches

III. Elementary Examples

3.1. Preliminaries

3.2. Spurious Asymptotic Numerical Solutions for Constant Step Sizes

3.2.1. Explicit Methods

3.2.2. Fixed Point Diagrams

3.3. Bifurcation Diagrams

3.4. Strong Dependence of Solutions on Initial Data (*Numerical Basins of Attraction*)

3.5. Global Asymptotic Behavior of Superstable Implicit LMMs

3.5.1. Super-stability Property

3.5.2. Implicit LMMs

3.5.3. Numerical Examples

3.6. Does Error Control Suppress Spuriousity?

3.7. Dynamics of Numerics of a Reaction-Convection Model

3.7.1. Spurious Asymptotes of Full Discretizations

3.7.2. Linearized Behavior vs. Nonlinear Behavior

3.7.3. Spurious Steady States & Nonphysical Wave Speeds

3.7.4. Numerical Basins of Attraction

3.8. Spurious Dynamics in Time-Accurate (Transient) Computations

IV. Spurious Dynamics in Steady-State Computations

4.1. A 1-D Chemically Relaxed Nonequilibrium Flow Model

4.2. Convergence Rate & Spurious Dynamics of High-Resolution Shock-Capturing Schemes

4.2.1. Convergence Rate of Systems of Hyperbolic Conservation Laws

4.2.2. Spurious Dynamics of TVD Schemes for the Embid et al. Problem

4.2.3. The Dynamics of Grid Adaption

4.3. Mismatch in Implicit Schemes for Time-Marching Approaches

V. Spurious Dynamics in Unsteady Computations

- 5.1. Chaotic Transient Near the Onset of Turbulence in Direct Numerical Simulations of Channel Flow
 - 5.2. Oscillations Induced by Numerical Viscosities in 1-D Euler Computations
 - 5.2.1. Introduction
 - 5.2.2. Numerical Solutions of a Slowly Moving Shock
 - 5.2.3. The Momentum Spikes
 - 5.2.4. The Downstream Oscillations
 - 5.2.5. Discussions and Conclusions
 - 5.3. Spurious Vortices in Under-Resolved Incompressible Thin Shear Layer Flow Simulations
 - 5.4. Convergence Rate of Systems of Hyperbolic Conservation Laws
- VI. Concluding Remarks

Invited review paper for Journal of Computational Physics (*invitation from the Editor-in-Chief of Journal of Computational Physics Dr. Jerry Brackbill*).

NONLINEAR DYNAMICS & NUMERICAL UNCERTAINTIES IN CFD¹

H.C. Yee²

NASA Ames Research Center, Moffett Field, CA., 94035, USA

P.K. Sweby³

University of Reading, Whiteknights, Reading RG6 2AX, England

Abstract

The application of nonlinear dynamics to improve the understanding of numerical uncertainties in computational fluid dynamics (CFD) is reviewed. Elementary examples in the use of dynamics to explain the nonlinear phenomena and spurious behavior that occur in numerics are given. The role of dynamics in the understanding of long time behavior of numerical integrations and the nonlinear stability, convergence, and reliability of using time-marching approaches for obtaining steady-state numerical solutions in CFD is explained. The study is complemented with examples of spurious behavior observed in CFD computations.

¹Portion of this work appeared as AIAA 96-2052, an invited paper for the 27th AIAA Fluid Dynamics Conference, June 18-20, 1996, New Orleans, LA. The full text was published as an internal report – NASA Technical Memorandum 110398, April 1996. Submitted to J. of Comput. Phys., April 1996

²Senior Staff Scientist

³Lecturer, Department of Mathematics; part of this work was performed as a visiting scientist at RIACS, NASA Ames Research Center.

I. Introduction

The authors' view and experience in the application of nonlinear dynamics and bifurcation theory to improve the understanding of numerical uncertainties and their effects in computational fluid dynamics (CFD) are reviewed. The use of dynamics to illuminate how numerical methods work for strongly nonlinear problems is indirectly addressed. Simple nonlinear model equations are used to illustrate how the recent advances in nonlinear dynamical system theory can provide new insights and further the understanding of nonlinear effects on the asymptotic behavior of numerical algorithms commonly used in CFD. The discussion is complemented with CFD examples containing spurious behavior (numerical artifacts) in steady and unsteady flows. This topic is part of a long term research referred to as the "Dynamics of Numerics for CFD". Here "dynamics" is used loosely to mean the dynamical behavior of nonlinear dynamical systems (continuum or discrete) and "numerics" is used loosely to mean the numerical methods and procedures in solving dynamical systems. For this paper, the phrase "to study the dynamics of numerics" (dynamical behavior of a numerical scheme) is restricted to the study of nonlinear and long time behaviors of nonlinear difference equations resulting from finite discretizations of a nonlinear differential equation (DE) subject to the variation of discretized parameters such as the time step, grid spacing, numerical dissipation coefficient, etc. This topic belongs to a subset of a rather new field in numerical analysis and dynamical system theory sometimes referred to as "The Dynamics of Numerics and The Numerics of Dynamics," named after the First IMA Conference on Dynamics of Numerics and Numerics of Dynamics, University of Bristol, England, July 31 - August 2, 1990. We emphasize here that in the study of the dynamics of numerics, unless otherwise stated, we always assume the continuum (governing equations) is nonlinear. Although this paper is intended primarily for computational fluid dynamicists, it can be useful for computational scientists, physicists, engineers and computer scientists who have a need for reliable numerical simulation.

Since the late 1980's, many CFD related journals imposed an editorial policy statement on numerical uncertainty which pertained mainly to the accuracy issue. However, the study of numerical uncertainties in practical computational physics encompasses very broad subject areas. These include but are not limited to (a) problem formulation and modeling, (b) type, order of accuracy, nonlinear stability, and convergence of finite discretizations, (c) limits and barriers of existing finite discretizations for highly nonlinear stiff problems with source terms and forcing, and/or for wave propagation phenomena, (d) numerical boundary condition procedures, (e) finite representation of infinite domains (f) solution strategies in solving the nonlinear discretized equations, (g) procedures for obtaining the steady-state numerical solutions, (h) grid quality and grid adaptations, (i) multigrids, and (j) domain decomposition (zonal or multicomponent approach) in solving large problems. See the last six years of AIAA conference papers on numerical uncertainties in CFD and guidelines for code verification, validation and certification. See, for example, Mehta (1995), Melnik et al. (1994), Cosner et al. (1995), Demuren & Wilson (1994) Marvin (1993), Marvin & Holst (1990) and references cited therein. At present, some of the numerical uncertainties can be explained and minimized by traditional numerical analysis and standard CFD practices. Highly nonlinear and/or stiff

problems, however, do not always lend themselves to such treatment. At the same time, the understanding of the dynamics of numerics, in general, is at a very early stage of development and much remains to be learned. More theoretical development and extensive numerical experimentation are needed. Nevertheless, we believe that this approach can improve the understanding of numerical uncertainties and computational barriers in CFD in general, and in particular in combustion, direct numerical simulations, high speed and reacting flows, and certain turbulence models in compressible Navier-Stokes computations.

A major stumbling block in genuinely nonlinear studies is that unlike the linear model equations used for conventional stability and accuracy considerations in time-dependent partial differential equations (PDEs), there is no equivalent unique nonlinear model equation for nonlinear hyperbolic and parabolic PDEs for fluid dynamics. A numerical method behaving in a certain way for a particular nonlinear DE (PDE or ordinary differential equation (ODE)) might exhibit a different behavior for a different nonlinear DE even though the DEs are of the same type. See Jackson (1989) for the definition of genuinely (or strongly) nonlinear problems. On the other hand, even for simple nonlinear model DEs with known solutions, the discretized counterparts can be extremely complex, depending on the numerical methods. Except in special cases, there is no general theory at the present time to characterize the various nonlinear behaviors of the underlying discretized counterparts. Most often, the only recourse is a numerical approach. Under this constraint, whenever analytical analysis of the discretized counterparts is not possible, the associated dynamics of numerics such as bifurcation phenomena and asymptotic behavior are obtained numerically using supercomputers. The term “**discretized counterparts**” is used to mean the finite difference equations (or “**discrete maps**”) resulting from finite discretizations of the underlying differential equations (DEs). Analysis here means analysis of the discretized counterparts by (a) available theory (b) searching for asymptotic solution behavior without resorting to purely numerical computations and (c) using continuation types of approaches to trace out the bifurcation diagrams (Keller 1977). This is the case for most of the illustrations throughout this paper. It is hoped that we can encourage numerical analysts to construct practical algorithms (to avoid spurious dynamics) based on the numerical phenomena observed using supercomputers to balance advances of computations and analyses. We also hope that it will strengthen the interface of numerical analysis with practical CFD applications and motivate CFD researchers who are looking for new approaches and solutions to new or old but challenging problems.

Due to the rapid independent development of dynamics of continuum and discrete maps, and the numerics of dynamics and the dynamics of numerics, it is extremely difficult to write a review paper on the subject. Topics discussed and references cited are only representative of the subject and reflect the authors’ experiences and preference toward certain areas at the time of this writing. Only selected properties of the observed phenomena are discussed.

Outline: A rather detailed background, motivation and subtleties of the subject will be given in Section II due to the relatively new yet interdisciplinary nature of this research topic for CFD. The subtleties discussed are necessary to illuminate and isolate the sources of numerical uncertainties due to factors such as slow convergence or nonconvergence of numerical schemes,

and nonlinear behavior of high-resolution shock-capturing schemes. These include but are not limited to spurious nonlinear behavior of numerics such as “spurious chaos”, “spurious traveling waves”, “spurious chaotic transient” in transition to turbulence flows, “spurious steady-state numerical solutions” and “spurious asymptotes” (e.g., spurious limit cycles). Here “spurious numerical solutions (and asymptotes)” is used to mean numerical solutions (asymptotes) that are solutions (asymptotes) of the discretized counterparts but are not solutions (asymptotes) of the underlying DEs. Asymptotic solutions here include steady-state solutions, periodic solutions, limit cycles, chaos and strange attractors. See Thompson & Stewart (1986) and Hoppensteadt (1993) for the definition of chaos and strange attractors. The background material includes the connection between nonlinear dynamics and fluid dynamics, between nonlinear dynamics and CFD, between nonlinear dynamics and time-marching approaches.

Section III reviews the basic terminology in nonlinear dynamics and reviews selected examples from our previous work. These examples consist of nonlinear model ODEs and PDEs. Particular attention is paid to the isolation of the different nonlinear behavior and spurious dynamics due to some of the numerical uncertainties mentioned earlier. The numerical schemes considered are selected to illustrate the following different spurious behavior of the dynamics of numerics.

- (a) Occurrence of stable and unstable spurious asymptotes above the linearized stability limit of the scheme (for constant step sizes)
- (b) Occurrence of stable and unstable spurious steady states below the linearized stability limit of the scheme (for constant step sizes)
- (c) Interplay of initial data and time steps on the permissibility of spurious asymptotes
- (d) Linearized behavior vs. nonlinear behavior of numerical solutions
- (e) Stabilization of unstable steady states by super-stable implicit methods
- (f) Interference with the dynamics of the underlying implicit scheme by procedures in solving the nonlinear algebraic equations (resulting from implicit discretization of the continuum)
- (g) Dynamics of the linearized implicit Euler scheme vs. Newton’s method
- (h) Local error control in ODE solvers and the conferrance of global properties of the nonlinear ODEs
- (i) Spurious chaos and chaotic transients
- (j) Spurious dynamics independently introduced by spatial and time discretizations

Sections IV and V illustrate examples of CFD computations that exhibit spurious behavior due to numerics. The discussion is divided into transient and steady-state computations with several examples for each category. Sections 4.2.1, 5.1, 5.2 and 5.4 were written by the original contributors of the respective work. Section IV was taken from Yee & Sweby (1996). It is mainly concerned with convergence rate and spurious behavior of time-marching to the steady states of high-resolution shock-capturing methods. Section V is concerned with a “numerically induced chaotic transient” computation, and spurious behavior and convergence rate of transient computations of high-resolution shock-capturing schemes. The final section discusses how to use existing tools in bifurcation theory to avoid convergence to the wrong steady states or asymptotes. These tools are based on the combined knowledge of recent

advances in the dynamics of the physical equations and the dynamics of the underlying finite discretizations using existing tools in bifurcation theory and nonlinear dynamics. Note that the reference list contains more references than are cited inside the text. These extra references are intended for interested readers to pursue this subject further.

II. Background & Motivations

Starting in the late 1970's, there have been important developments and breakthroughs concerned with the theory of nonlinear dynamical systems. There was also an explosion of journal and conference papers, texts and reference books on the subject in the 1980's and early 1990's. See for example, Guckenheimer & Holmes (1983), Thompson & Stewart (1988), Seydel (1988), Hales & Kocak (1991), Stewart (1990), Wiggins (1990), and Hoppensteadt (1993). During the early 1980's, a new area of applied mathematics emerged from the interaction of dynamical system theory and numerical analysis. These developments addressed mainly mathematical principles and their applications of numerics in the understanding of the dynamics of DEs without discussing the connection between dynamics and numerics for initial value problems (IVPs) and initial boundary value problems (IBVPs). There was, however, some discussion on this connection for boundary value problems (BVPs) (Doedel & Beyn 1981, Doedel 1986, Shubin et al. 1981, Kellogg et al. 1980, Peitgen et al. 1981 and Shreiber & Keller 1983). Studies of BVPs of the elliptic type continue to the present day. See, for example, the SIAM Conference on Dynamical Systems, October 15-19, 1992, and the Proceedings of IMA Conferences on Dynamics of Numerics and Numerics of Dynamics, July 31 - Aug. 2, 1990, Bristol, England.

Why is it important to understand the connection between dynamics and numerics for BVPs, IVPs and IBVPs? It stems from the fact that it is a standard practice to use numerics to discover dynamical properties of continuous systems. As a matter of fact, much of what we know about specific dynamical systems is usually obtained from numerical experiments. One not only can visualize the dynamics and the bifurcation phenomena associated with numerics, but in most of the cases the dynamical behaviors of the DEs are not amenable otherwise. Consequently, developments concerned with the connection between dynamics and numerics are necessary to bridge the gap in a better understanding of the dynamics of numerics and the numerics of dynamics.

In the late 1980's, developments concerned with the connection between dynamics and numerics for IVPs and IBVPs slowly emerged. See for example, Mitchell & Griffiths (1985), Griffiths & Mitchell (1988), Pruffer (1985), Iserles (1988), Lorenz (1989) and Sanz-Serna (1985, 1990), and Salas et al. (1986). These developments raised many interesting and important issues of concern that are useful to practitioners in computational sciences. The following lists some of the issues:

(a) Can recent advances in dynamical systems provide new insights into better understanding of numerical algorithms and the construction of new ones?

(b) Can these advances aid in the determination of a more reliable criterion on the use of existing numerical schemes for strongly nonlinear problems?

(c) Under what conditions should a nonlinear problem be treated as a genuinely nonlinear problem rather than as a simplified linear problem?

(d) Do traditional convergence and linear stability analyses apply to asymptotic nonlinear behavior and in particular to long time numerical simulation of nonlinear evolutionary PDEs?

(e) Does error control suppress spuriousity? To what extent does local error control confer global properties in IVPs (long time integration) of nonlinear DEs?

(f) What is the influence of finite time steps and grid spacings rather than time steps and grid spacings approaching zero on the overall nonlinear behavior and stability of the scheme in terms of allowable initial data and discretized parameters?

(g) How different is the dynamical behavior of different procedures in solving the nonlinear algebraic equations resulting from using implicit time discretizations?

Since the early 1990's, the use of dynamics to address long time behavior of numerical schemes for IVPs and IBVPs began to flourish. The more recent work includes the Conference on Dynamics of Numerics and Numerics of Dynamics (University of Bristol, July 31 - August 2, 1990), the Chaotic Numerics Workshop (Deakin University, Geelong, Australia, July 12-16, 1993), the Conference on Dynamical Numerical Analysis (Georgia Institute of Technology, Atlanta, Georgia, December 14-16, 1995), and the "Innovative Time Integrators Workshop" (Center for Mathematics and computer Science, Amsterdam, November 6-8, 1996, the Netherlands). These conferences were devoted almost entirely to dynamical numerical analysis. See the proceedings and references cited therein. See also Stuart (1994, 1995), Humphries (1992), Hairer et al. (1989), Aves et al. (1995), Corless (1994a,b), Dieci & Estep (1991), and Poliashenko & Aidun (1995). The majority of the later developments concentrated on long time behavior of ODE solvers using variable step size based on local error controls (Butcher 1987). This type of local error controls enjoyed much success in controlling accuracy and stability for transient computations.

On the other hand, even though standard practice in ODE solvers uses local error control for the selection of step size, practical CFD applications rarely employ this type of variable step size control due to the lack of efficient and practical theory for highly coupled nonlinear time-dependent PDEs. See Section 3.6 for a discussion. It should also be noted that finite element methods use ODEs solvers for the time integration part of the solution. There is also some preliminary work on computability and error control in finite element methods. See Johnson (1995) and Johnson et al. (1995) and references cited therein. Indirectly, this type of approach does make use of adaptive step size error controls. There still remains the question of spurious dynamics due to spatial discretizations. In practical CFD computations, one usually uses fixed grid spacings and time step constraints based on a linearized stability requirement or the Courant-Friedrich-Lewy (CFL) condition. Usually, after the initial transient dies down, the

step sizes are nearly constant from one step to the next in time marching to the steady state.

The caveat is that regardless of whether finite difference (and finite volume) or finite element methods are employed, when time-marching approaches are used to obtain steady-state numerical solutions, local error controls similar to that used in ODE solvers that were designed for accuracy purposes are neither practical nor appropriate to use, since such local step size error control methods might prevent the solution from reaching the correct steady-state solutions within a reasonable number of iterations. It is remarked that the standard practice of using “local time step” (varied from grid point to grid point with the same CFL) in time-marching to the steady state is not the same as the variable step size based on local error controls.

The authors believe that the understanding of the dynamics of numerics for fixed step size is necessary from that aspect. Besides, the study of the dynamics of ODE solvers using variable step size based on local error control requires the knowledge of the constant step size case (Aves et al. 1995). In a series of papers, Yee et al. (1991), Yee & Sweby (1994, 1995a,b), Sweby et al. (1990, 1995), Sweby & Yee (1992, 1994), and Lafon & Yee (1991, 1992) studied the dynamics of finite discretization for fixed (constant) time steps. The examples used in these papers were deliberately kept simple to permit explicit analysis. The approach was to take nonlinear model ODEs and PDEs with known explicit solutions (the most straight forward way of being sure what is ‘really’ happening), discretize them according to various standard numerical methods, and apply techniques from discrete dynamics to analyze the behavior of the discretized counterparts. Particular attention was paid to the isolation of the different nonlinear behavior and spurious dynamics due to some of the numerical uncertainties listed in Section I. These studies revealed much rich dynamical phenomena that we believe are useful for CFD and at the same time were not amenable with available theory at the time. The present paper alludes mainly to this aspect of the dynamics of numerics.

2.1. Nonlinear Dynamics and Fluid Dynamics

Most of the available fluid dynamics and CFD related texts and reference books describe the Euler and Navier-Stokes equations in differential form as coupled systems of nonlinear PDEs. These equations are rarely classified as dynamical systems. However, fluid dynamicists are often interested in how the flow behaves as a function of one or more physical parameters. Of particular interest to fluid dynamicists is locating the critical value of the physical parameter where the fluid undergoes drastic changes in the flow behavior. Some examples are the prediction of transition to turbulence or laminar instability as a function of the Reynolds number, flow separation and stall as a function of Reynolds number and angle of attack, rotorcraft vibration as a function of rotation speed and flight speed, the occurrence of shock waves as a function of the body shape and/or Mach number, and the formation of vortices, flutter, and other flow phenomena as a function of the angle of attack or other physical parameters. Another application is in the area of aiding the understanding of the topology of flow patterns (flow visualizations) of laboratory experiments, observable physical phenomena and numerical data. An additional important topic for CFD is the control and optimization

of dynamical systems. This involves the application of optimization and control theory to dynamical systems. Researchers are beginning to use these interdisciplinary ideas to study, for example, the control of turbulence, the control of vortex generation and/or shock waves, the control of vibration in rotorcraft, and the control of aerodynamic noise such as sonic boom and jet noise.

The application of dynamical system theory to the study of spatio-temporal instabilities of aerodynamic and hydrodynamic flows and chaotic systems in fluid dynamics was discussed respectively in the 1994 and 1996 von Karman Institute for Fluid Dynamics Lecture Series. How the solution behaves as one or more of the system parameters is varied is precisely the definition of dynamical systems and bifurcation theory. According to Ian Stewart (1990)

“Bifurcation theory is a method for finding interesting solutions to nonlinear equations by tracking dull ones and waiting for them to lose stability.”

As evident from the Third SIAM Conference on the Application of Dynamical Systems, May 21-24, 1995, Snowbird, Utah, presentations in treating the various fluid flow equations as dynamical systems have pushed these topics to the forefront of applied mathematical research.

2.2. Nonlinear Dynamics and CFD

When we try to use numerical methods to gain insight into the fluid physics, there is an added new dimension to the overall problem. Even though we freeze the physical parameters of the governing equations, the resulting discretized counterparts (from finite discretizations of the governing equations) are **not just** a nonlinear system of difference equations, but are **also** a nonlinear but **discrete** dynamical system **on their own**. From nonlinear dynamics, we know that discrete dynamical systems possess much richer dynamical behavior than the continuum dynamical systems. These resulting discrete dynamical systems are a function of **all** of the discretized parameters which are not present in the governing equations. See Section III for a discussion. This is one of the key factors in influencing the numerical solution to depart from the physical ones if the governing equations are strongly nonlinear and stiff.

Of course, before analyzing the dynamics of numerics, it is necessary to analyze (or understand) as much as possible the dynamical behavior of the governing equations and/or the physical problems using theories of ODEs, PDEs, dynamical systems of ODEs and PDEs, and also physical guidelines. In fact, a knowledge of the theories of ODEs, PDEs, dynamical behavior of nonlinear DEs, and the dynamical behavior of nonlinear discrete maps (difference equations) is a prerequisite to the study of dynamics of numerics. In an idealized situation, if one knows the dynamical behavior of the governing equations, one can then construct suitable numerical methods for that class of dynamical systems. Consequently, spurious dynamics due to numerics can be minimized and that computation and analysis kept pretty much in tune. However, as applied scientists want to push the envelope of understanding of realistic flows and configurations further, dependence on the numerics takes over even though rigorous analysis

lags behind. Starting in the late 1970's the advances in computer power resulted in attempts to use CFD to replace wind tunnel experiments and use numerics to understand dynamical systems. The gap between computation and analysis increased. The nonlinear behavior of commonly used algorithms in CFD was not well understood but at the same time applied CFD increased the intensity of using these algorithms to solve more complex practical problems where the flow physics and configurations under consideration were not understood, and were either too costly for or not amenable to laboratory experiments. CFD was and remains in a stage where computation is ahead of analysis. In other words, we usually do not know enough about the solution behavior of the underlying DEs in practice, and we are at the stage where the understanding of the dynamics of the DEs and the understanding of the dynamics of numerics are in tandem, and they both are rapidly growing research areas. With this in mind, we summarize some of the sources of nonlinearities in the study of dynamics of numerics for CFD.

The sources of nonlinearities that are well known in CFD are due to the physics. Examples of nonlinearities due to the physics are convection, diffusion, forcing, turbulence source terms, reacting flows, combustion related problems, or any combination of the above. The less familiar sources of nonlinearities are due to the numerics. There are generally three major sources:

(a) Nonlinearities due to time discretizations -- the discretized counterpart is nonlinear in the time step. Examples of this type are Runge-Kutta methods. It is noted that linear multistep methods (LMMs) are linear in the time step. See Lambert (1973) for the forms of these methods.

(b) Nonlinearities due to spatial discretizations -- in this case, the discretized counterpart can be nonlinear in the grid spacing and/or the scheme. Examples of nonlinear schemes are the total variation diminishing (TVD) and essentially nonoscillatory (ENO) schemes. See Yee (1989) and references cited therein for the forms of these schemes.

(c) Nonlinearities due to complex geometries, boundary interfaces, grid generation, grid refinements and grid adaptations -- each of these procedures can introduce nonlinearities.

The behavior of the above nonlinearities due to the numerics are not well understood. Only some preliminary development is beginning to emerge recently.

2.3. Dynamics of Numerical Approximations of ODEs vs. Time-Dependent PDEs

Recent analyses and studies have shown that spurious numerical solutions can be independently introduced by time and spatial discretizations. Take the case when the ODEs are obtained from semi-discrete approximations of PDEs, the resulting system of ODEs contains **more** parameters (due to spatial discretizations) as opposed to physical problems governed by ODEs. The parameters due to spatial discretizations for the semi-discrete approximation becomes the system parameter (instead of the discretized parameter) of the resulting system of ODEs. Depending on the differencing scheme the resulting discretized counterparts of a PDE can be nonlinear in Δt , the grid spacing Δx and the numerical dissipation parameters, even though the PDEs have only one parameter or none. One major consideration is that one might

be able to choose a “safe” numerical method to solve the resulting system of ODEs to avoid spurious stable numerical solutions due to time discretizations. However, spurious numerical solutions and especially spatially varying steady states introduced by spatial discretizations in nonlinear hyperbolic and parabolic PDEs for CFD applications appear to be **more difficult** to avoid due to the use of a **fixed mesh**. In the case of the semi-discrete approach such as methods of lines or finite element methods, if spurious numerical solutions due to spatial discretizations exist, the resulting ODE system has already **inherited** this spurious feature as part of the exact solution of the semi-discrete case. Thus care must be taken in using the ODE solver computer packages for PDE applications. See Lafon & Yee (1991, 1992) and Section 3.7 for a discussion.

2.4. Nonlinear Dynamics and Time-Marching Approaches

The use of time-marching approaches to obtain steady-state numerical solutions has been considered the method of choice in CFD for nearly two decades since the pioneering work of Crocco (1965) and Moretti & Abbett (1966). Moretti and Abbett used this approach to solve the inviscid supersonic flow over a blunt body without resorting to solving the steady form of PDEs of the mixed type. The introduction of efficient CFD algorithms of MacCormack (1969), Beam & Warming (1978), Briley & McDonald (1977) and Steger (1978) marked the beginning of numerical simulations of 2-D and 3-D Navier-Stokes equations for complex configurations. It enjoyed much success in computing a variety of weakly and moderately nonlinear fluid flow problems. For strongly nonlinear problems, the situation is more complicated. To aid the understanding of the scope of the situation, first, we have to identify all the sources of nonlinearities. Second, we have to isolate all elements and issues of numerical uncertainties due to these nonlinearities in time-marching to the steady state. The following isolates some of the key elements and issues of numerical uncertainties in time-marching to the steady state.

Solving an IBVP with Unknown Initial Data: In time-marching approaches, one transforms a BVP to an IBVP with **unknown** initial data. Elements such as reliability, convergence with unknown initial data and rapid convergence to the **correct** steady state are the predominant requirements. The time differencing in this case acts as a pseudo time. Although it is well known from linearized stability analysis that only a subset of the numerical solutions for certain ranges of the discretized parameters (these ranges can be continuous or disjoint for problems with source terms) and boundary conditions mimic the true solution behavior of the governing equations, it is less well known that outside these safe regions the numerical solution, **depending on the initial data**, do not necessarily undergo instabilities. In addition, there exist asymptotic numerical solutions that are not solutions of the continuum even inside the safe regions. Unlike nonlinear problems, the numerical solutions of linear or nearly linear problems are “independent” of the discretized parameters and **initial data** as long as the discretized parameters are inside the stability limit (CFL condition). We put “independent” in quotations here to mean that the numerical solutions behave the same up to the order of accuracy and grid spacing of the scheme. That is, the topological shapes of these solutions remain the same within the stability limit and accuracy of the scheme for linear behavior. Section 3.4 illustrates

the strong dependence of the numerical solution on initial data for nonlinear DEs. It turns out that if constant step sizes are used, stability, convergence rate and permissibility of spurious numerical solutions are intimately related to the choice of initial data (or start up solution).

Reliability of Residual Test: The deficiency of the use of residual tests in detecting the convergence rate and the convergence to the correct steady-state numerical solutions is now briefly discussed. Consider a quasilinear PDE of the form

$$\mathbf{u}_t = G(\mathbf{u}, \mathbf{u}_\bullet, \mathbf{u}_{\bullet\bullet}, \alpha, \epsilon), \quad (2.1)$$

where G is nonlinear in \mathbf{u} , \mathbf{u}_\bullet and $\mathbf{u}_{\bullet\bullet}$. The values α and ϵ are system parameters. For simplicity, consider a two time level and a $(p + q + 1)$ point grid stencil numerical scheme of the form

$$\mathbf{u}_j^{n+1} = \mathbf{u}_j^n - H(\mathbf{u}_{j+q}^n, \dots, \mathbf{u}_j^n, \dots, \mathbf{u}_{j-p}^n, \alpha, \epsilon, \Delta t, \Delta \mathbf{x}) \quad (2.2)$$

for the PDE (2.1). Note that the discussion need not be restricted to explicit methods or two time level schemes. Let U^* , a vector representing $(\mathbf{u}_{j+q}^*, \dots, \mathbf{u}_j^*, \dots, \mathbf{u}_{j-p}^*)$, be a steady-state numerical solution of (2.2). When a time-marching approach such as (2.2) is used to solve the steady-state equation $G(\mathbf{u}, \mathbf{u}_\bullet, \mathbf{u}_{\bullet\bullet}, \alpha, \epsilon) = 0$, the iteration typically is stopped when the residual H and/or some ℓ_2 norm of the dependent variable \mathbf{u} between two successive iterates is less than a pre-selected level.

Aside from the various standard numerical errors such as truncation error, machine round-off error, etc., there is a more fundamental question of the validity of the residual test and/or ℓ_2 norm test. If the spatial discretization happens to produce spurious steady-state numerical solutions, these spurious solutions would still satisfy the residual and ℓ_2 norm tests in a deceptively smooth manner. Moreover, aside from the spurious solution issue and depending on the combination of time as well as spatial discretizations, it is not easy to check whether $G(\mathbf{u}^*, \mathbf{u}_\bullet^*, \mathbf{u}_{\bullet\bullet}^*, \alpha, \epsilon) \rightarrow 0$ even though $H(U^*, \alpha, \epsilon, \Delta t, \Delta \mathbf{x}) \rightarrow 0$, since spurious steady states (and asymptotes) can be independently introduced by spatial and time discretizations. This is contrary to the ODE case, where if \mathbf{u}^* is a spurious steady state of $d\mathbf{u}/dt = S(\mathbf{u})$, then $S(\mathbf{u}^*) \neq 0$. If a steady state has been reached with a rapid convergence rate, it does not imply that the obtained steady state is not spurious.

Methods Used to Accelerate Convergence Process: Methods such as iterations and relaxation procedures, and/or convergence acceleration methods such as conjugate gradient methods have been utilized to speed up the convergence process (Saad 1994). Also techniques such as preconditioning (Tukel 1993) and multigrid (Wesseling 1992) combined with iteration, relaxation and convergence acceleration procedures are commonly used in CFD. Depending on the type of PDEs, proper preconditioners can be established for the PDEs or for the particular discretized counterparts. Multigrid methods can be applied to the steady PDEs or the time-dependent PDEs. In either case, a combination of these methods can still be viewed as pseudo time-marching methods (but not necessarily of the original PDE that was under consideration).

However, if one is not careful, numerical solutions other than the desired one can be obtained in addition to spurious asymptotes due to the numerics. From here on the term “time-marching approaches” is used loosely to include all of the above. It is remarked that multigrid methods can be viewed as the (generalized) spatial counterpart of variable time step control in time discretizations.

Methods in Solving the Nonlinear Algebraic Equations From Implicit Methods: When implicit time discretizations are used, one has to deal with solving systems of nonlinear algebraic equations. Aside from the effect of the different methods to accelerate the convergence process discussed previously, we need to know how different the dynamical behavior is for the different procedures (e.g., iterative vs. non-iterative) in solving the resulting nonlinear difference equations. See Yee & Sweby (1994, 1995a,b) and the next section for a discussion.

Mismatch in Implicit Schemes: It is standard practice in CFD to use a simplified implicit operator (or mismatched implicit operators) to reduce CPUs and to increase efficiency. These mismatched implicit schemes usually consist of the same explicit operator but different simplified implicit operators. The implicit time integrator is usually of the LMM type. One popular form of the the implicit operator is the so called “delta formulation” (Beam & Warming 1978). The advantage of the delta formulation is that if a steady state has been reached, the numerical solution is independent of the time step. The original logic in constructing this type of scheme is that the implicit operators act as a relaxation mechanism. However, from a dynamical system standpoint, before a steady state is reached, the nonlinear difference equations representing each of these simplified implicit operators are different from each other. They have their own dynamics as a function of the time step, grid spacing and initial data. They also can exhibit different types of nonlinear behavior if one is solving strongly nonlinear time-dependent PDEs. Thus, even when steady states have been reached, they might not converge to the same steady state due to the different forms of the implicit operator. In addition, even if they converge to the same steady state, that steady state can still be spurious since the same explicit operator is used. This might be due to the fact that spatial discretizations can introduce spurious steady states. Consequently, these mismatched implicit operators can have different spurious dynamics and/or different convergence rates for the entire solution procedure. Section 4.3 describes some examples.

Nonlinear Schemes: It is well known that all of the TVD, total variation bounded (TVB) and ENO schemes (see Yee (1989) or references cited therein) are *nonlinear schemes* in the sense that the final algorithm is *nonlinear even for the constant-coefficient linear PDE*. These types of schemes are known to have a slower convergence rate than classical shock-capturing methods and can occasionally produce unphysical solutions for certain combinations of entropy satisfying parameters and flux limiters (in spite of the fact that entropy satisfying TVD, TVB and ENO schemes can suppress unphysical solutions). See Yee (1989) for a summary of the subject. The second aspect of these nonlinear schemes is that even if the numerical method is formally of more than first-order and if the approximation converges, the rate may still be only first-order behind the shock (not just around the shock). This can happen for systems where one

characteristic may propagate part of the error at a shock into the smooth domain. Engquist & Sjögreen (1996) illustrate this phenomena with examples. See Section 4.2 for a discussion. The third aspect of these higher-order nonlinear schemes is their true accuracy away from shocks. See Donat (1994), Casper & Carpenter (1995) and Section 5.4 for a discussion.

Schemes That are Linear vs. Nonlinear in Δt : The obvious classification of time-accurate schemes for time-marching approaches to the steady state are explicit, implicit, and hybrid explicit and implicit methods. Although many of the added numerical procedures, discussed in the previous paragraph, used to help speed up convergence to steady states can apply to both explicit and implicit methods, there are distinct differences between the two. Usually, one tries to enlarge what is the equivalent of the linearized time step constraints imposed by the explicit schemes for rapid convergence. On the other hand, if implicit methods are used, unconditionally stable implicit methods are usually employed. Linearized stability constraints are not the problem. Efficient methods for solving the nonlinear algebraic equations which guarantee rapid convergence to the correct steady states are then the main concern.

A less commonly known classification of numerical schemes for time-marching approaches is the identification of schemes that are linear or nonlinear in the time step (Δt) parameter space when applied to nonlinear DEs. As mentioned before, all LMMs (explicit or implicit) are linear in Δt and all multistage Runge-Kutta methods are nonlinear in Δt . Lax-Wendroff and MacCormack type of non-separable full discretizations also are nonlinear in Δt . A desirable property for a scheme that is linear in Δt is that, if the numerical solution converges, its steady-state numerical solutions are independent of the time step. On the other hand, the accuracy of the steady-state numerical solutions (also for time-accurate numerical solutions) depends on Δt if the scheme is nonlinear in Δt . Certain of these types of schemes are more sensitive to Δt than others. For example, Lax-Wendroff and MacCormack methods (MacCormack 1969) are more sensitive than the Lerat variant (Lerat & Sides 1988). A less known property of schemes that are nonlinear in Δt is that this type of scheme has an important bearing on the existence of spurious steady-state numerical solutions due to time discretizations. Although schemes like LMMs are immune from exhibiting spurious steady-state numerical solutions, as seen in Yee & Sweby (1994, 1995a,b), a wealth of surprisingly nonlinear behavior of implicit LMMs that had not been observed before were uncovered by the dynamical approach. See the next section for a review.

Adaptive Time Step Based on Local Error Control: It is a standard practice in CFD to use “local time step” (varied from grid point to grid point using the same CFL) for nonuniform grids. However, except in finite element methods, adaptive time step based on local error control is rarely use in CFD. Adaptive time step is built in for standard ODE solver computer packages (Butcher 1987). It enjoyed much success in controlling accuracy and stability for transient (time-accurate) computations. The issue is to what extent does this adaptive local error control confer global properties in long time integration of time-dependent PDEs? Can one construct similar error control that has guaranteed and rapid convergence to the correct steady-state numerical solutions in the time-marching approaches for time-dependent PDEs?

Nonunique Steady-State Solutions of Nonlinear DEs vs. Spurious Asymptotes: The phenomenon of generating spurious steady-state numerical solutions (or other spurious asymptotes) by certain numerical schemes is often **confused** with the nonuniqueness (or **multiple steady states**) of the governing equation. In fact, the existence of nonunique steady-state solutions of the continuum can complicate the numerics tremendously (e.g., the basins of attraction -- which initial data lead to which asymptote) and is **independent** of the occurrence of spurious asymptotes of the associated scheme. But, of course, a solid background in the theory of nonlinear ODEs and PDEs and their dynamical behavior is a prerequisite in the study of the dynamics of numerical methods for nonlinear PDEs. A full understanding of the subject can shed some light on the controversy about the “true” existence of multiple steady-state solutions through numerical experiments for certain flow types of the Euler and/or Navier-Stokes equations.

III. Elementary Examples

This section reviews the fundamentals of and illustrates with elementary examples, the spurious behavior of commonly used time discretizations in CFD. Except for Section 3.6, details of these examples can be found in our earlier papers.

3.1. Preliminaries

Consider an autonomous nonlinear ODE of the form

$$\frac{du}{dt} = \alpha S(u), \quad (3.1)$$

where α is a parameter and $S(u)$ is nonlinear in u . Autonomous here means that t does not appear explicitly in the function S . For simplicity of discussion, we consider only autonomous ODEs where α is linear in (3.1); i.e., α does not appear explicitly in S .

A fixed point u^* of an autonomous system (3.1) is a constant solution of (3.1); that is

$$S(u^*) = 0. \quad (3.2)$$

We remark that the terms “equilibrium points”, “critical points”, “singular points”, “stationary points”, “asymptotic solutions” (we are excluding periodic solutions for the current definition), “steady-state solutions” and “fixed points” are sometimes used with slightly different meanings in the literature, for example, in bifurcation theory. However, for the current discussion and for the majority of the nonlinear dynamics literature, these terms are used interchangeably. Note that certain researchers reserve the term “fixed point” for discrete maps (difference equations) only.

Consider a nonlinear discrete map from the finite discretization of (3.1)

$$\mathbf{u}^{n+1} = \mathbf{u}^n + D(\mathbf{u}^n, \mathbf{r}), \quad (3.3)$$

where $\mathbf{r} = \alpha \Delta t$ and $D(\mathbf{u}^n, \mathbf{r})$ is linear or nonlinear in \mathbf{r} depending on the numerical scheme. Here the analysis is similar if (3.3) involves more than two time levels. Examples to illustrate the dependence on the numerical schemes for cases where D is linear or nonlinear in the parameter space will be given in a subsequent section.

A fixed point \mathbf{u}^* of (3.3) (or fixed point of period 1) is defined by $\mathbf{u}^{n+1} = \mathbf{u}^n$, or

$$\mathbf{u}^* = \mathbf{u}^* + D(\mathbf{u}^*, \mathbf{r}), \quad (3.4a)$$

i.e.,

$$D(\mathbf{u}^*, \mathbf{r}) = 0. \quad (3.4b)$$

One can also define a fixed point of period p (or periodic solution of period p), where p is a positive integer by requiring that $\mathbf{u}^{n+p} = \mathbf{u}^n$ or

$$\mathbf{u}^* = E^p(\mathbf{u}^*, \mathbf{r}) \quad \text{but} \quad \mathbf{u}^* \neq E^k(\mathbf{u}^*, \mathbf{r}) \quad \text{for} \quad 0 < k < p. \quad (3.5)$$

Here, $E^p(\mathbf{u}^*, \mathbf{r})$ means that we apply the difference operator E p times, where $E(\mathbf{u}^n, \mathbf{r}) = \mathbf{u}^n + D(\mathbf{u}^n, \mathbf{r})$. For example, a fixed point of period 2 means $\mathbf{u}^{n+2} = \mathbf{u}^n$ or

$$\mathbf{u}^* = E(E(\mathbf{u}^*, \mathbf{r})). \quad (3.6)$$

In the context of discrete systems, the term ‘‘fixed point’’ without indicating the period means ‘‘fixed point of period 1’’ or the steady-state solution of (3.3). Interchangeably, we also use the term asymptote to mean a fixed point of any period.

In order to illustrate the basic idea, the simplest form of the Riccati ODE, i.e., the logistic ODE with

$$\frac{du}{dt} = \alpha S(u) = \alpha u(1 - u) \quad (3.7a)$$

is considered. For this ODE, the exact solution is

$$u(t) = \frac{u^0}{u^0 + (1 - u^0)e^{-\alpha t}}, \quad (3.7b)$$

where u^0 is the initial condition. The fixed points of the logistic equation are roots of $u^*(1 - u^*) = 0$; it has two fixed points $u^* = 1$ and $u^* = 0$.

To study the stability of these fixed points, we perturb the fixed point with a disturbance ξ , and obtain the perturbed equation

$$\frac{d\xi}{dt} = \alpha S(u^* + \xi). \quad (3.8)$$

Next, $S(\mathbf{u}^* + \xi)$ can be expanded in a Taylor series around \mathbf{u}^* , so that

$$\frac{d\xi}{dt} = \alpha \left[S(\mathbf{u}^*) + S_u(\mathbf{u}^*)\xi + \frac{1}{2}S_{uu}(\mathbf{u}^*)\xi^2 + \dots \right], \quad (3.9)$$

where $S_u(\mathbf{u}^*) = \left. \frac{dS}{d\mathbf{u}} \right|_{\mathbf{u}^*}$. Stability can be detected by examining a small neighborhood of the fixed point provided that, for a given α , \mathbf{u}^* is a **hyperbolic point** (Seydel 1988) (i.e., if the real part of $\alpha S_u(\mathbf{u}^*) \neq 0$). Under this condition ξ can be assumed small, its successive powers ξ^2, ξ^3, \dots can normally be neglected and the following linear perturbed equation is obtained

$$\frac{d\xi}{dt} = \alpha S_u(\mathbf{u}^*)\xi. \quad (3.10)$$

The fixed point \mathbf{u}^* is asymptotically stable if $\alpha S_u(\mathbf{u}^*) < 0$ whereas \mathbf{u}^* is unstable if $\alpha S_u(\mathbf{u}^*) > 0$. If $\alpha S_u(\mathbf{u}^*) = 0$, a higher order perturbation is necessary. If \mathbf{u}^* is not a hyperbolic point, the behavior of (3.10) does not infer the behavior of the original unperturbed equation.

For the logistic ODE, the fixed points are hyperbolic. Thus the linearized analysis suffices (i.e., the original equation has the same local behavior as the perturbed equation (3.10)). If we perturb the logistic equation around the fixed point with $\alpha > 0$, we find that $\mathbf{u}^* = 1$ is stable and $\mathbf{u}^* = 0$ is unstable. It is well known that the global asymptotic solution behavior of the logistic ODE is that for any $\mathbf{u}^0 > 0$, the solution will eventually tend to $\mathbf{u}^* = 1$. Figure 3.1 shows the asymptotic solution behavior of the logistic ODE.

Now, let us look at three of the well known schemes for IVPs of ODEs. These are explicit Euler (Euler or forward Euler), leapfrog and Adams-Bashforth. For the ODE (3.1), the dynamical behavior of their corresponding discrete maps is well established. The explicit Euler method is given by

$$\mathbf{u}^{n+1} = \mathbf{u}^n + rS(\mathbf{u}^n), \quad (3.11)$$

and after a linear transformation it is the well known logistic map (Hoppensteadt 1993). The leapfrog method can be written as

$$\mathbf{u}^{n+1} = \mathbf{u}^{n-1} + 2rS(\mathbf{u}^n), \quad (3.12)$$

and it is a form of the Henon map (Devaney 1987). The Adams-Bashforth method yields

$$\mathbf{u}^{n+1} = \mathbf{u}^n + \frac{r}{2} \left[3S(\mathbf{u}^n) - S(\mathbf{u}^{n-1}) \right], \quad (3.13)$$

again a variant of the Henon map that has been discussed by Pruffer (1985) in detail.

We can determine fixed points of the discrete maps (3.11)-(3.13) and their stability properties in a manner similar to that for the ODE. It turns out that all three of the discrete maps have the same fixed points as the ODE (3.1) --- a desired property which is important for obtaining the

correct steady states of nonlinear DEs numerically. An examination of (3.11)-(3.13) reveals that the discretized parameter r appears linearly in these discrete maps. As will be seen in the next section, a necessary condition for the occurrence of spurious steady states by any scheme is that the discretized parameter should appear nonlinearly in the underlying discrete map. Consequently the existence of spurious steady states is not possible for (3.11)-(3.13).

The corresponding linear perturbed equation for the discrete map (3.3), found by substituting $u^n = u^* + \xi^n$ in (3.3) and ignoring terms higher than ξ^n , is

$$\xi^{n+1} = \xi^n [1 + \Delta t D_u(u^*, \Delta t)]. \quad (3.14)$$

Here the parameter α of the ODE has been absorbed in the parameter Δt based on the assumption that α does not appear explicitly in $S(u)$. Depending on the scheme, $D(u^n, \Delta t)$ might be nonlinear in Δt . If nonlinearity in the parameter space Δt is introduced into the discretized counterpart, it increases the possibility that the dynamics of numerics deviates from the dynamics of the continuum.

For stability we require

$$|1 + \Delta t D_u(u^*, \Delta t)| < 1. \quad (3.15)$$

Again, for $|1 + \Delta t D_u(u^*, \Delta t)| = 1$, a higher order perturbation is necessary. For a fixed point of period p the corresponding linear perturbed equation and stability criterion are

$$\xi^{n+p} = \xi^n E_u^p(u^*, \Delta t), \quad (3.16a)$$

and

$$|E_u^p(u^*, \Delta t)| < 1, \quad (3.16b)$$

with

$$E_u^p(u^n, \Delta t) = \frac{d}{du} E(u^{n+p-1}, \Delta t) \dots \frac{d}{du} E(u^n, \Delta t). \quad (3.16c)$$

For $S(u) = u(1 - u)$, the stability of the stable fixed points of period 1 and 2 for discrete maps (3.11)-(3.13) with $r = \alpha \Delta t$ are

Explicit Euler:

$$\begin{array}{ll} u^* = 1 & \text{stable if } 0 < r < 2 \\ \text{period 2} & \text{stable if } 2 < r < \sqrt{6} \end{array}$$

Leapfrog:

$$\begin{array}{ll} u^* = 1 & \text{unstable for all } r \geq 0 \\ & \text{chaotic solutions exist for all } r \text{ no matter how small} \end{array}$$

Adams-Bashforth:

$$\begin{array}{ll} u^* = 1 & \text{stable if } 0 < r < 1 \\ \text{period 2} & \text{stable if } 1 < r < \sqrt{2}. \end{array}$$

Figure 3.2a shows the **stable** fixed point diagram of period 1, 2, 4, 8 obtained for the explicit Euler scheme by solving numerically the roots of (3.11) (by setting $u^{n+1} = u^n$) for $S(u) = u(1 - u)$. The r axis is divided into 1000 equal intervals. The numeric labeling of the branches denotes their period. The subscript ‘‘E’’ on the period 1 branch indicates the stable fixed point of the DE. From here on, $r = a\Delta t$ where $a = \alpha$ in all of the plots. The change of notation inside the plots is due to the plotting package.

All of these three examples share a common property of not exhibiting spurious steady states. Two of these three examples serve to illustrate that operating with a time step beyond the linearized stability limit of the stable fixed points of the nonlinear ODEs does not always result in a divergent solution; spurious asymptotes of higher period can occur. This is in contrast to the ODE solution, where only a single stable asymptotic value $u^* = 1$ exists for any $\alpha > 0$ and any initial data $u^0 > 0$. The spurious asymptotes, regardless of the period, stable or unstable, are solutions in their own right of the discrete maps resulting from a finite discretization of the ODE.

3.2. Spurious Asymptotic Numerical Solutions for Constant Step Sizes

For the previous section we purposely picked the type of schemes that do not exhibit spurious fixed points, but allow spurious fixed points of period higher than 1. In this section numerical methods are purposely chosen so that the discretized parameter appears nonlinearly in the underlying discrete maps. Consequently, existence of spurious steady-state numerical solutions in these examples is possible.

3.2.1. Explicit Methods

Consider two second- and third-order Runge-Kutta schemes, namely, the modified Euler (R-K 2) and the improved Euler (R-K 2), Heun (R-K 3), Kutta (R-K 3), the fourth-order Runge-Kutta method (R-K 4), and two predictor-corrector methods (P-C 2 and P-C 3) (Lambert 1973) of the forms

Modified Euler (R-K 2) method:

$$u^{n+1} = u^n + rS\left(u^n + \frac{r}{2}S^n\right), \quad S^n = S(u^n), \quad (3.17)$$

Improved Euler (R-K 2) method:

$$u^{n+1} = u^n + \frac{r}{2} \left[S^n + S(u^n + rS^n) \right], \quad (3.18)$$

Heun (R-K 3) method:

$$u^{n+1} = u^n + \frac{r}{4} (k_1 + 3k_3) \quad (3.19)$$

$$k_1 = S^n$$

$$k_2 = S\left(u^n + \frac{r}{3}k_1\right)$$

$$k_3 = S\left(u^n + \frac{2r}{3}k_2\right),$$

Kutta (R-K 3) method:

$$u^{n+1} = u^n + \frac{r}{6} (k_1 + 4k_2 + k_3) \quad (3.20)$$

$$k_1 = S^n$$

$$k_2 = S\left(u^n + \frac{r}{2}k_1\right)$$

$$k_3 = S\left(u^n - rk_1 + 2rk_2\right),$$

R-K 4 method:

$$u^{n+1} = u^n + \frac{r}{6} (k_1 + 2k_2 + 2k_3 + k_4) \quad (3.21)$$

$$k_1 = S^n$$

$$k_2 = S\left(u^n + \frac{r}{2}k_1\right)$$

$$k_3 = S\left(u^n + \frac{r}{2}k_2\right)$$

$$k_4 = S\left(u^n + rk_3\right),$$

Predictor-corrector for $m = 2, 3$ (P-C 2 & P-C 3):

$$\begin{aligned}
 u^{(0)} &= u^n + rS^n \\
 u^{(k+1)} &= u^n + \frac{r}{2} \left[S^n + S^{(k)} \right], \quad k = 0, 1, \dots, m-1 \\
 u^{n+1} &= u^n + \frac{r}{2} \left[S^n + S^{(m-1)} \right].
 \end{aligned} \tag{3.22}$$

3.2.2. Fixed Point Diagrams

Using the same procedures as before, one can obtain the fixed points for each of the above schemes (3.17) - (3.22). Figures 3.2b - 3.2f show the **stable** fixed point diagrams of period 1,2,4 and 8 for selected schemes for $S(u) = u(1 - u)$. The unstable fixed points of any period are not plotted. See Yee et al. (1991) for the unstable fixed point diagrams. Some of the fixed points of lower period were obtained by closed form analytic solution and/or by a symbolic manipulator such as MAPLE (1988) to check against the computed fixed point. The majority were computed numerically. The stability of these fixed points was examined by checking the discretized form of the appropriate stability conditions. The domain is chosen so that it covers the most interesting part of the scheme and ODE combinations, and is divided into 1000 equal intervals. In other words, spurious asymptotes may occur in other parts of the domain as well. The numeric labeling of the branches denotes their period, although some labels for period 4 and 8 are omitted due to the size of the labeling areas. Again, the subscript ‘E’ on the main period one branch indicates the stable fixed point of the DE while the subscript ‘S’ indicates the spurious stable fixed points introduced by the numerical scheme. Spurious fixed points of period higher than one are obvious (since the ODEs under discussion only possess steady-state solutions) and are not labeled with a subscript ‘S’. Note that these diagrams, which for the most part appear to consist of solid lines, **actually consist of points**, which are only apparent in areas with high gradients.

To contrast the results, similar stable fixed point diagrams were also computed for the ODE

$$\frac{du}{dt} = \alpha u(1 - u)(b - u), \quad 0 < b < 1, \tag{3.23}$$

that is, for a cubic nonlinearity for $S(u) = u(1 - u)(b - u)$. The stable fixed point for the ODE (3.23) in this case is $u^* = b$ and the unstable ones are $u^* = 0$ and $u^* = 1$. For any $0 < u^0 < 1$ and any $\alpha > 0$, the solution will asymptotically approach the only stable asymptote of the ODE $u^* = b$.

By looking at the roots of the underlying discrete maps, it is readily realized that r appears nonlinearly in these discrete maps. In fact, the maximum number of stable and unstable fixed

points (real and complex) for each of the studied schemes (3.17)-(3.22) varied from 4 to 16 for $S(u) = u(1 - u)$ and 9 to 81 for $S(u) = u(1 - u)(b - u)$, depending on the numerical method and the r value. For certain r values, aside from the real steady states, these roots might be unstable and/or complex, but not for others. Fig. 3.3 shows the **stable** fixed point diagram by the modified Euler for four different values of b .

Aside from the striking difference in topography in the stable fixed point diagrams of the above methods and ODE combinations, all of these diagrams (except the P-C 2 method) have one common feature: they all exhibit **stable** spurious steady states, as well as spurious stable fixed points of period higher than one. In the majority of cases, these occur for values of r above the linearized stability limit of the true fixed point. But this is not always the case, as is demonstrated in the modified Euler scheme applied to the logistic ODE (3.7) and (3.23) for $0 < b < 0.5$, and the R-K 4 applied to the logistic ODE. For these two methods and ODE combinations, stable spurious fixed points occur below the linearized stability limit. In some of the instances, these spurious fixed points are outside the interval of the stable and unstable fixed points of the ODEs. Others not only lie below the linearized stability limit but also in the region between the fixed points of the DEs and so could be very easily achieved in practice. For example, in Fig. 3.2b, the modified Euler scheme for the logistic ODE, the linearized stability limit of period 1_E is $r = 2$. But depending on the value of r , two stable fixed points of period 1 (one is spurious) can exist at the same time for $0 < r < 1.236$. For the R-K 4 method applied to the logistic DE, one can see from Fig. 3.2d that spurious steady states which exist for $2.75 < r < 2.785$ are below the linearized stability limit of the 1_E branch. For the modified Euler method applied to $du/dt = \alpha u(1 - u)(b - u)$, it is interesting to see the changing behavior of stable spurious steady states as the stable fixed point $u^* = b$ is varied between 0 and 0.5.

A unified analysis for the above for the standard explicit Runge-Kutta methods is reported in Griffiths et al. (1992a). Tables 3.1 - 3.4, taken from Griffiths et al. (1992a), show the true and spurious asymptotes of selected schemes. Some entries are marked with an asterisk to indicate where stable fixed points are known to exist but no closed analytic form has yet been found.

Historically, Iserles (1988) was the first to show that while LMMs for solving ODEs possess only the fixed points of the original DEs, popular Runge-Kutta methods may exhibit spurious fixed points. Iserles et al. (1990) and Hairer et al. (1989) classified and gave guidelines and theory on the types of Runge-Kutta methods that do not exhibit spurious period one or period two fixed points. Humphries (1991) showed that under appropriate assumptions if stable spurious fixed points exist as the time-step approaches zero, then they must either approach a true fixed point or become unbounded. Hence repeating the integration with a smaller step size will ultimately make spurious behavior apparent. However, convergence in practical calculations involves a finite time step Δt that is not small as the number of integrations $n \rightarrow \infty$ rather than $\Delta t \rightarrow 0$, as $n \rightarrow \infty$. The work in Yee et al. (1991), Yee & Sweby (1994, 1995a,b), and Lafon & Yee (1991, 1992), Sweby et al. (1990, 1995), Sweby & Yee (1991), and Griffiths et al (1992) attempted to provide some of the global asymptotic behavior of time discretizations when finite **fixed** but not extremely small Δt is used. As mentioned in Section II, constant

step size algorithms are relevant to many applications in CFD as well as in other science and engineering disciplines. Thus a clear understanding of the dynamics of constant step sizes is necessary to isolate some of the sources and cures of numerical uncertainties in computational sciences.

3.3. Bifurcation Diagrams

This section discusses another method for obtaining the **stable** fixed point diagrams or bifurcation diagrams before illustrating the symbiotic relationship between permissibility of spurious steady states and initial data in fixed time step computations.

“Full” Bifurcation Diagram (“Complete Fixed Point Diagram”): If one obtains the full spectrum of these fixed points of any order as a function of the step size, the fixed point diagram is sometimes referred to as the “full” bifurcation diagram. In other words, the “full” bifurcation diagram exhibits the complete asymptotic solutions of the discretized counterparts as a function of the discretized parameter τ . In computing the “full” bifurcation diagram, searching for the roots and testing for stability of highly complicated nonlinear algebraic equations (for fixed points of higher period and/or complex nonlinear DEs combination) can be expensive and might lead to inaccuracy. In certain instances, one might be able to obtain the bifurcation diagram by some type of continuation method. The most popular one is called the pseudo arclength continuation method and was devised by Keller (1977). However, the majority of the continuation type methods require **known start up solutions** for each of the main bifurcation branches before one can continue the solution along a specific main branch. For problems with complicated bifurcation patterns, the arclength continuation method cannot provide the complete bifurcation diagram without the known start up solutions. In fact, it is usually not easy to locate even just one solution on each of these branches, especially if spurious asymptotes exist.

Computed Bifurcation Diagram: A numerical approach in obtaining a “computed” bifurcation diagram (not necessarily the full bifurcation diagram, as explained later) of the resulting discretized counterpart is by iterations of the underlying discrete map. In other words, this type of computed bifurcation diagram for the one-dimensional discrete map displays the iterated solution u^n vs. τ after iterating the discrete map for a given number of iterations with a chosen initial condition for each of the τ parameter values. For the figures shown later, with a given interval of τ and a chosen initial condition, the τ axis is divided into 500 equal spaces. In each of the computations, the discrete maps were iterated with 600 preiterations (more or less depending on the DE and scheme combinations) and the next 200 iterations were over plotted in the same diagram for each of the 500 τ values. The preiterations are necessary in order for the solutions to settle to their asymptotic value. A high number of iterations are overlaid on the same plot in order to detect periodic orbits (in this case periods of up to 200) or invariant sets. The reader is reminded that with this method of computing the bifurcation diagrams, **only the stable branches** are obtained. The domains of the τ and u^n axes are chosen to coincide with the stable fixed point diagrams shown previously. As explained later, even though all of these

discrete maps possess periodic solutions of period n for arbitrarily large n and stable chaotic solutions, no attempt was made to compute all of the spurious orbits of any order or chaotic solutions. The purpose of the present discussion is to show the spurious behavior and these computations suffice to serve the purpose.

Examples: Figure 3.4 shows the bifurcation diagram of the Euler scheme applied to the logistic DE with an initial condition $u^0 > 0$. It is of interest to know that in this case the bifurcation diagram looks practically the same for any $u^0 > 0$. This is due to the fact that no spurious fixed points exist for $r \leq 2$ and no spurious asymptotes of low period exist for $r < 2.627$. One quickly observes that using the arclength continuation method for this discrete map is the most efficient way to obtain its bifurcation diagram. However, this is not the case for other methods to be discussed later. Comparing the bifurcation diagram with Fig. 3.2a, one can see that if we had computed all of the fixed points of period up to 200 for Fig. 3.2a, the resulting fixed point diagram would look the same as the corresponding bifurcation diagram (assuming 600 iterations of the logistic map are sufficient to obtain the converged stable asymptotes of period up to 200 and the chosen initial data are appropriate to cover the basins of all of the periods in question). The numeric labeling of the branches in the bifurcation diagram denote their period, with only the essential ones labeled for identification purposes.

The noise appearing on the 1_E branch near the bifurcation point $r = 2$ of the linearized stability limit of the fixed point $u^* = 1$ indicates that 600 iterations of the logistic map are not sufficient to obtain the converged stable asymptotes. This phenomenon is common to other bifurcation points of higher periods as well as the rest of the corresponding bifurcation for the studied schemes. See Yee et al. (1991), and Yee & Sweby (1994, 1995a,b) for additional details. In fact, the **slow convergence** of using a time step that is near the linearized stability of the scheme (bifurcation point) might be due to this fact.

It is remarked that the explicit Euler applied to the logistic ODE resulted in the famous logistic map. Unlike the underlying logistic ODE, it is well known that the logistic map possesses very rich dynamical behavior such as period-doubling (of period 2^n for any positive n) cascades resulting in chaos (Feigenbaum, 1978). One can find Fig. 3.4 appearing in most of the elementary dynamical systems text books. The exact values of r for all of the period-doubling bifurcation points and chaotic windows (intervals of r) are known and were discovered by Feigenbaum in the late 1970's. Interested readers should consult these elementary text books for details. In other words, one can obtain the analytical (exact) behavior of the spurious asymptotes and numerical (spurious) chaos of the logistic map. The next section explains why using a single initial datum in computing the bifurcation diagrams for schemes that exhibit spurious asymptotes does not necessarily coincide with the fixed point diagram (or full bifurcation diagram). It is interesting to note that the corresponding bifurcation diagrams of the respective discrete maps produced by the remaining studied schemes consist of unions of "logistic-map-like" bifurcations and/or "inverted logistic-map-like" bifurcations with similar yet slightly complicated period-doubling cascades resulting in chaos. See Section 3.4 for additional discussions.

Types of Bifurcations: In all of the fixed point diagrams shown previously, the majority of the bifurcation phenomena can be divided into three kinds; these are flip, supercritical and transcritical bifurcations (Seydel 1988). Figure 3.5 shows examples of these three types of bifurcation for the logistic ODE using the modified Euler, improved Euler and R-K 4. Figure 3.5 also shows a comparison of the stable and unstable fixed points of periods 1 and 2. Although the modified Euler and the R-K 4 experience a transcritical bifurcation, they have different characteristics.

For the bifurcation of the first kind, the paths (spurious or otherwise) resemble period doubling bifurcations (flip bifurcation) similar to the logistic map. See Fig. 3.2a (for $r = 2$) and Fig. 3.2e (for $r = 2$) for examples. The second kind is the steady or supercritical bifurcation. It occurs, most often, at the main branch 1_E , with the spurious paths branching from the correct fixed point as it reaches the linearized stability limit, and quite often even bifurcating more than once, as r increases still further before the onset of period doubling bifurcations. See Fig. 3.2c (for $r = 2$) and Fig. 3.2f (for $r = 2$) for examples. Using the P-C 3 method to solve (3.7) more than one consecutive steady bifurcation occurs before period doubling bifurcations. Follow the 1_S labels on Fig. 3.2f. Although figures are not shown for ODE (3.23) with $b = 0.5$, the improved Euler experiences two consecutive steady bifurcations before period doubling bifurcation occurs (see original paper for details). Using the P-C 3 method to solve (3.23), four consecutive steady bifurcations occur before period doubling bifurcations. The modified Euler and R-K 4 methods, however, experience only one steady bifurcation before period doubling bifurcations occur.

The third kind of bifurcation again occurs most often at the main branch 1_E . The spurious paths near the linearized stability limit of 1_E experience a transcritical bifurcation. See Fig. 3.2b (for $r = 2$), Fig. 3.2d (for r near 2.75), Fig. 3.2f (for r near 3.4) and Fig. 3.3 (follow the 1_E branch) for examples. Notice that the occurrence of transcritical and supercritical bifurcations is not limited to the main branch 1_E . See Fig. 3.3 for examples. At the stability limit of the true fixed point, only the modified Euler and R-K 4 undergo transcritical bifurcation.

As can be seen, the occurrence of flip and supercritical bifurcations is more common. In fact, most of the bifurcation points shown in previous figures are of these types. The other commonly occurring bifurcation phenomenon is the subcritical bifurcation which was not observed in our two chosen $S(u)$ functions. With a slight change in the form of our cubic function $S(u)$, a subcritical bifurcation can be achieved (Seydel 1988). See elementary text books on bifurcations of discrete maps (Seydel 1988) for a discussion of these four types of bifurcation phenomena. The consequence of the latter three bifurcation behaviors is that bifurcation diagrams computed from a single initial condition u^0 will appear to have missing sections of spurious branches, or even seem to jump between branches. This is entirely due to the existence of spurious asymptotes of some period or more than one period, and its dependence on the initial data.

Slow Convergence Near Bifurcation Points: As discussed previously, the number of iterations for the computed asymptotes that are near or at the bifurcation point can be orders of magnitude higher than away from the bifurcation points. In fact, depending on the type of

bifurcation and initial data, one might experience slow convergence using a time step that is near the linearized stability of the scheme (bifurcation points of the above four types). See Yee & Sweby (1994, 1995a,b) for some examples. In the worst case scenario, if the bifurcation is of the transcritical or subcritical type and the time step is within that range, the numerical solution can get trapped in a spurious steady state or a spurious limit cycle, causing nonconvergence of the numerical solution. Due to the fact that if the spurious steady state or spurious limit cycle is very close to the true steady state with a time step that is near the bifurcation point, it is not easy to distinguish it from a pure slow convergence issue or a spurious issue.

3.4. Strong Dependence of Solutions on Initial Data (*Numerical Basins of Attraction*)

Computing Bifurcation Diagrams Using A Single Initial Datum: Figures 3.6a - 3.6c show the bifurcation diagram by the modified Euler method for the logistic ODE with three different starting initial conditions (I.C.). In contrast to the explicit Euler method as shown in Fig. 3.4, none of these diagrams look alike. One can see the influence and the strong dependence of the asymptotic solutions on the initial data. For certain initial data and Δt value combinations, spurious dynamics can be avoided. Yet for other combinations, one can never get to the correct steady state. In other words, it is possible that for the same Δt but two different initial data or vice versa, the scheme can converge to two different distinct numerical solutions of which one or neither of them is the true solution of the underlying DE. Thus in a situation where there is no prior information about the exact steady-state solution, and where a time-marching approach is used to obtain the steady-state numerical solution when initial data are not known, a stable spurious steady-state could be computed and mistaken for the correct steady-state solution. Figure 3.6d shows the corresponding “full” bifurcation diagram, their earlier stages resembling the fixed point diagram 3.2b which showed only fixed points up to period 8. See Yee et al. (1991) for an example that overplotting a number of initial data, but not the appropriate ones, would not be sufficient to cover all of the essential spurious branches. The strong dependence of solutions on initial data is evident from the various examples in which this type of behavior is present. It is remarked that if one uses the pseudo arclength continuation type method without solving for the roots of the spurious fixed point, one only knows one starting solution (i.e., the exact steady states of these two ODEs). The continuation method, in this case, only produces the branch of the bifurcation diagram originating from the 1_E branch of the curve.

Computed Full Bifurcation Diagram: In order to compute a “full” bifurcation diagram using this numerical approach, we must overplot all of the individual bifurcation diagrams of existing asymptotes of any period and chaotic attractors obtained by using the entire domain of u values as starting initial data. Thus, a better method in numerically approximating the full bifurcation diagram is dividing the domain of interest of the u axis into equal increments and using these u values as initial data. The “full” bifurcation diagram is obtained by simply overplotting all of these individual diagrams on one. Figs. 3.7 and 3.8 show the “full” bifurcation diagrams for the corresponding fixed point diagrams shown previously. Note that the full bifurcation computed this way might miss some of the windows of bifurcations that occur inside the intervals of the

adjacent r and/or the initial data values.

It is noted that for the cases when one knows the bifurcation pattern of a specific discrete map, the actual number of the initial data points used for that full bifurcation diagram computations do not have to completely cover the entire domain of u as long as these initial data cover all of the basins of attraction of the asymptotes (which initial data lead to which asymptotes). See next section for definition and discussion. That is, at least one initial data point is used from each of the basins of the asymptotes. No attempt has been made to compute the complete full bifurcation diagram, since this is very costly and involves a complete picture of the existing asymptotes of any period and chaotic attractors for the domain of interest in question. See remarks in Section 3.2 on computed bifurcation diagrams for explanation. Here, we use the term “full bifurcation diagram” to mean “computed bifurcation diagram with sufficient initial data to cover the essential lower order periods”. Without loss of generality, from here on we use the word bifurcation diagram to mean the computed (and approximated) full bifurcation diagram.

From Figs. 3.7 and 3.8, one can conclude that all of the studied explicit methods undergo “period doubling bifurcations” leading to the “logistic-map-type bifurcations”. The term “logistic-map-type bifurcations” here means that the behavior and shape of the bifurcations resemble the logistic map as shown in Fig. 3.4. The ranges of the r values in which logistic-map-type bifurcations occur are not restricted to the 1_E branch of the bifurcation diagram. The birth of the logistic-map-type bifurcations can occur below or beyond the linearized stability limit of the true steady state of the governing equation. To aid the readers, Figs. 3.7 and 3.8 indicate the major stable fixed points of periods up to 4. Basically (not restricted to), each of the 1_S branches of the bifurcations are logistic-map-type. For example, the modified Euler experiences two period doubling bifurcations for the ODE (3.7). For the ODE (3.23), the modified Euler experiences at least two to three period doubling bifurcations, depending on the b values. For other methods, the situation is slightly more complicated.

Besides the regular logistic-map-type bifurcations, some of these methods undergo the so called “inverted logistic-map-type” of period doubling bifurcations. The shape of this type of bifurcation resembles the reverse image of Fig. 3.4. See, for examples, Fig. 3.7b for $1.62 < r < 1.67$ and Fig. 3.7c for $3.15 < r < 3.3$.

The above example explains the **role of initial data** in the **generation** of spurious steady-state numerical solutions, stable and unstable spurious numerical chaos and other asymptotes. Section 3.5 illustrates the **role of initial data** in the permissibility of **stabilizing** unstable steady states of the governing equation and the introduction of stable and unstable spurious numerical chaos and other asymptotes by implicit LMMs. Next, how basins of attraction can complement the bifurcation diagrams in gaining more detailed global asymptotic behavior of time discretizations for nonlinear DEs will be illustrated.

“Exact” Basin of Attraction vs. “Numerical” Basin of Attraction: The basin of attraction of an asymptote (for the DEs or their discretized counterparts) is a set of all initial data

asymptotically approaching that asymptote. We use the terms “exact” basin of attraction and “numerical” basin of attraction to mean the basin of attraction of the DE and basin of attraction of the underlying discretized counterpart. Although all of the numerical basins of attraction shown later are obtained numerically, the term “numerical basin of attraction” here pertains to the true basins of attraction of all of the asymptotes for the underlying discrete map.

For the logistic ODE, the “exact” basin of attraction for the only stable fixed point $u^* = 1$ is the entire positive plane for all values of $\alpha > 0$. The basin of attraction for the ODE (3.23) for the stable fixed point $u^* = b$ is $0 < u < 1$ for all $\alpha > 0, 0 < b < 1$. However, the situation for the corresponding numerical basins of attraction for the various schemes is more complicated since each asymptote, stable or unstable, spurious or otherwise, possesses its own numerical basin of attraction. Intuitively, in the presence of stable and unstable spurious asymptotes, the basins of the true stable and unstable steady states (and asymptotes if they exist) can be separated by the numerical basins of attraction of the stable and unstable spurious asymptotes. Consequently, what is part of the true basin of a particular fixed point of the governing equation might become part of the basin of the spurious asymptotes. For implicit methods that can stabilize unstable steady states of the governing equation (to be discussed later), the basin of attraction associated with the particular stabilizing steady state can consist of the union of part of basins from other true asymptotes. In other words, the allowable initial data of the numerical method associated with a particular asymptote of the DE can experience enlargement or contraction, and can become null or consist of a union of disjoint regions. These regions can be fractal like. Therefore, keeping track of which initial data lead to which asymptotes (exact or spurious) of the underlying discrete maps becomes more complicated as the number of spurious asymptotes increases.

On the other hand, the computed bifurcation diagram cannot distinguish the types of bifurcation and the periodicity of the spurious fixed points of any order. With the numerical basins of attraction and their respective bifurcation diagrams superimposed on the same plot, the type of bifurcation and which initial data lead to which stable asymptotes become apparent. In order to obtain the corresponding numerical basins of attraction for the schemes discussed above, one immediately realizes that, in most cases, a numerical approach is the only recourse until more theoretical tools for searching for the basin boundaries of general discrete maps become available. We would like to add that there are isolated theories or approximate methods to locate some basin boundaries for simple discrete maps or special classes of discrete maps. Even in this case, these methods are neither practical nor are there fixed guidelines for the actual implementation of discrete maps for more complex ones of similar type. See Hsu (1987) for an approximate method and Friedman (1995) for numerical algorithms which compute connecting orbits.

Computing Numerical Basins of Attraction on the Connection Machine: The nature of this type of computation, especially for systems of nonlinear ODEs or PDEs, requires the performance of a very large number of simulations with different initial data; this can be achieved efficiently by the use of the highly parallel Connection Machine (CM-2 or CM-5) or the IBM SP2 machine whereby each processor could represent a single initial datum and

thereby all the computations can be done in parallel to produce detailed global stability behavior and the resulting basins of attraction. With the aid of highly parallel Connection Machines, we were able to detect a wealth of the detailed nonlinear behavior of these schemes for systems of ODEs and PDEs which would have been overlooked had isolated initial data been chosen on the Cray or other serial or vector machine.

Figure (3.9) shows the bifurcation diagram with numerical basins of attraction superimposed for the logistic ODE for four Runge-Kutta methods. (Even though one might not need to use a highly parallel machine to compute the basins of attraction for the scalar ODE, nevertheless this figure was computed on the CM-5 requiring only a few minutes for each plot). The major work on the CM-5 coding is on the efficient handling of data for plotting. The same plots would have required at least an order of magnitude more CPU time on a serial or vector machine. To obtain a bifurcation diagram with numerical basins of attraction superimposed using the CM-5, the preselected domain of initial data and the preselected range of the Δt parameter are divided into 512 equal increments. For the bifurcation part of the computations, the discretized equations are, in general, preiterated 3000 steps for each initial datum and Δt before the next 1000 iterations (more or less depending on the problem and scheme) are plotted. The preiterations are necessary in order for the trajectories to settle to their asymptotic value. The high number of iterations are plotted (overlaid on the same plot) to detect periodic solutions. The bifurcation curves appear on the figures as white curves, white dots and dense white dots. While computing the bifurcation diagrams it is possible to overlay basins of attraction for each value of Δt used. For the numerical basins of attraction part of the computations, with each value of Δt used, we keep track where each initial datum asymptotically approaches, and color code each basin (appearing as a multi-color vertical line) according to the individual asymptotes. Black regions denote basins of divergent solutions. While efforts were made to match color coding associated with a particular asymptote of adjacent multi-color vertical lines on the bifurcation diagram (i.e., from one Δt to the next), it was not always practical or possible. Care must therefore be taken when interpreting these overlays. In an idealized situation it is best if we also know the critical value of Δt for the onset of unstable spurious asymptotes. However, with the current method of detecting the bifurcation curve only the stable ones are detected. For example, a steady bifurcation would break the domain immediately after the bifurcation point into two different color domains immediately after the bifurcation point.

Examples: Any initial data residing in the green region in Fig. 3.9 for the modified Euler method belongs to the numerical basin of attraction of the spurious (stable) branch emanating from $u = 3$ and $r = 1$. Thus, if the initial data is inside the green region, the solution can never converge to the exact steady state using even a small fixed but finite Δt (all below the linearized stability limit of the scheme). Although not shown, we have computed the bifurcation diagram with wider ranges of r and initial data. In fact, the green region actually extends upward as r decreases below 1. Thus for a small range of r values very near zero, the entire domain is divided into two basins (same as the ODE). As r increases, the domain can divide into more than two basins (instead of two for the ODE). But of course higher period spurious fixed points exist for other ranges of r and more basins are created within the same u domain. For r near

2 (i.e., near the linearized stability limit of the true steady state $u^* = 1$, the bifurcation is transcritical. Using an r value slightly bigger than 2 will lead to the spurious steady state until r increases beyond 3.236. Consequently, there are large ranges of r below and beyond the linearized stability limit of the true steady state for which spurious dynamics occur. Observe the size and shape of these basins as r varies. The majority of these basin boundaries are fractal like.

A similar situation exists for the R-K 4 method (Fig. 3.9), except that now the numerical basins of attraction of the spurious fixed points occur very near the linearized stability limit of the scheme, with a small portion occurring below the linearized stability limit. Although both the modified Euler and the R-K 4 methods experience a transcritical bifurcation for the logistic ODE. The transcritical bifurcation for the R-K 4 is more interesting. See Fig. 3.5 for the distinction between the two transcritical bifurcations. In contrast to the improved Euler method, the green region represents the numerical basin of attraction of the upper spurious branch of the transcritical bifurcation. The bifurcation curve directly below it with the corresponding red portion is the basin of the other spurious branch. With this way of color coding the basins of attraction, one can readily see (from the plots) that for the logistic ODE (3.7), the improved Euler method experience one steady bifurcations before period doubling bifurcation occurs. The modified Euler and R-K 4 methods, however, experience a transcritical bifurcation before period doubling bifurcations occur. The Kutta method experiences period doubling bifurcation at the linearized stability limit. One way to detect the steady bifurcation from these plots is to look for a separate color associated with each branch of the associated bifurcation. A similar interpretation holds for certain type of transcritical bifurcation. See R-K 4 in Fig. 3.9. One way to detect the period doubling bifurcation from these plots is to look for no change in colors associated with each branch of the associated bifurcation. For subcritical bifurcation, it is slightly more complicated.

The above discussion shows the interplay between initial data, step size and permissibility of spurious asymptotes. It indicates that it is not just the occurrence of stable spurious numerical solutions that causes difficulty. Indeed such cases may be easier to detect. These spurious features of the discretizations often occur but are unstable; i.e., they do not appear as an actual (spurious) solution because one usually cannot obtain an unstable asymptotic solution by mere forward time integration. However, far from being benign, they can have severe detrimental effects on the allowable initial data of the true solution for the particular method, hence causing slow convergence or possibly even nonconvergence from a given set of initial data, even though the data might be physically relevant.

Due to space limitations, interested readers are referred to Yee & Sweby (1994, 1995a) for results for four 2×2 systems of nonlinear model ODEs. Classification of fixed points of systems of equations are more involved than the scalar case. See elementary dynamical systems text books for details. The corresponding bifurcation diagrams and numerical basins of attraction of these schemes are even more involved. New phenomena exist that are absent from the scalar case. For example, in the presence of multiple steady states, even for explicit methods, depending on the step size and initial data combination, the associated numerical

basins of attraction for a true steady state might experience an enlargement of their basins at the expense of a contraction of the other asymptotes. For the scalar case, this is only possible for superstable implicit methods (see next section). See Yee & Sweby (1994, 1995a,b) for more details. Another example is that the fixed point can change type as well as stability (e.g., from a saddle point to a stable or unstable node). It is remarked that for systems beyond 3×3 , it is impossible to conduct a detailed analysis as shown above.

3.5. Global Asymptotic Behavior of Superstable Implicit LMMs

This section reviews the superstable property of some implicit LMMs and summarizes their global asymptotic nonlinear behavior using the dynamical approach. Recall that the underlying discrete maps from using LMMs are linear in the discretized parameter Δt and they are exempt from spurious steady states. As can be seen later, the combination of implicit LMMs and the superstable property produce asymptotic behavior that is very different from schemes that were studied in the previous section. One distinct property of these types of schemes is that they can **stabilize unstable steady states** of the governing equation. Another property is that the numerical basins of attraction of the stable steady state can **include** regions of the basins of the unstable steady states of the governing equation.

3.5.1. Super-stability Property

Dahlquist et al. (1982) first defined super-stability in ODE solvers to mean the region of numerical stability that encloses regions of physical instability of the true solution of the ODE. Dieci & Estep (1991) subsequently gave a broader definition as one in which an ODE solver does not detect that the underlying solution is physically unstable. They observed that super-stability can occur also when the ODE solver is not super-stable in terms of Dahlquist et al. They concluded that the key factor which determines the occurrence of super-stability is the iterative solution process for the nonlinear algebraic equations. They indicated that the iterative solution process has its own dynamics, which might be in conflict (as for Newton's method) with the dynamics of the problem. They also indicated that super-stability can arise because of this fact. Their viewpoint is that the numerical scheme and the methods for solving the nonlinear algebraic equations should be considered as a unit. Neglecting this latter aspect and basing step size selection purely on accuracy considerations leads to faulty analysis. They believe that error control strategies for stiff initial value problems ought to be redesigned to take into account stability information of the continuous problem.

In Yee & Sweby (1994, 1995a,b) we exploited the global asymptotic behavior of some of the superstable implicit LMMs for *constant step sizes*. We concentrated on four of the typical unconditionally stable implicit LMMs. These are backward Euler, trapezoidal rule, midpoint implicit, and three-point backward differentiation (BDF), each with noniterative (linearized implicit), simple, Newton and modified Newton iterative procedures for solving the resulting nonlinear algebraic equations. A semi-implicit predictor method of Gresho (1996) also was

investigated.

We believe that some of the phenomena observed in our study were not observed by Dieci & Estep (1991) or by Iserles (1988). Based on our study, we now give a loose definition of an implicit time discretization as having a super-stability property if, within the linearized stability limit for a combination of initial data and time step (fixed) or starting time step (using standard variable time step control based on accuracy requirements), the scheme stabilizes unstable steady states of the governing equations in addition to having the property of Dieci and Estep. The definition includes the procedures in solving the nonlinear algebraic equations. This loose definition fits the behavior that was observed in Yee & Sweby (1994, 1995a,b), while at the same time it fits the framework of dynamics of numerics in time-marching approaches in CFD. This is not a re-definition of Dieci and Estep, but rather a clarification of their definition when asymptotic numerical solutions of the governing equations are desired. In this case, superstable schemes might have the property of a numerical basin of attraction of the true steady state that is larger than the underlying exact basin of attraction. As can be seen in Yee & Sweby (1994, 1995a,b), the trapezoidal method is more likely to exhibit this property than the other three LMMs. The stabilization of unstable steady states by LMMs was also observed by Salas et al. (1986), Embid et al. (1984), Burton & Sweby (1995) and Poliashenko (1995). Section 4.2.2 gives a summary of the work of Burton and Sweby.

3.5.2. Implicit LMMs

The four LMMs and a semi-implicit predictor method considered are

Implicit Euler Method

$$\mathbf{u}^{n+1} = \mathbf{u}^n + \Delta t \mathbf{S}^{n+1}, \quad (3.24)$$

Trapezoidal Method

$$\mathbf{u}^{n+1} = \mathbf{u}^n + \frac{1}{2} r (\mathbf{S}^n + \mathbf{S}^{n+1}), \quad (3.25)$$

Midpoint Implicit Method

$$\mathbf{u}^{n+1} = \mathbf{u}^n + r \mathbf{S} \left(\frac{(\mathbf{u}^{n+1} + \mathbf{u}^n)}{2} \right), \quad (3.26)$$

3-Level Backward Differentiation Formula (BDF)

$$\mathbf{u}^{n+1} = \mathbf{u}^n + \frac{2}{3} r \mathbf{S}^{n+1} + \frac{1}{3} (\mathbf{u}^n - \mathbf{u}^{n-1}), \quad (3.27)$$

Semi-Implicit Predictor Method of Gresho (Gresho 1996).

The semi-implicit predictor method is the same as (3.24) but with an added predictor step using the explicit Euler before the implicit step (3.24) to make the final scheme second-order accurate. The four methods of solving the resulting nonlinear algebraic equations are as follows.

Linearization (a noniterative procedure) is achieved by expanding S^{n+1} as $S^n + J(\mathbf{u}^n)(\mathbf{u}^{n+1} - \mathbf{u}^n)$, where $J(\mathbf{u}^n)$ is the Jacobian of S .

Simple Iteration is the process where, given a scheme of the form $\mathbf{u}^{n+1} = G(\mathbf{u}^n, \mathbf{u}^{n+1})$, we perform the iteration

$$\mathbf{u}_{(\nu+1)}^{n+1} = G(\mathbf{u}^n, \mathbf{u}_{(\nu)}^{n+1}), \quad (3.28)$$

where $\mathbf{u}_0^{n+1} = \mathbf{u}^n$ and “ (ν) ” indicates the iteration index. The iteration is continued either until some tolerance between iterates is achieved or a limiting number of iterations has been performed. In all of our computations the tolerance “tol” is set as $\|\mathbf{u}_{(\nu)}^{n+1} - \mathbf{u}_{(\nu-1)}^{n+1}\| \leq \text{tol}$ and the maximum number of iterations is 15. The major drawback with simple iteration is that for guaranteed convergence the iteration must be a contraction; i.e.

$$\|G(\mathbf{u}^n, \mathbf{v}) - G(\mathbf{u}^n, \mathbf{w})\| \leq \alpha \|\mathbf{v} - \mathbf{w}\|, \quad (3.29)$$

where $\alpha < 1$. Whether or not the iteration is a contraction at the fixed points will influence the stability of that fixed point, overriding the stability of the implicit scheme. Away from the fixed points the influence will be on the basins of attraction. In other words, “implicit method + simple iteration” behaves like explicit methods. As can be seen in Yee & Sweby (1994, 1995a,b), numerical results illustrate this limitation in terms of basins of attraction as well. One advantage of the “implicit method + simple iteration” over non-LMM explicit methods is that spurious steady states cannot occur. Due to this fact, results using simple iteration will not be presented here.

Newton Iteration for the implicit schemes is of the form

$$\mathbf{u}_{(\nu+1)}^{n+1} = \mathbf{u}_{(\nu)}^{n+1} - F'(\mathbf{u}^n, \mathbf{u}_{(\nu)}^{n+1})^{-1} F(\mathbf{u}^n, \mathbf{u}_{(\nu)}^{n+1}), \quad (3.30)$$

where $\mathbf{u}_0^{n+1} = \mathbf{u}^n$. The differentiation is with respect to the second argument and the scheme has been written in the form (for two-level schemes) $F(\mathbf{u}^n, \mathbf{u}^{n+1}) = 0$.

Modified Newton iteration is the same as (3.30) except it uses a frozen Jacobian $F'(\mathbf{u}^n, \mathbf{u}^n)$. The same tolerance and maximum number of iterations used for the simple iteration are also used for the Newton and modified Newton iterations. In all of the computations, the starting scheme for the 3-level BDF is the linearized implicit Euler.

We also considered two variable time step control methods. The first one is “implicit Euler + Newton iteration with local truncation error control”

$$\begin{aligned} \mathbf{u}_{(0)}^{n+1} &= \mathbf{u}^n \\ \mathbf{u}_{(\nu+1)}^{n+1} &= \mathbf{u}_{(\nu)}^{n+1} + \left[I - \Delta t^n J(\mathbf{u}_{(\nu)}^{n+1}) \right]^{-1} \left[\mathbf{u}_{(\nu)}^{n+1} - \mathbf{u}^n - \Delta t^n S(\mathbf{u}_{(\nu)}^{n+1}) \right] \quad \nu = 1, \dots \end{aligned} \quad (3.31a)$$

with

$$\Delta t^n = 0.9 \Delta t^{n-1} \left\{ \text{tol}_1 / \|u^n - u^{n-1} - \Delta t^{n-1} S(u^n)\| \right\}^{1/2}, \quad (3.31b)$$

where the $(n + 1)$ th step is rejected if $\|u^n - u^{n-1} - \Delta t^{n-1} S(u^n)\| > 2\text{tol}_1$. In this case, we set $\Delta t^n = \Delta t^{n-1}$. The value “ tol_1 ” is a prescribed tolerance and the norm is an infinity norm. The second one is the popular “ode23” method

$$\begin{aligned} k_1 &= S(u^n) \\ k_2 &= S(u^n + \Delta t^n k_1) \\ k_3 &= S(u^n + \Delta t^n (k_1 + k_2)/4) \\ u^{n+1} &= u^n + \Delta t^n (k_1 + k_2 + 4k_3)/6 \\ \Delta u^{n+1} &= \Delta t^n (k_1 + k_2 - 2k_3)/3 \end{aligned} \quad (3.32a)$$

with

$$\Delta t^n = 0.9 \Delta t^{n-1} \sqrt{\frac{\text{tol}_1}{\|\Delta u^n\|}}, \quad (3.32b)$$

where the $(n + 1)$ th step is rejected if $\|\Delta u^{n+1}\| > \text{tol}_1 \max\{1, \|u^{n+1}\|\}$. In that case, we set $\Delta t^{n+1} = \Delta t^n$. Again, “ tol_1 ” is a prescribed tolerance and the norms are infinity norms. We also use the “straight Newton” method to obtain the numerical solutions of $S(u) = 0$, which is the one-step Newton iteration of the implicit Euler method of (3.30).

We mapped out the bifurcation diagrams and numerical basins of attraction for these five schemes as a function of the time step for different nonlinear model equations with known analytical solutions (scalar and 2×2 systems of autonomous nonlinear ODEs). The computations were performed on the CM-5. In general, we preiterated the discretized equations 3000 - 5000 steps before the next 3000 iterations are plotted. Comparing the results with the explicit methods, it was found that aside from exhibiting spurious asymptotes, all of the four implicit LMMs can **change the type** and stability (unstable to stable) of the steady states of the differential equations (DEs). See the next section for some examples. They also exhibit a drastic distortion but less shrinkage of the basin of attraction of the true solution than standard non-LMM explicit methods. In some cases with smaller Δt , the implicit LMMs exhibit enlargement of the basins of attraction of the true solution. Overall, the numerical basins of attraction of the linearized implicit procedure mimics more closely the basins of attraction of the continuum than the studied iterative implicit procedures for the four implicit LMMs. In general the numerical basins of attraction bear no resemblance to the exact basins of attraction. The size can increase or decrease depending on the time step. Also, the possible existence of the largest numerical basin of attraction that is larger than the exact one does not necessarily occur when the time step is the smallest. Although unconditionally stable implicit methods allow a theoretically large time step Δt , the numerical basins of attraction for large Δt sometimes are so fragmented and/or so small that the safe (or practical) choice of Δt is only slightly larger or

comparable to the stability limit of standard explicit methods (but with larger numerical basins of attraction than the explicit method counterparts). In general, if one uses a Δt that is a fraction of the stability limit, one has a higher chance of convergence to the correct asymptote than when one uses standard explicit methods. Comparing the results of Yee & Sweby (1994, 1995b) with Yee & Sweby (1995a), the implication is that unconditionally stable implicit methods are, in general, safer to use and have larger numerical basins of attraction than explicit methods. However, one cannot use too large a time step since the numerical basins of attraction can be so small and/or fragmented that the initial data has to be very close to the exact solution for convergence. This knowledge improved the understanding of the basic ingredients needed for a time-marching method using constant step sizes to have a rapid and guaranteed convergence to the correct steady states.

Numerical experiments performed on the two variable time step control methods also indicated that, although variable time step controls are not foolproof, they might alleviate the spurious dynamics most of the time. One shortcoming is that in order to avoid spurious dynamics, the required size of Δt is impractical to use in CFD, especially for the explicit ode23 method. The next section shows some representative global asymptotic behavior of these implicit LMMs.

3.5.3. Numerical Examples

Selected results in the form of bifurcation diagrams and basins of attraction are shown in Figs. 3.10-3.16 for the logistic ODE model (3.7) and Figs. 3.17-3.19 for the second model (3.23). In Figs. 3.10, 3.12, 3.14, 3.16-3.19, the left diagrams show the bifurcation diagrams and the right diagrams show the bifurcation diagrams with basins of attraction superimposed on the same plot. However, Figs. 3.11, 3.13 and 3.15 show only the bifurcation diagrams with basins of attraction superimposed on the same plot. In all of Figs. 3.10-3.19, the abscissa is $r = a\Delta t$.

Note that the preselected regions of Δt and the initial data were determined by examining a wide range of Δt and initial data. In most cases, we examined Δt from close to zero up to one million. What is shown in these figures represents some of the Δt and initial data ranges that are most interesting. Due to this fact, the Δt and initial data ranges shown are different from one method to another for the same model problem. The streaks on some of the plots are either due to the non-settling of the solutions within the prescribed number of iterations or the existence of small isolated regions of spurious asymptotes. Due to the high cost of computation, no further attempts were made to refine their detailed behavior since our purpose was to show how, in general, the different numerical methods behave in the context of nonlinear dynamics.

Due to the method of tracking the basins of attraction the color coding of the basin of attraction associated with a particular asymptote might vary from one vertical line to the next vertical line (i.e, from one Δt to the next). This is the case for Figs. 3.10, 3.11, 3.14, 3.18 and 3.19. For example in Fig. 3.10 the basin of attraction (as a function of Δt) for the steady state $u = 1$ is the red region before the appearance of the light blue strip. After the appearance of the blue strip, it is the region above the envelope that separates the green and red regions. When in

doubt, use the bifurcation diagram as a guide and identify the r value where the sudden birth of stable spurious asymptotes occurred. Incidentally, for this particular discrete map, this envelope and the critical value r which undergoes stabilization of the fixed point $u = 0$ can be obtained analytically. Independently, Arriola (1993) derived the analytical form of the envelope.

The midpoint implicit method behaves similarly to the trapezoidal method. In fact their linearized forms are identical. From here on, the midpoint implicit method is not discussed.

As mentioned before, for unconditionally stable LMMs, the scheme should not experience any steady bifurcation from the stable branch because unconditionally stable LMMs preserve the stability of the stable steady states. This rule does not apply to **unstable** steady states using super-stable LMMs. Before stabilization of the unstable steady state, super-stable LMMs typically undergo “inverted period doubling bifurcations” or the “inverted logistic-map-type bifurcations” (or crisis in terms of Grebogi et al. 1983). See Fig. 3.10 for $0.2 < u^n < -1$ for an example. For the ODE (3.23), all of the implicit methods experience at least two inverted logistic-map-type bifurcations. See Figs. 3.17-3.19. From these figures, we can observe that all of the studied implicit methods can introduce stable spurious chaos since a logistic-map-type of spurious bifurcations occur.

Figures 3.10, 3.11, 3.14, 3.16-3.19 show other situations where the rest of three implicit LMMs and the Gresho method stabilize the unstable steady states of the ODEs. It appears that the onset of stabilization of the unstable steady states arises in two ways. One way is the birth of stable spurious asymptotes or stable spurious chaos in the form of an inverted logistic map. The second way is the birth of unstable spurious asymptotes (fixed points other than period one) leading to the onset of stabilization of unstable steady states. Although the two ways of stabilization of the unstable steady states are similar, their corresponding basins of attraction are very different. See Figs. 3.10, 3.14, 3.16-3.19.

The critical value of Δt_c for the onset of stabilization is not very large. It is problem dependent, method dependent and also procedure dependent (the various ways of solving the nonlinear algebraic equations). In most cases, the value of the Δt_c is comparable to or smaller than the equivalent of the stability limit of standard explicit Runge-Kutta methods. It is not uncommon for the underlying basins of attraction to be larger than the exact basin of attraction for $\Delta t < \Delta t_c$.

Among the three procedures, the linearized noniterative forms have a higher tendency to stabilize unstable steady states. See Figs. 3.10, 3.14, 3.16-3.19. Here the word “procedure” excludes the simple iteration method. Among the three LMMs, the trapezoidal method is the least likely to stabilize unstable steady states, but the corresponding basins of attraction can be very small and more fragmented than for the other two LMMs. Also, the Δt_c for stabilization is bigger than for the other two LMMs. For a particular LMM not all three procedures for solving the nonlinear algebraic equation necessarily stabilize the unstable steady states (see Figs. 3.14 and 3.15). But, if they do, the pattern or the method for the onset of the stabilization does not have to be the same (see Figs. 3.10 and 3.11) but the value of Δt_c is the same for all models

and methods studied.

For the case of the semi-implicit predictor method, the onset of the stabilization can be accompanied by the birth of other spurious asymptotes (other than steady state). See Fig. 3.16 for $r \geq 2$. It is fascinating to see how complicated the basins of attraction are which compose the many disjoint and fractal like regions. Similar behavior is also observed for the “implicit Euler + modified Newton” but is less pronounced than the semi-implicit predictor method. See Figs. 3.11 and 3.16.

Compared with the three implicit LMMs, and independent of the method of solving the nonlinear algebraic equation, the Gresho method exhibits the smallest basin of attraction (compared with the exact basin of attraction of the stable steady state) and is more fragmented for $\Delta t < \Delta t_c$. Aside from the efficiency issue, the implication is that a higher order accuracy scheme might not be as desirable for the time-marching approach.

Since straight Newton is just a one step “implicit Euler + Newton”, its basins of attraction (for Δt larger than explicit Runge-Kutta) are almost the same even with more than one step iterations. Studies indicated that contrary to popular belief the initial data using the straight Newton method may not have to be close to the exact solution for convergence. Straight Newton exhibits stable and unstable spurious asymptotes. Initial data can be reasonably removed from the asymptotic values and still be in the basin of attraction. However, the basins can be fragmented even though the corresponding exact basins of attraction are single closed domains. See Fig. 6.25 of Yee & Sweby (1995a). The cause of nonconvergence may just as readily be due to the fact that the numerical basins of attraction are fragmented. If one uses a time step slightly bigger than the stability limit of standard explicit methods for the three LMMs, straight Newton can have similar or better performance. In fact, using a large Δt with the linearized implicit Euler method or the implicit Euler + Newton procedure has the same chance of obtaining the correct steady state as the straight Newton method if the initial data are not known or arbitrary initial data are taken.

A consequence of all of the observed behavior is that part or all of the flow pattern can change topology as the discretized parameter is varied. An implication is that the numerics might predict, for example, a nonphysical reattachment flow. Thus even though LMMs preserve the same number (but not the same types or stability) of fixed points as the underlying DEs, the numerical basins of attraction of LMMs do not coincide with the exact basins of attraction of the DEs even for small Δt . Some of the dynamics of the LMMs observed in our study can be used to explain the root of why one cannot achieve the theoretical linearized stability limit of the typical implicit LMMs in practice when solving strongly nonlinear DEs (e.g., in CFD).

3.6. Does Error Control Suppress Spuriousity?

The previous sections discussed mainly the spurious behavior of long time integrations of initial value problems of nonlinear ODE solvers for constant step sizes. The use of adaptive

step size based on local error control for implicit methods was studied by Dieci & Estep (1991). Dieci and Estep concluded that for superstable LMMs with local step size error control and depending on the method of solving the resulting nonlinear algebraic equations, spurious behavior can occur. Our preliminary study on the two variable step size control methods discussed in the previous section indicated that one shortcoming is that the size of Δt needed to avoid spurious dynamics is impractical (too small) to use, especially for the ode23 method. Theoretical studies on the adaptive explicit Runge-Kutta method for long time integration have been gaining more attention recently. Recent work by Stuart (1994, 1995), Humphries (1992), Higham and Stuart (1995) and Aves et al. (1995) showed that local error control offers benefits for long-term computations with certain problems and methods. Aves et al. addressed the heart of the question of whether local error control confers global properties of steady states of the IVP of autonomous ODEs using adaptive Runge-Kutta type methods.

Aves et al.'s work is concerned with long term behavior and global quantities of general explicit Runge-Kutta methods with step size control for autonomous ODEs. They believed that the limit $t_n \rightarrow \infty$ is more relevant than the limit of the variable step sizes $h_n \rightarrow 0$. They studied spurious fixed points that persist for arbitrarily small error tolerances τ . This type of adaptive Runge-Kutta method usually consists of a primary and secondary Runge-Kutta methods of different order. Their main result is positive. When standard local error control is used, the chance of encountering spuriousity is extremely small. For general systems of ODEs, the constraints imposed by the error control criterion make spuriousity extremely unlikely. For scalar problems, however, the mechanism by which the algorithm succeeds is indirect -- spurious fixed points are not removed, but those that exist are forced by the step size selection mechanism to be locally repelling (with the relevant eigenvalues behaving like $O(1/\tau)$).

To be more precise, adaptive time stepping with Runge-Kutta methods involves a pair of Runge-Kutta formulae and a tolerance parameter " τ ", which is usually small. See for example the "ode23" method (3.32). Hence a spurious fixed point of the adaptive procedure requires:

- 1) A spurious fixed point **common** to both methods must exist. This is usually easy to achieve since the bifurcation diagrams of individual Runge-Kutta methods have so many branches.
- 2) This spurious fixed point must be **stable**. This is much more difficult to achieve - essentially since the bifurcation curves for the two methods must intersect **tangentially**; otherwise there will be an eigenvalue of the Jacobian of $O(1/\tau)$.

They then show that the probability of 2) occurring is zero. However, for a given pair one can generally construct functions for which it holds (generally stability will only hold for $\tau >$ lower bound). In any event, the basin of attraction of this spurious fixed point will only be $O(\tau)$. These results were derived for scalar problems.

In the worst scenario problem classes exist where, for arbitrary τ , stable spurious fixed points persist with significant basins of attraction. They derived a technique for constructing ODEs for which an adaptive explicit Runge-Kutta method will behave badly. They showed that this can be accomplished using a locally piecewise constant function $S(\mathbf{u})$. Since the disjoint pieces can

be connected in any manner, S can be made arbitrarily smooth. Hence, smoothness of S alone is not sufficient to guarantee that spurious behavior will be eliminated. These examples highlight the worst-case behavior of adaptive explicit Runge-Kutta methods. They also mentioned that they can construct similar examples involving systems. However, these types of examples are somewhat contrived.

Griffiths is currently working on the application to hyperbolic PDEs. Preliminary results (private communication with David Griffiths (1996)) showed that it is by no means clear at the moment whether stable spurious solutions may be eliminated. The difference is that, unlike physical problems governed by nonlinear ODEs, nonlinear PDEs may have wave-like solutions rather than fixed points due to the spatial derivatives.

3.7. Dynamics of Numerics of a Reaction-Convection Model

This section further studies the dynamics of selected finite difference methods in the framework of a scalar model reaction-convection PDE (LeVeque & Yee 1990) and investigates the possible connection of incorrect propagation speeds of discontinuities with the existence of some stable spurious steady-state numerical solutions. The effect of spatial as well as time discretizations on the existence and stability of spurious steady-state solutions will be discussed. This is a summary of the work of Lafon & Yee (1991, 1992).

A nonlinear reaction-convection model equation in which the exact solution of the governing equations are known (LeVeque & Yee 1990) is considered. The model considered in LeVeque and Yee is

$$u_t + au_x = \alpha S(u) \quad 0 \leq x \leq 1 \quad (3.33a)$$

$$u(x, 0) = u^0(x) \quad (3.33b)$$

where a and α are parameters, and $S(u) = -u(1-u)(2-u)$. The boundary condition given by

$$u(0, t) = u_0 \quad t \geq 0 \quad (3.33c)$$

or, periodic boundary condition given by

$$u(0, t) = u(1, t) \quad t \geq 0 \quad (3.33d)$$

is used to complete the system.

The exact steady-state solutions u^* of the continuum PDE (3.33) can be obtained by integration by parts of $adu^*/dx = \alpha S(u^*)$ which yields

$$\frac{\alpha x}{a} + c = \int \frac{du^*}{S(u^*)} = \log \left[\frac{|u^*(x) - 1|}{\sqrt{|u^*(x)(2 - u^*(x))|}} \right], \quad (3.34)$$

where c is the integration constant.

In the case where the boundary condition $u(0, t) = u_0$, there is a unique steady state and its value is determined by u_0 . If u_0 is a root of S , (i.e., $u_0 = 0, 1$, or 2), then the exact steady state is constant in x and is equal to u_0 . But if u_0 is not a root of S , then the exact steady state satisfies

$$x = \frac{a}{\alpha} \log \left[\frac{u^*(x) - 1}{(u_0 - 1)} \sqrt{\frac{u_0(u_0 - 2)}{u^*(x)(u^*(x) - 2)}} \right]. \quad (3.35)$$

Although, the domain is confined to $0 \leq x \leq 1$, the steady-state solution is defined for $0 \leq x < \infty$. The limit of $u^*(x)$ is 0 as $x \rightarrow \infty$ for $-\infty < u_0 < 0$ or $0 < u_0 < 1$. The limit of $u^*(x)$ is 2 if $1 < u_0 < 2$, or $2 < u_0 < \infty$. One can show that this exact steady-state solution is stable.

In the case of the periodic boundary condition where $u(0, t) = u(1, t)$ and $u^*(0)$ is not a root of S , it can be shown that there exist three exact steady-state solutions; namely $u^*(x) \equiv 0, 1$, or 2 . One can also show that $u^* = 0$ and $u^* = 2$ are stable while $u^* = 1$ is unstable.

Denote the basin of attraction for the steady state u^* by $BA(u^*)$. Then it is obvious that $BA(0)$, the basin of attraction for the steady-state solution $u^* = 0$, is the set of initial data $u^0(x) < 1$ for all real values of x . In mathematical notation

$$BA(0) = \{u^0 : u^0(x) < 1 \ \forall x\}. \quad (3.36)$$

Similarly, the basin of attraction for the steady state $u^* = 2$ is

$$BA(2) = \{u^0 : u^0(x) > 1 \ \forall x\}. \quad (3.37)$$

Later we contrast these exact basins of attraction with the numerical basins of attraction $\widehat{BA}(0)$ and $\widehat{BA}(2)$ for the various schemes under discussion.

For the numerical methods, semi-discrete (method of lines) finite difference methods (FDMs) and implicit treatment of the source terms (semi-implicit) with noniterative linearization using a characteristic form are considered.

Spatial Discretizations: Let $u_j(t)$ represent an approximation to $u(x_j, t)$ where $x_j = j\Delta x$ and $j = 0, \dots, J$ with $\Delta x = 1/J$ the uniform grid spacing ($J + 1$ grid points). Let the parameter

$$p_1 = \frac{a}{\alpha\Delta x}. \quad (3.38)$$

Define the flow residence time in a cell $\tau_c = \Delta x/a$ (characteristic time due to convection) and the time required by the reaction to reach equilibrium $\tau_r = 1/\alpha$. Then a simple physical interpretation of the parameter p_1 comes from the fact that p_1 is equal to the ratio τ_r/τ_c . Note also that this ratio is the inverse of a Damkohler number. Therefore, the parameter p_1 is a measure of the stiffness of the problem. The smaller p_1 is, the stiffer the problem becomes.

A semi-discrete approximation (for a chosen spatial discretization for the convection and source term) of the reaction-convection PDE (3.33a) is then

$$\frac{1}{\alpha} \frac{dU}{dt} = F, \quad (3.39)$$

where U is the vector whose components are $u_j(t)$, $1 \leq j \leq J$. The function F is a discrete J -dimensional vector which depends on the grid function U , the parameter p_1 , and the particular spatial finite difference approximation. For simplicity the commonly used spatial discretizations (the first-order upwind (UP1), second-order upwind (UP2) and second-order central (C2) schemes) are considered for the convection term, and the pointwise evaluation (PW), upwind interpolation (UI), and mean average between two neighboring grid points (MA) are considered for the (spatial) numerical treatments of the source term. The combination of the three numerical treatments of the source term and the three basic schemes used for the discretization of the convection term yields 9 spatial finite difference approximations for the reaction-convection PDE (3.33a).

The expressions of the elements f_j of F corresponding to the 9 spatial difference approximations for (3.33a) and (3.33c) are given below, where we use the obvious notations $u_{-1} = u_{J-1}$, $u_0 = u_J$ and $u_1 = u_{J+1}$ for the periodic boundary condition (3.33c).

1. First-order upwind for convection - pointwise evaluation for source term (UP1PW)

$$f_j(U) = -p_1(u_j - u_{j-1}) + S(u_j). \quad (3.40a)$$

2. Second-order upwind for convection - pointwise evaluation for source term (UP2PW)

$$f_j(U) = -p_1\left(\frac{3}{4}u_j - u_{j-1} + \frac{1}{4}u_{j-2}\right) + S(u_j). \quad (3.40b)$$

3. Second-order central for convection - pointwise evaluation for source term (C2PW)

$$f_j(U) = -\frac{1}{2}p_1(u_{j+1} - u_{j-1}) + S(u_j). \quad (3.40c)$$

4. First-order upwind for convection - upwind evaluation for source term (UP1UI)

$$f_j(U) = -p_1(u_j - u_{j-1}) + \theta S(u_{j-1}) + (1 - \theta)S(u_j). \quad (3.41a)$$

5. Second-order upwind for convection - upwind evaluation for source term (UP2UI)

$$f_j(U) = -p_1\left(\frac{3}{4}u_j - u_{j-1} + \frac{1}{4}u_{j-2}\right) + \theta S(u_{j-1}) + (1 - \theta)S(u_j). \quad (3.41b)$$

6. Second-order central for convection - upwind evaluation for source term (C2UI)

$$f_j(U) = -\frac{1}{2}p_1(u_{j+1} - u_{j-1}) + \theta S(u_{j-1}) + (1 - \theta)S(u_j). \quad (3.41c)$$

7. First-order upwind for convection - mean average evaluation for source term (UP1MA)

$$f_j(U) = -p_1(u_j - u_{j-1}) + \frac{1}{2} \left[S(u_{j+1}) + S(u_{j-1}) \right]. \quad (3.42a)$$

8. Second-order upwind for convection - mean average evaluation for source term (UP2MA)

$$f_j(U) = -p_1\left(\frac{3}{4}u_j - u_{j-1} + \frac{1}{4}u_{j-2}\right) + \frac{1}{2} \left[S(u_{j-1}) + S(u_{j+1}) \right]. \quad (3.42b)$$

9. Second-order central for convection - mean average evaluation for source term (C2MA)

$$f_j(U) = -\frac{1}{2}p_1(u_{j+1} - u_{j-1}) + \frac{1}{2} \left[S(u_{j-1}) + S(u_{j+1}) \right]. \quad (3.42c)$$

The parameter θ associated with the upwind interpolation of the source term in formula (3.41) is an extra parameter in the discretization, lying between 0 and 1. For ease of referencing, the above 9 spatial discretizations will be denoted by the symbols UP1PW, UP1UI, UP1MA, UP2PW, UP2UI, UP2MA, C2PW, C2UI and C2MA.

Time Discretizations: To contrast the nonlinear behavior between LMMs and explicit Runge-Kutta methods, for simplicity, the explicit Euler and the modified Euler schemes are considered.

Let u_j^n represent an approximation of $u(j\Delta x, n\Delta t)$ with a fixed time step Δt . Also let U^n denote a vector with elements u_j^n . Then the fully discrete approximation of the PDE (3.33a) with explicit Euler time discretization is

$$U^{n+1} = U^n + p_2 F(U^n), \quad (3.43)$$

where the parameter p_2 is simply related to the time step through

$$p_2 = \alpha \Delta t. \quad (3.44)$$

With modified Euler time discretization, the fully discrete approximation is

$$U^{n+1} = U^n + p_2 F(\bar{U}) \quad ; \quad \bar{U} = U^n + \frac{p_2}{2} F(U^n). \quad (3.45)$$

In the following the above 18 fully discrete approximations will be denoted for ease of reference by the symbols UP1PW/EE, UP1PW/ME, etc. (where EE stands for explicit Euler and ME for modified Euler). In all of the computations $\theta = c = \alpha \frac{\Delta t}{\Delta x}$ in (3.41) is used.

FDMs Based on the Characteristic Form: A more physical approach to updating the grid value u_j at time level $n + 1$ is to trace back the characteristic passing through $(x_j, (n + 1)\Delta t)$. Denote by $(\hat{x}, n\Delta t)$ the coordinates of the point on the characteristic at time $n\Delta t$. Along this characteristic, the problem reduces to solving the ODE

$$v_\tau = \alpha S(v) \quad n\Delta t < \tau \leq (n+1)\Delta t \quad (3.46a)$$

with the initial condition

$$v(n\Delta t) = u^n(\hat{x}), \quad (3.46b)$$

where $u^n(\hat{x})$ denotes the value of u at point \hat{x} and time level $n\Delta t$, obtained by some interpolation method on the adjacent grid function u_j^n . For this approach, explicit and implicit time discretizations of (3.46a) or, equivalently, explicit and implicit treatments of the source term of the PDE (3.33a) are considered. To facilitate the analysis, the convection part of the PDE (3.33a) is handled in an explicit way. This means that for the homogeneous part of the PDE (3.33a) all the underlying schemes are under the CFL restriction

$$c = \frac{a\Delta t}{\Delta x} = p_1 p_2 < 1. \quad (3.47)$$

An immediate consequence is that \hat{x} lies between $x_{j-1} = (j-1)\Delta x$ and $x_j = j\Delta x$. Then, from a linear interpolation we get

$$\hat{u}^n = u^n(\hat{x}) = cu_{j-1}^n + (1-c)u_j^n. \quad (3.48)$$

For fully explicit schemes, the same two explicit time discretizations for the method of lines approach are considered here. With explicit Euler, the fully discrete approximation (denoted by CHA/EE) takes the form

$$u_j^{n+1} = cu_{j-1}^n + (1-c)u_j^n + p_2 S(\hat{u}^n). \quad (3.49)$$

With the modified Euler time discretization the fully discrete approximation (denoted by CHA/ME) takes the form

$$u_j^{n+1} = cu_{j-1}^n + (1-c)u_j^n + p_2 S(\bar{u}), \quad (3.50)$$

where

$$\bar{u} = cu_{j-1}^n + (1-c)u_j^n + \frac{p_2}{2} S(\hat{u}^n). \quad (3.51)$$

For a less restricted time step, the implicit Euler (IE) and the trapezoidal implicit scheme (T) are considered for the source term. With implicit Euler, the fully discrete approximation, denoted by CHA/IE, takes the form

$$u_j^{n+1} - p_2 S(u_j^{n+1}) = \hat{u}^n, \quad (3.52)$$

while with the trapezoidal rule, the fully discrete approximation, denoted by CHA/T, takes the form

$$u_j^{n+1} - \frac{p_2}{2} S(u_j^{n+1}) = cu_{j-1}^n + (1-c)u_j^n + \frac{p_2}{2} S(\hat{u}^n). \quad (3.53)$$

The corresponding linearized implicit scheme CHA/LIE associated with the fully discrete approximation CHA/IE is given by

$$u_j^{n+1} = u_j^n + \frac{cu_{j-1}^n - cu_j^n + p_2 S(u_j^n)}{1 - p_2 S'(u_j^n)}, \quad (3.54)$$

with $S' = dS/du = -2 + 6u - 3u^2$. The linearized trapezoidal method CHA/LT is

$$u_j^{n+1} = u_j^n + \frac{cu_{j-1}^n - cu_j^n + \frac{p_2}{2} [S(u_j^n) + S(\hat{u}^n)]}{1 - \frac{p_2}{2} S'(u_j^n)}. \quad (3.55)$$

3.7.1. Spurious Asymptotes of Full Discretizations

Besides the three exact steady-state solutions, depending on the numerical methods, either the spatial discretizations and/or the time differencing can independently introduce spurious asymptotic numerical solutions (see Lafon & Yee (1991) for a detailed analysis). Bifurcation diagrams and stability analysis for the exact and spurious asymptotes of the above schemes and source term treatments were discussed in Lafon & Yee (1991, 1992). Interested readers are referred to these references for more details.

Since the explicit Euler and the implicit methods are LMMs, no spurious steady state due to time discretizations are possible. But, consider for example the various FDMs involving modified Euler time differencing (method of lines or characteristic form) and look for the simple case of spatially invariant steady states (i.e., the value of u_j is the same for all j , $1 \leq j \leq J$). Then it is found that for such FDMs, the value u^* of a spatially invariant steady-state must satisfy

$$u^* + \frac{p_2}{2} S(u^*) = \bar{u}, \quad S(\bar{u}) = 0. \quad (3.56)$$

It can be shown that (3.56) admits the following 9 solutions

$$0, \quad \frac{1}{2} \left[3 \pm \sqrt{1 + \frac{8}{p_2}} \right], \quad 1, \quad 1 \pm \sqrt{1 + \frac{2}{p_2}}, \quad 2, \quad \frac{1}{2} \left[1 \pm \sqrt{1 + \frac{8}{p_2}} \right] \quad (3.57)$$

in which $u^* = 0, 1$ or 2 are the exact steady-state solutions while the rest are spurious steady-state numerical solutions introduced by the modified Euler time discretization.

3.7.2. Linearized Behavior vs. Nonlinear Behavior

To illustrate the differences between the linearized analysis and the nonlinear solution behavior, Fig. 3.20 shows the spectral radius around the exact steady-state solution $u^* = 2$ and the bifurcation diagram obtained with initial data $U^0 = (2., 2.1, 2., 2.1, 2., 2.1, 2.)$ for the scheme UP1UI/EE and $p_1 = 7$. Similar results for the scheme UP1UI/ME are shown in Fig. 3.21. For $p_1 = 7$, the scheme UP1UI/ME exhibited **two disjoint linearized stability intervals**. From Fig. 3.21 we observe that outside these stability intervals the scheme does not necessarily diverge (as indicated by the linearized analysis) but can converge to a spurious asymptotic solution.

Another example which shows the importance of nonlinear analysis is that of two schemes that exhibit the same linearized behavior yet have different nonlinear behavior (true behavior). For example, the linearized stability analyses for schemes UP1UI/EE and CHA/EE (see Figs. 5a and 7a of Lafon & Yee (1992)) are identical even though the bifurcation diagrams obtained with the same initial data and $p_1 = 7$ are different (see Figs 19a and 20a of Lafon & Yee (1992)).

3.7.3. Spurious Steady States and Nonphysical Wave Speeds

The possible connection of the numerical phenomenon of incorrect propagation speeds of discontinuities with the existence of some stable spurious steady states introduced by the spatial discretization is discussed here. The boundary condition (3.33c) and the following piecewise constant initial data

$$u^0(x) = \begin{cases} 2 & 0 < x < x_d, \\ 0 & x_d < x < 1 \end{cases} \quad (3.58)$$

are considered. The constant value x_d denotes the location of the discontinuity. The exact solution of (3.33a,b,c) with initial data (3.58) is simply

$$u(x, t) = u^0(x - at) \quad (3.59)$$

which is a wave traveling at constant speed a .

For an explanation of how numerical methods applied to this model PDE are likely to produce wrong speeds of propagation for the initial data (3.58), the reader is referred to LeVeque & Yee (1990). This phenomenon lies with the smearing of the discontinuity caused by the spatial discretization of the advection term. This introduces a nonequilibrium state into the calculation. Thus, as soon as a nonequilibrium value is introduced in this manner, the source term turns on and immediately tries to restore equilibrium, while at the same time shifting the discontinuity to a cell boundary.

For simplicity, consider the first-order upwind spatial discretization with the explicit Euler

time discretization for (3.33a,c) and (3.58). Assume an equal spatial increment of J intervals so that the discretized initial data associated with (3.59) is

$$u_j^0 = \begin{cases} 2 & 1 \leq j \leq K \\ 0 & K < j \leq J + 1 \end{cases} \quad (3.60)$$

with the index K depending on the constant α_d . In addition, assume that the convection speed $\alpha = 1$ so that $\Delta t = c/J$. In the computation $J = 20$ and the Courant number $c = .05$. With these assumptions, only the stiffness α of the source term is a free parameter. Define the average wave speed W for the numerical solution as follows

$$W = \frac{\Delta x}{2n\Delta t} \left[\sum_{j=1}^{J+1} u_j^n - \sum_{j=1}^{J+1} u_j^0 \right], \quad (3.61)$$

where the average is taken on the time interval 0 to $n\Delta t$. Figure 3.22 shows this average speed versus p_1 (proportional to $1/\alpha$). It reveals the fact that when p_1 becomes large (or, similarly when the source term is not stiff) the numerical wave speed tends to the exact solution ($\alpha = 1$), while for $p_1 < .25$ the numerical solution is a standing wave (the average speed being 0).

This zero wave speed is indeed a stable steady-state solution of the discretized equation but not a solution of the continuum PDE. Since the explicit Euler time differencing has the property of not producing spurious steady-state numerical solutions, this spurious stable steady-state numerical solution must have been introduced by the spatial discretization. In fact, it is evident from the bifurcation diagram shown in Fig. 2 of Lafon & Yee (1991) that this spurious steady state lies on the stable branch originating at $p_1 = 0$ from the state $u_1 = 2, \dots, u_k = 2, u_{k+1} = 0, \dots, u_J = 0$.

3.7.4. Numerical Basins of Attraction

In order to show the global nonlinear solution behavior of the schemes, numerical basins of attraction (of the underlying schemes) are compared with each other as well as with the exact basin of attraction for $u^* = 2$ ($BA(2)$). Due to the complexity and CPU intensive nature of the computation, unlike the detailed basins of attraction presented in Yee & Sweby (1994, 1995a,b), only a fraction of the basins of attraction are computed.

To compute a partial view of some numerical basins of attraction for $u^* = 2$ ($\widehat{BA}(2)$), a set of initial data in a two-dimensional plane was selected. Even with this restriction, the analysis is still very complex and the computation is CPU intensive; it was performed only for the case $J = 4$ (5 grid points). The equation of the chosen plane is

$$u_1 = 2; u_4 = 2. \quad (3.62)$$

A set of 121 initial data in the plane (3.62) were obtained by confining u_2 and u_3 in the square $1.1 \leq u_2 \leq 3.1, 1.1 \leq u_3 \leq 3.1$ with a uniform increment of $\Delta u_2 = \Delta u_3 = 0.2$. For each

initial datum, 5000 preiterations were performed. The asymptotic behavior is plotted in the (u_2, u_3) plane. In all of the figures, open triangles belong to the numerical basin of attraction $\overline{BA}(2)$. Dark squares belong to the numerical basin of attraction of a spurious steady state. Dark circles are the numerical basins of attraction of other (exact or spurious) asymptotic solutions, while a blank space denotes a divergent solution. Note that the whole square domain $1.1 \leq u_2 \leq 3.1$, $1.1 \leq u_3 \leq 3.1$ is inside the true basin of attraction of the exact steady state $u^* = 2$ and therefore the true behavior should be an open triangle for all the initial data considered. The study in Lafon & Yee (1991) indicated that the modified Euler time differencing has a smaller attractive region than the explicit Euler for the domain considered even though in terms of linearized stability and accuracy, the modified Euler exhibits an advantage over the explicit Euler.

For example, for $p_1 = 0.1$ and $p_2 = 0.5$, implicit treatments of the source term exhibit a larger attractive region of initial data than the explicit treatments of the source term. However, as the time step is further increased, an adverse behavior is observed contrary to the common belief that implicit schemes can operate with much higher time step and still produce the correct steady-state numerical solution. Since the source term is handled implicitly, the classical guideline for the time step constraint is given by the explicit discretization of the convective term (homogeneous part of the PDE (3.33a)), or equivalently by the CFL constraint $c = p_1 p_2 < 1$. Thus, the permissible time step for the implicit treatments of the source term is larger than explicit treatments of the source term. However, it is evident from the computation shown on Figs. 3.23 - 3.25 for implicit schemes CHA/LIE and CHA/LT with a Courant number set equal to 0.3 ($p_2 = 3$) and 1 ($p_2 = 10$) respectively, that these implicit schemes no longer give the correct asymptotic solution, in particular for the scheme CHA/LT.

3.8. Spurious Dynamics in Time-Accurate (Transient) Computations

In the examples chosen by Lorenz (1989), he showed that numerical chaos always precedes divergence of a computational scheme. He suggested that computational chaos is a prelude to computational instability. Poliashenko & Aidun (1995) showed that this is not a universal scenario. In previous sections, we have shown that numerics can introduce chaos. Using a simple example, Corless (1994b) showed that numerics can suppress chaotic solutions. The work of Poliashenko and Aidun also discussed spurious numerics in transient computations. Adams et al. (1993) discussed spurious chaotic phenomena in astrophysics and celestial mechanics. They showed that the source of certain observed chaotic numerical solutions might be attributed to round-off errors. Adams also discussed the use of interval arithmetics (interval mathematics or enclosure methods) to avoid this type of spurious behavior. Moore et al. (1990) discussed the reliability of numerical experiments in thermosolutal convection. Keener (1987) discussed the uses and abuses of numerical methods in cardiology.

It is a common misconception that inaccuracy in long-time behavior of numerical schemes poses no consequences for transient or time-accurate solutions. This is not the case when one is dealing with ‘genuinely nonlinear DEs (Jackson 1989)’. For genuinely nonlinear problems,

due to the possible existence of spurious solutions, larger numerical errors can be introduced by the numerical methods than one can expect from a local linearized analysis or weakly nonlinear behavior. Lafon & Yee (1991) illustrated this connection. Section 3.7.3 summarizes their result. The situation can become more intensified if the initial data of the DE is in the basin of attraction of a chaotic transient (Grebogi et al. 1983) of the discretized counterpart. In fact, it is possible that part or all of the solution trajectory is erroneous. Section V shows a practical example of a chaotic transient near the onset of turbulence in direct numerical simulations of channel flow by Keefe (1996). Since numerics can introduce and suppress chaos, and can also introduce chaotic transients, the dangers of relying on numerical tests for the onset of turbulence and chaos is evident.

There has been much debate on the overall accuracy away from shocks of high-resolution shock-capturing methods. Donat (1994) addressed this issue from a theoretical standpoint while Casper & Carpenter (1995) illustrated it with a shock induced sound wave model. Casper and Carpenter concluded that there is only first-order accuracy downstream of the sound-shock interaction using a spatially 4th-order ENO scheme. Sections 5.2 and 5.3 illustrate two additional types of spurious numerics in transient computations.

IV. Spurious Dynamics in Steady-State Computations

Any CFD practitioner would agree that making a time-marching CFD computer code converge efficiently to a correct steady state for a new physical problem, that was previously not understood, is still an art rather than a science. One usually has to tune the code and still encounters one or more problems such as blow-up, nonconvergence, nonphysical, or slow convergence of the numerical solution. Some of these phenomena have been reported in conference proceedings and reference journals, but the majority have been left unreported. Although these behaviors might be caused by factors such as poor grid quality, under-resolved grids, improper numerical boundary conditions, etc., most often they can be overcome by employing standard procedures such as using physical guidelines, grid refinement, improved numerical boundary treatments, halving of the time step, and using more than one scheme to double check if the numerical solution is accurate and physically correct. However, these standard practices alone may sometimes be misleading, not possible (e.g., too CPU intensive) or inconclusive due to the various numerical uncertainties (see section I) that can be attributed to the overall solution process. Consequently, isolation of the sources of numerical uncertainties is of fundamental importance. Section III isolates some of the spurious numerics for elementary models. Complementing the phenomena observed in Section III, this section illustrates examples from CFD computations. These examples were published in Yee & Sweby (1996). We concentrate mainly on the convergence issues that are contributed by the spurious dynamics that are inherent in the schemes. Section 4.2.1 was written by Bjorn Sjogreen of the Uppsala University, Sweden.

4.1. A 1-D Chemically Relaxed Nonequilibrium Flow Model⁴

The model considered is a nonequilibrium flow field relaxation of the one-dimensional Euler equations for a (N_2, N) mixture. This type of flow is encountered in various physical situations, such as shock tube experiments (the mixture behind the shock being in a highly nonequilibrium state) or an hypersonic wind tunnel. Under these assumptions the model can be expressed as a single ODE,

$$\frac{dz}{dx} = S(\rho, T, z), \quad (4.1)$$

where z is the mass fraction of the N_2 species, ρ is the density of the mixture and T is the temperature. There are two algebraic equations for ρ and T .

This system consists of a disparity range of parameter values (many orders of magnitude) and is stiff and highly nonlinear. Even when care is taken, the following features are observed when Runge-Kutta schemes are used for the integration (Sweby et al. 1995):

- restricted basins of attraction
- spurious equilibrium values
- oscillatory solutions

The derivation of the model is as follows. The one-dimensional steady Euler equations for a reacting (N_2, N) mixture are

$$\frac{d}{dx} (\rho_{N_2} u) = \dot{w}_{N_2} \quad (4.2a)$$

$$\frac{d}{dx} (\rho u) = 0 \quad (4.2b)$$

$$\frac{d}{dx} (\rho u^2 + p) = 0 \quad (4.2c)$$

$$\frac{d}{dx} [u(E + p)] = 0, \quad \dots \quad (4.2d)$$

where (4.2a) is the balance equation for the N_2 species and \dot{w}_{N_2} is the production rate of the N_2 species with density ρ_{N_2} . Equation (4.2b) is the continuity equation, (4.2c) the momentum equation and (4.2d) the energy equation, in which ρ , u , E and p are density, velocity, total internal energy per unit volume, and pressure, respectively.

The production rate \dot{w}_{N_2} of species N_2 is the sum of the production rates for the two reactions

⁴We would like to acknowledge Andre Lafon for the original formulation and the earlier study used in this section; presented at the ICFD Conference on Numerical Methods for Fluid Dynamics, April 3-6, 1995, Oxford, UK.

$$N_2 + N_2 \rightleftharpoons 2N + N_2 \quad (4.3a)$$

$$N_2 + N \rightleftharpoons 2N + N \quad (4.3b)$$

and are computed using the Park's model (Park 1985) that has been largely used for hypersonic computations. See the Workshop on Hypersonics (1991) for some discussion. These reaction rates involve an equilibrium constant, K_{eq} (see below), which is determined by a polynomial fitting to experimental data, and as such is only valid for a certain range of temperatures. In particular, a cut-off value has to be introduced for low temperatures, a typical choice being $T_{min} = 1000K$ (Mulard & Moules 1991).

The system (4.2) and (4.3) must be closed by a thermodynamical representation of the mixture. Here a simple model, with no vibrational effects, has been chosen. The details have been omitted for brevity.

Equations (4.2b)-(4.2d) simply integrate to give

$$\rho u = q_\infty, \quad (4.4a)$$

$$\rho u^2 + p = P_\infty, \quad (4.4b)$$

$$H = \frac{E + p}{\rho} = H_\infty, \quad (4.4c)$$

where H is the total enthalpy and q_∞ , P_∞ and H_∞ are all constants. Finally, denoting the mass fraction of the N_2 species by

$$z = \frac{\rho N_2}{\rho}, \quad (4.5)$$

and using the Park's reaction rate model and the thermodynamical closure, (4.1) can be written as

$$\begin{aligned} \frac{dz}{dz} &= S(\rho, T, z) \\ &= \frac{1}{M_1 q_\infty} \rho^2 T^B \exp\left(-\frac{\theta}{T}\right) \\ &\quad \times [\alpha A_1 z(1-z)^2 - A_1 z^2 + 2\alpha A_2 (1-z)^3 - 2A_2 z(1-z)], \end{aligned} \quad (4.6a)$$

where

$$\alpha = \frac{4\rho}{M_1 K_{eq}}, \quad K_{eq} = 10^6 \exp [c_1 + c_2 Z + c_3 Z^2 + c_4 Z^3 + c_5 Z^4], \quad Z = \frac{10^4}{T}. \quad (4.6b)$$

The density ρ is obtained from

$$q_\infty^2(8 - 2z)\left(\frac{1}{\rho}\right)^2 - (10 - 3z)P_\infty\left(\frac{1}{\rho}\right) + 2(2 - z)[H_\infty - (1 - z)e_2^0] = 0 \quad (4.6c)$$

and the temperature T from

$$T = \frac{M_1 p}{R(2 - z)\rho} \quad (4.6d)$$

with pressure

$$p = P_\infty - \frac{q_\infty^2}{\rho}. \quad (4.6e)$$

The model uses the constants

$$\begin{bmatrix} c_1 = 3.898 \\ c_2 = -12.611 \\ c_3 = 0.683 \\ c_4 = -0.118 \\ c_5 = 0.006 \\ M_1 = 28 \times 10^3 \end{bmatrix} \quad \begin{bmatrix} A_1 = 3.7 \times 10^{15} \\ A_2 = 1.11 \times 10^{16} \\ B = -1.6 \\ \theta = 1.132 \times 10^5 \\ e_2^0 = 3.355 \times 10^7 \\ R = 8.3143 \end{bmatrix}$$

where q_∞ , P_∞ and H_∞ are input parameters set to be 0.0561, 158,000 and 27,400,000, respectively, in our calculations. A limitation of the model is $T > T_{\min} = 1000K$. In addition, solutions are nonphysical if $z \notin [0, 1]$, if $p < 0$ or if ρ is complex.

Equation (4.6a) was integrated using the Euler, modified Euler, improved Euler, Heun (R-K 3), Kutta (R-K 3) and R-K 4 Runge-Kutta schemes. In each case the computations were performed for a range of initial z and integration steps Δz . The discretized equations were preiterated 1000 steps before a full bifurcation diagram together with basins of attraction were produced. (The computations were carried out on the CM-200 Connection Machine at the Edinburgh Parallel Computing Centre, UK.)

There are two strategies possible when implementing the Runge-Kutta schemes. One is to freeze the values of ρ and T at the beginning of each step when calculating $S(\rho, T, z)$ at the intermediate stages. The other is to update the values at each evaluation of the function S . The results presented here employ the latter strategy since this is the more proper implementation; however, it is interesting to note (see below) that results obtained by freezing ρ and T for intermediate calculations exhibit a slightly richer dynamical structure.

Figure (4.1) shows the results obtained from our calculations. In all of these plots the shaded region denotes the basin of attraction in which combinations of initial z values and step size Δz converge to the fixed point, depicted by the solid black line. The unshaded regions indicate

regions where the combinations of z and Δz do not converge to a physical solution of the problem.

As can be seen in all cases the basins of attraction narrow considerably for the larger values of Δz . (Note that the axis scale is 10^{-5} !) The explicit Euler scheme (Fig. 4.1a) obtains the correct fixed point up to its stability limit, where there is a very small region of period 2 (oscillatory) behavior before it becomes nonphysical. Similar behavior is observed for the improved Euler (Fig. 4.1c) and Kutta (Fig. 4.1e) schemes, the latter also exhibiting a much more constricted basin of attraction for any given Δz . The Heun scheme (Fig. 4.1d) exhibits a distinct region of oscillatory behavior just above the linearized stability limit.

As is typical with the modified Euler scheme (Fig. 4.1b), a transcritical bifurcation occurs at its stability limit which leads to a spurious (Δz dependent) solution. Note also the solid line at about $z = 0.25$ down on the plot, outside of the shaded region. This appears to be an unstable feature picked up by our method of fixed point detection (comparison of initial data with the 1000th iterate) and is unlikely to arise in practical calculations unless the initial data are on this curve. The R-K 4 scheme (Fig. 4.1f) also exhibits a transcritical bifurcation at the linearized stability limit; however this is discernible more by the sudden narrowing of the basin of attraction since the spurious fixed point varies only slightly with Δz .

Finally we note that if the values of ρ and T are frozen for intermediate calculations the dynamics are somewhat modified. All schemes with the exception of explicit Euler have a slightly larger basin of attraction for values of Δz within the stability limit and all schemes have period two behavior at the stability limit, there being no transcritical bifurcations for any of the schemes. The modified Euler scheme also has embedded period doubling and chaotic behavior below the linearized stability limit.

What we have shown with this example is that, although the dynamical behavior is perhaps not as rich as in some of our simple examples, spurious features can still occur in practical calculations and so care must still be taken in both computation and in interpretation.

4.2. Convergence Rate & Spurious Dynamics of High-Resolution Shock-Capturing Schemes

We have seen in Section III elementary examples and references cited therein on how the proper choice of initial data and the step size combination can avoid spurious dynamics. Yet for other combinations the numerical solutions can get trapped in a spurious limit cycle. We have also seen that the convergence rates of the schemes are greatly affected by the step sizes that are near bifurcation points. Here we include the dynamics of full discretization of two nonlinear PDE examples. The spatial discretizations are of the high-resolution shock-capturing type (nonlinear schemes). This includes TVD and ENO schemes. Section 4.2.1 discusses how this nonlinear scheme affects the convergence rate of systems of hyperbolic conservation laws. Section 4.2.2 illustrates the existence of spurious asymptotes due to the various flux limiters that are built in to TVD schemes.

4.2.1. Convergence Rate for Systems of Hyperbolic Conservation Laws

This section summarizes the results of Engquist & Sjögreen (1995) and Sjögreen (1996, private communication). These results concern the convergence rate for discontinuous solutions of a system of hyperbolic conservation laws. For a scalar nonlinear conservation law, the characteristics point into the shock. According to the linear theory of Kreiss & Lundqvist (1968), dissipative schemes damp out errors propagating backwards against the direction of the characteristics. Thus it is reasonable to expect that the locally large errors at the shock stay in a layer near the shock. In numerical experiments we usually obtain $O(h^p)$ convergence away from the shock with difference schemes of formally p th order.

For the systems case, the same reasoning from the scalar conservation law cannot be applied. In this case, we have other families of characteristics intersecting the shock causing the situation to be more involved. Thus it is possible that the large error near the shock propagates out into the entire post shock region by following a characteristic which emerges from the shock.

This effect cannot be seen in a simple scalar Riemann problem (problem with jump initial data), because exact global conservation determines the post shock states. The system model problem, taken from Engquist & Sjögreen (1995),

$$u_t + (u^2/4)_x = 0, \quad -\infty < x < \infty, \quad 0 < t \quad (4.7a)$$

$$v_t + v_x + g(u) = 0, \quad g(u) = (u + 1)(u - 1)(1/2 - u) \quad (4.7b)$$

gives an example of propagation of large errors. The function $g(u)$ has the properties $g(1) = g(-1) = g(1/2) = 0$, and $g(u) \neq 0$ for $-1 < u < 1$ except at $u = 1/2$. The initial data was given as

$$u_0(x) = \begin{cases} 1 & x \leq 0 \\ -1 & x > 0 \end{cases}, \quad v_0(x) = 1 \quad (4.7c)$$

so that the exact solution of the u equation is a steady shock. The eigenvalues of the Jacobian matrix of the flux $(u^2/4, v)^T$ for (4.7) are $\lambda_1 = u/2$ and $\lambda_2 = 1$. The eigenvalue $\lambda_1 = u/2$ corresponds to a strictly nonlinear field, and $\lambda_2 = 1$ corresponds to a linearly degenerate field.

With this initial data (4.7c), it gives rise to a steady 1-shock, with the 1-characteristics having a slope 1/2 to the left of the shock and a slope -1/2 to the right of the shock. These thus intersect the shock when time increases. The 2-characteristics of the linear field, have slope 1 on both sides of the shock. These characteristics thus enter the shock from the left and exit to the right. The v component of the solution is passively advected along the 2-characteristics. When these characteristics exit from the shock at $x = 0$, an error, coming from poor accuracy locally at the shock, is picked up and advected along with the solution into the domain $x > 0$. The shock curve $x = 0$ (in the $x-t$ plane) acts as an inflow boundary for the domain $x > 0$. The error coming from the shock is similar to an error in given inflow data, and is therefore not affected

by the numerical method used in the interior of the domain. Thus is not surprising that this error is of first order, even when the equation is solved by a method of higher formal order of accuracy.

Figure 4.2 shows the numerical solution, computed by a second-order accurate ENO method using 50 grid points at the time $T = 5.68$. The points in the shock give a large error which is coupled to the v equation through $g(u)$. The exact solution for v is 1. Numerical investigation of the convergence rate of the error in v to the right gave the exponent 1.047. One thus has first-order convergence for this second-order accurate method.

Similar effects can be seen in computing the quasi one-dimensional nozzle flow. Engquist & Sjogreen (1996) computed the solution on the domain $0 < x < 10$ for a nozzle with the following cross sectional area variation

$$A(x) = 1.398 + 0.347 \tanh(0.8x - 4). \quad (4.8)$$

This problem is studied in Yee et al. (1985) for a class of explicit and implicit TVD schemes. The solution has a steady shock in the middle of the domain. Figure 4.3 shows the error in momentum for the steady-state solution on grids of 50, 100, and 200 points for a fourth-order ENO scheme and a second-order TVD scheme. For the fourth-order method, the convergence exponent is 3.9 before the shock and 1.0 after the shock, when going from 100 to 200 points. For the second-order TVD the same quantities have the values 2.2 and 1.1 respectively.

Sjogreen (1996) recently conducted the same numerical study for the two-dimensional compressible Euler equations for a supersonic flow past a disk with Mach number 3. The equations were discretized by a second-order accurate uniformly nonoscillatory (UNO) scheme (Harten 1986), which unlike TVD schemes, is formally second-order everywhere including smooth extrema. He computes the error in entropy along the stagnation line for the steady-state solution on grids with 33×17 , 65×33 , and 129×65 grid points. The result is shown in Fig. 4.4, where the error and convergence exponent in the region behind the bow shock are plotted. The convergence exponent is between the 65×33 and 129×65 grids. The disk has radius 0.5, and it is centered at the origin, which means that the line is attached to the wall for $-0.5 < x$. A convergence exponent of 1.5 is observed for this formally second-order method.

4.2.2. Spurious Dynamics of TVD Schemes for the Embid et al. Problem⁵

It has long been observed that the occurrence of residual plateauing is common when TVD and ENO types of schemes are used to time march to the steady state. That is, the initial decrease in the residual levels out and never reaches the convergence tolerance. See Yee (1986, 1989) and Yee et al. (1990) for some discussion. This has often been overcome by *ad hoc* modification of the flux limiter or similar device in problem regions.

⁵We would like to acknowledge Paul Burton for the computations used in this section.

A recent study (Burton & Sweby 1995) investigated this phenomenon using a dynamical systems approach for the one-dimensional scalar test problem of Embid et al. (1984)

$$u_t + \left(\frac{1}{2}u^2\right)_x = g(x)u = (6x - 3)u, \quad x \in (0, 1), \quad (4.9a)$$

with boundary conditions

$$u(0) = 1, \quad u(1) = -0.1. \quad (4.9b)$$

This equation with the flux function $f(u) = u^2/2$ has the property that there are two entropy satisfying steady solutions, consisting of stationary shocks jumping between the two solution branches

$$u^l(x) = 3x(x - 1) + 1 \quad (4.10a)$$

$$u^r(x) = 3x(x - 1) - 0.1. \quad (4.10b)$$

For this problem the two possible solutions consist of a single shock, either approximately at $x_1 = 0.18$ or $x_2 = 0.82$. It can then be shown (see Embid et al. 1984 for details) that the solution with a shock at x_1 is stable to perturbations while the solution with a shock at x_2 is unstable.

Embid et al. solved (4.9) using three different methods, the first-order implicit upwind scheme of Engquist and Osher, its second-order counterpart, and the second-order explicit MacCormack scheme. All three schemes used time stepping as a relaxation technique for solving the steady-state equation. The initial conditions were taken to follow the solution branches (4.10) from the boundary values, with a single jump between the two branches. The results obtained showed that, although the implicit schemes allowed large time steps and hence fast convergence, if the initial jump was taken too near the unstable shock position x_2 , then for some ranges of Courant number,

$$c = u \frac{\Delta t}{\Delta x}, \quad (4.11)$$

the schemes would converge to the physically unstable shock. This phenomenon was studied both for these three schemes and a variety of flux limited TVD schemes (Sweby 1984) in Burton & Sweby (1995), where not only the full problem was studied but also a reduced 2×2 system was investigated using a dynamical system approach. We report on this investigation here.

The schemes investigated were explicit and implicit versions of the Engquist-Osher and TVD flux limiter schemes using the minmod, van Leer, van Albada and superbee flux limiters. In all cases a method of lines implementation was adopted, the spatial discretization being performed separately from the time discretization. (This is necessary so that the final state does not depend on the Courant number, which would be the case if a Lax-Wendroff type

discretization were used.) For the time discretization, forward Euler was used for the explicit implementations while linearized implicit Euler was used for the implicit computations. For the second-order flux limiter schemes the Jacobian matrix used was taken to be that of the first-order Engquist-Osher in order to allow easy inversion.

The schemes are

(a) **Explicit Scheme**

$$\begin{aligned} u_j^{n+1} = & u_j^n - \lambda \Delta_- (f_{j+1}^- + f_j^+) + \Delta t g(x) u_j^n \\ & - \frac{1}{2} \lambda \Delta_- [\phi(r_j^+) (\Delta f_{j+\frac{1}{2}})^+ - \phi(r_{j+1}^-) (\Delta f_{j+\frac{1}{2}})^-], \end{aligned} \quad (4.12)$$

(b) **Linearized Implicit Scheme**

$$\begin{aligned} J(u_j^n)[u_j^{n+1} - u_j^n] = & - \lambda \Delta_- (f_{j+1}^- + f_j^+) + \Delta t g(x) u_j^n \\ & - \frac{1}{2} \lambda \Delta_- [\phi(r_j^+) (\Delta f_{j+\frac{1}{2}})^+ - \phi(r_{j+1}^-) (\Delta f_{j+\frac{1}{2}})^-], \end{aligned} \quad (4.13)$$

where f_j^\pm are the Engquist-Osher numerical fluxes

$$f_j^+ = f(\max(u_j, 0)), \quad (4.14a)$$

$$f_j^- = f(\min(u_j, 0)). \quad (4.14b)$$

The flux differences are given by

$$(\Delta f_{j+\frac{1}{2}})^+ = -(f_{j+1}^+ - f(u_{j+1})), \quad (\Delta f_{j+\frac{1}{2}})^- = (f_j^- - f(u_j)), \quad (4.15)$$

and the solution monitors by

$$r_j^\pm = \left[\frac{(\Delta f_{j-\frac{1}{2}})^\pm}{(\Delta f_{j+\frac{1}{2}})^\pm} \right]^{\pm 1}. \quad (4.16)$$

Finally, J is the Jacobian matrix and the flux limiter $\phi(r)$ is one of

$$\phi_0(r) = 0 \text{ --- first-order Engquist-Osher (E-O) scheme,} \quad (4.17)$$

$$\phi_1(r) = \max(0, \min(r, 1)) \text{ --- the minmod limiter,} \quad (4.18)$$

$$\phi_2(r) = \max(0, \min(2r, 1), \min(r, 2)) \text{ --- Roe's superbee limiter,} \quad (4.19)$$

$$\phi_{VL}(r) = \frac{r + |r|}{1 + |r|} \text{ --- van Leer's limiter,} \quad (4.20)$$

$$\phi_{VA}(r) = \frac{r + r^2}{1 + r^2} \text{ --- van Albada's limiter.} \quad (4.21)$$

The experiments reported in Burton & Sweby (1995) used a grid spacing of $\Delta x = 0.025$ with initial conditions consisting of a single jump between the solution branches (4.10) near either the stable shock (\mathbf{x}_1) or the unstable shock (\mathbf{x}_2). The convergence criterion used was the following bound on the residual

$$\sum_j |\mathbf{u}_j^{n+1} - \mathbf{u}_j^n| \leq 10^{-15}, \quad (4.22)$$

with an upper limit of **2000** iterations being performed.

The results of applying these schemes to problem (4.9) largely echoed those reported by Embid et al. For the explicit schemes convergence, when it occurred, was to the stable shock. It was found that there were regions of Courant number ($c \leq c_i$) for which the schemes converged, regions ($c_i < c < c_j$) for which convergence did not take place using (4.22) within **2000** iterations, and regions ($c > c_j$) for which the schemes were unstable. This is summarized in Table 4.1. The absence of an entry in Table 4.1 corresponds to residual plateauing.

Notice that for the superbee flux limiter there was no range of Courant numbers for which the scheme converged. Closer inspection reveals residual (defined as $r^n = |\mathbf{u}^{n+1} - \mathbf{u}^n|$) plateauing at around 10^{-3} . For the other schemes when $c_i < c < c_j$ the nonconvergence observed arises from a similar process, except that the residual does not necessarily level out completely, but decreases at a very gradual rate, resulting in very slow convergence.

The implicit scheme experiments revealed that the choice of initial conditions could cause convergence to the unstable shock for certain ranges of Courant number. For an initial jump near the stable shock, the schemes (with the exception of the van Leer limiter) converge to the stable shock for $c < 11$. However, for an initial discontinuity near the unstable shock, convergence could sometimes be towards the unstable shock. The situation is summarized in Table 4.2, where again the absence of an entry corresponds to residual plateauing.

To gain further insight into this problem, Burton & Sweby (1995) considered a reduced problem consisting of two free points at one of the shocks, with exact solution values being imposed as boundary conditions on either side. This then leads to a two dimensional dynamical system which, although obviously a gross simplification of the full problem, was hoped to still maintain some of the qualitative behavior.

The situation is as shown in Fig. 4.5, where the free points are X and Y , the remaining points (U_u, U_l, U_{rr} and U_r) being set at exact analytic values to provide boundary conditions. Two such values are needed on either side to provide the necessary information for the flux limiters. Substitution of these points into the numerical scheme then leads to a two-dimensional system. For example, the explicit Engquist-Osher scheme yields

$$X^{n+1} = X^n - \frac{\Delta t}{40} \left[f^-(Y^n) + f^+(X^n) - f^-(X^n) - f^+(U_l) \right] - \frac{39}{20} \Delta t X^n \quad (4.23a)$$

$$Y^{n+1} = Y^n - \frac{\Delta t}{40} \left[f^-(U_r) + f^+(Y^n) - f^-(Y^n) - f^+(X^n) \right] - \frac{36}{20} \Delta t Y^n, \quad (4.23b)$$

where a step size of $\Delta x = \frac{1}{40}$ has been used.

For the first-order explicit and implicit schemes some analysis on the reduced problem can be performed. Table 4.3 summarizes the findings. Note that for both schemes spurious fixed points are introduced by the simplification of the problem. These both have X and Y of the same sign and would not be tolerated for the full problem. It is only the proximity of the boundary conditions for the reduced problem which allow them to exist as fixed points. However, the remaining fixed points and their stability agree well with numerical results obtained for the full problem.

Analytical results could only be obtained for the first-order scheme and so numerical experiments were performed for the flux limiter schemes. These consisted of generating bifurcation diagrams for X and Y against Δt and the plotting of basins of attraction in the (X, Y) plane for fixed values of Δt . The explicit schemes were shown to possess no spurious dynamics below their respective stability limits, apart from that introduced by the simplification of the problem (i.e. outside of the quadrant $(X > 0, Y < 0)$). As Δt was increased above the stability limit the schemes entered a period of bifurcation and chaos accompanied by a dramatic shrinkage in the numerical basins of attraction.

The dynamics of the implicit schemes at the unstable shock showed the falsely stable fixed point becoming stable for large values of Δt . For all the limiters tested the stabilizing of the fixed point was accompanied by the introduction of additional, spurious (period 2) fixed points. These spurious solutions caused a reduction in size of the basin of the falsely stable fixed point. The fact that the more compressive limiters took longer to recover from the effects of the spurious fixed points seems a possible cause of the phenomenon of residual plateauing experienced in the full problem. Due to a space limitation, see Burton & Sweby (1995) for the illustrations.

It must be realized that although the residual plateauing illustrated is around the physically unstable shock (to which we would usually not wish to converge), the fact that it is not a repelling phenomenon will in itself have repercussions on convergence to the correct, physically stable shock. Indeed no such nonconvergence was observed for Courant numbers greater than 11. We conclude this section by emphasizing that the reduced problem indicated a possible cause for residual plateauing. However, for certain situations the dynamics of the full problem does not coincide precisely with that of the reduced problem.

4.2.3. The Dynamics of Grid Adaption

Consider a model convection-diffusion equation of the form

$$u_t + f(u)_x = \epsilon u_{xx} \quad (4.24)$$

with the linear case, $f(u) = u$ and the nonlinear case, $f(u) = \frac{1}{2}u^2$ (the Burgers equation) respectively. The boundary conditions for the linear case are $u(0, t) = 0$ and $u(1, t) = 1$ and for the nonlinear case, $u(0, t) = 1$ and $u(1, t) = -1$. These boundary conditions result in steady-state solutions of a boundary layer at $x = 1$ and a viscous shock at $x = 1/2$, respectively. In both cases the steepness of the feature is governed by the diffusion coefficient parameter ϵ . Besides its steepness feature, one of the main reasons for considering the linear convection-diffusion equation is to show that grid adaptation alone and/or nonlinear schemes such as TVD schemes can introduce unwanted dynamics to the overall solution procedure. The authors realize that model (4.24) is not the best model to illustrate the dynamics of the studied schemes since the model is not stable under perturbations. However, it serves to show what type of spurious numerics would occur under such an environment.

One common criterion used for grid adaptation is the equidistribution of a positive definite weight function $w(x, t)$, often taken to be some monitor of the numerical solution $u(x, t)$ of the underlying PDE. A grid $x_0 < x_1(t) < \dots < x_{J-1}(t) < x_J$, where x_0 and x_J are fixed, equidistributes $w(x, t)$ (at time t) if

$$\int_{x_{j-1}}^{x_j} w(x, t) dx = \int_{x_j}^{x_{j+1}} w(x, t) dx = \frac{1}{J} \int_{x_0}^{x_J} w(x, t) dx, \quad (4.25)$$

for $j = 1, \dots, J$. A one-parameter family of weight functions

$$w(x, t) = \sqrt{1 - \alpha + \alpha u_x^2(x, t)}, \quad \alpha \in [0, 1], \quad (4.26)$$

can be chosen where $\alpha = 1/2$ corresponds to equidistribution in the arc-length and $\alpha = 0$ yields a uniform grid. Approximating $w(x, t)$ to be constant in each interval (x_{j-1}, x_j) yields

$$\left(\sqrt{1 - \alpha + \alpha u_x^2} \right)_{j-1/2} (x_j - x_{j-1}) = \left(\sqrt{1 - \alpha + \alpha u_x^2} \right)_{j+1/2} (x_{j+1} - x_j). \quad (4.27)$$

Given a numerical solution of the PDE we can approximate the derivatives by

$$u_x|_{j-1/2} \approx \frac{u_j - u_{j-1}}{x_j - x_{j-1}}. \quad (4.28)$$

Equation (4.27) is nonlinear in $\{x_j\}$ if we use (4.28). However, (4.27) is linear in $\{x_j\}$ if $\{x_j\}$ in (4.28) uses the existing grid. In this case we can solve the tridiagonal system (4.27) for a new set of $\{x_j\}$ to obtain an updated grid.

Given a set of initial data and an initial grid, the procedure is to numerically solve the PDE and (4.27) in a time-lagged manner. We use nodal placement and the ℓ_2 norm of the solution to illustrate our results. We use the previous time step value for \mathbf{x}_j in (4.28) to achieve a linear tridiagonal system for the updated grid in (4.27). Our preliminary study shows that the solution procedure of Ren and Russel (1992), and Budd et al. (1995a) in solving the coupled PDE and (4.27) are less stable than the present linearized form. See also Neil (1994) for a similar study and conclusion. The regridding strategy adopted was to regrid after every time step of the PDE method, either interpolating updated solution values from the old grid or performing no adjustment at all due to grid movement. This latter approach in effect presents the PDE method with new initial data to the problem at each step.

The dynamics of the above one-parameter family of mesh equidistribution schemes coupled with different spatial and time discretization were studied numerically in Sweby & Yee (1994) and Yee & Sweby (1995a,b) using the above numerical procedure. The spatial discretizations include three-point central, second-order upwind and second-order TVD schemes. The time discretizations include explicit Euler, second- and fourth-order Runge-Kutta and the linearized implicit Euler methods. In a parallel study, Budd et al. (1995b) made use of the AUTO computer bifurcation package (Doedel 1986) to obtain bifurcation diagrams for similar grid adaptation methods for the steady part of the above PDEs with a different form than (4.27). However, the dependence on known solutions of the discretized PDEs and grid equations as starting values limits its usage. In Sweby & Yee (1994) we utilize the power of the highly parallel Connection Machine CM-5 to undertake a purely numerical investigation into the dynamics of the time-marching adaptive procedure.

We divided a chosen parameter space (e.g., ϵ) into 512 equal intervals, with all other parameters ($\alpha, \Delta t$, initial data) fixed. For each chosen parameter value, we iterated the discretized PDE and the grid function, in general, 4000 steps (8,000 steps for explicit methods) to allow the solution to settle to an asymptotic state. Then we performed a series of time step/regridding stages, during which we investigated the dynamics by producing an overlaid plot of the ℓ_2 norms of the numerical solution and the grid distribution at each step. This resulted in a bifurcation type diagram or the grid displacement diagram as a function of the physical or discretized parameters. We also performed numerical studies by only preiterating the discretized PDEs to the steady state for a fixed grid before solving both the discretized PDE and the grid adaptation function. We found in most cases the solution process is less stable and more likely to get trapped in a spurious mode than in the aforementioned process.

For this study, we took into consideration the grid density, an even and odd number of nodes, and whether or not there is interpolation after each regridding. The grid density studies consist of 4, 5, 6, 9, 10, 19, 20, 49 and 50 grid points. There is no apparent sign of even or odd grid dependence. The resolution and stability of TVD schemes are also grid independent. However, the central difference scheme experienced instability more often for coarser grids, and the second-order upwind is slightly more stable, with better resolution than the central scheme. As expected, the stable time step required for the explicit methods was orders of magnitude lower

than that for the implicit method. For the TVD schemes, comparison of the dynamical behavior of the five limiters of (3.50) of Yee (1989) was performed. Four of the limiters are the same as (4.17)-(4.21). Due to the simplicity of the PDEs, their dynamical behavior is similar, although there were slight differences in the stability and resolution. Due to space limitations, we summarize the results without presenting the actual computational figures. Interested readers should refer to our original papers for details.

Summary: We consider separately the cases “with” and “without” interpolations. The term “scheme” from here on means the overall adaptive scheme procedure.

(a) *No Interpolation:* For the linear problem, the behavior of the adaptive TVD schemes is similar to that of the classical shock-capturing methods. As opposed to the uniform grid case, the adaptive TVD schemes without interpolations behave rather poorly in terms of stability and allowable ϵ values. See Figs. 11 and 12 of Yee & Sweby (1995b). The solutions refuse to settle down for larger Δt and/or smaller ϵ . For the nonlinear problem, the behavior of the adaptive TVD schemes is similar to that of the uniform grid case. The range of allowable ϵ and Δt in terms of stability and convergence rate and settling of the grid distribution are far better than in the linear problem. It appears that for problems with shocks, adaptive TVD schemes prefer no interpolation after each regridding. See Figs. 13 and 14 of Yee & Sweby (1995b).

(b) *With Interpolations:* For the linear problem, as expected, both adaptive TVD schemes and adaptive classical schemes behave in a similar manner in terms of stability and convergence. Adaptive TVD schemes are less stable and have a smaller allowable range of ϵ than the uniform grid case. Overall, adaptive TVD schemes behave far better than their counterparts without interpolation for the linear problem as can be seen in Figs. 11 and 12 of Yee & Sweby (1995b). For the nonlinear problem, the adaptive TVD schemes with interpolations behave like the classical shock-capturing method. They experience nonconvergence of the solution, and the grid distribution cannot settle down for a certain range of Δt . This can be seen in Figs. 13 and 14 of Yee & Sweby (1995b).

It is surprising to see the opposite behavior of the adaptive implicit TVD schemes for the two model PDEs with and without interpolation combinations, especially when the same physical parameters, discretized parameters and initial data were used.

4.3. Mismatch in Implicit Schemes for Time-Marching Approaches

When implicit methods are used to time-march to the steady states, it is a common practice in CFD to use a linearized and/or a simplified implicit operator (or mismatched implicit/explicit operators) to reduce operation count. The simplified implicit operators usually are first-order and the explicit operator retains higher order spatial accuracy. The simplified implicit operator might not be consistent with the original implicit scheme. It might also be nonconservative even though the original and/or the explicit operator are conservative. One popular formulation with these mismatched implicit/explicit operators is the “delta formulation” of Beam & Warming (1978) in conjunction with implicit LMMs time discretizations. The logic is that

if the solution converges, the explicit operator dictates the final accuracy of the steady-state numerical solution. As discussed in Section 2.4, these mismatched implicit/explicit operators might induce unwanted spurious dynamics into and/or reduce the convergence rate of the overall solution procedure. To illustrate just this point, we summarize some old work of Mulder & van Leer (1984) and the first author's experiences (Yee 1986, 1989, 1990) in selecting the more desirable mismatch operators. These works use the delta formulation with a variant of the first-order upwind spatial discretizations for the implicit operator. The time discretization is the implicit Euler with the noniterative linearized form as discussed in Section 3.5.2. After the linearization in time and the drop in spatial discretization to first order, there are many ways to approximately evaluate the Jacobian matrix associated with the linearization for high-resolution and higher-order upwind shock-capturing schemes. Due to a space limitation, the readers are referred to the original papers for details or Yee (1989) for a summary.

Mulder and van Leer studied two first-order upwind spatial discretizations (van Leer's differentiable and Roe's nondifferential forms) for the implicit operator and a first-order or second-order upwind spatial discretization for the explicit operator. They concluded that the differentiable first-order upwind implicit operator gives quadratic convergence for flow of an isothermal gas along an almost circular path through the stellar gravitational field of a rotating two-armed spiral galaxy. The governing equations are a system of hyperbolic conservation laws. With Roe's nondifferentiable split flux-differences the iterations may get trapped in a limit-cycle. For a comparison of the two implicit operators, they used the same grid, physical parameters, explicit operator, initial data and numerical boundary treatment.

Yee (1986) constructed conservative and nonconservative linearized forms of implicit TVD schemes. A rather detailed study on the convergence properties of these forms was performed. Using the same notation as the original paper, both the linearized nonconservative implicit (LNI) and the linearized conservative implicit (LCI) forms can be of first or second-order accurate in space. Numerical experiments in Yee et al. (1985), Yee (1986), Yee & Harten (1987) and Yee (1989) showed that both the second-order LNI and LCI forms are very unstable even if a very small time step is used. The first-order LNI and LCI perform far better. However, the first-order LCI form is more stable and has a better convergence rate than the LNI counterpart. The first-order LNI form has a higher chance of converging to a nonphysical solution. Also the residual sometimes stagnates or gets trapped in a limit cycle. These conclusions are based on comparing the two forms for a variety of one-dimensional and two-dimensional practical problems containing complex shock waves. For both LCI and LNI forms, the more compressive limiters, such as the superbee, are very unstable. The residual stagnates even with very small time steps. See Yee et al. (1990) for their performance for hypersonic computations. Grid refinement in this case does not improve the situation. Again, in order to isolate the cause of the convergence problem, the same grid, physical parameters, explicit operator, initial data and numerical boundary condition treatment were used. In passing, both the first-order LCI and LNI are heavily used in the CFD community with TVD schemes other than the Harten & Yee type (Yee 1989). This includes but is not limited to the various UNO, ENO and high-order upwind schemes for the explicit operator.

The above convergence properties using pseudo time marching approaches in conjunction with high-resolution implicit TVD schemes contributed to yet another kind of spurious numerics, which are very different from that in Sections 4.1 and 4.2.

V. Spurious Dynamics in Unsteady Computations

In Section 3.8, we cited some of the spurious numerics in transient computations. We have also learned that numerics can introduce and suppress chaos and can also introduce chaotic transients, the danger of relying on numerical tests for the onset of turbulence and chaos is evident. Here, some examples from CFD computations that exhibit analogous spurious behavior are illustrated. Sections 5.1, 5.2 and 5.4 are written by the authors of the original work. Laurence Keefe of Nielsen Engineering summarizes his unpublished work on chaotic transient computation that he performed in the late 1980's. Shi Jin of the Georgia Institute of Technology summarizes his recent work on oscillations induced by numerical viscosities. Shi's work has an important implication in spurious dynamics using time-marching approaches as well as slowly moving shock waves in transient computations. Section 5.3. summarizes the work of Brown & Minion (1995). It is concerned with spurious vortices in two-dimensional thin shear layer incompressible flow simulations using high-resolution shock-capturing methods. Bjorn Sjogreen of the Uppsala University, Sweden summarizes his work on convergence rate for systems of hyperbolic conservation laws in transient computations in Section 5.4. For additional results concerning other issues, see Moore et al. (1990), Corless (1992, 1994), Poliashenko & Aidun (1995) and Read & Thomas (1995).

A brief background on chaotic transients and the significance and implications of Keefe's work on numerical uncertainties are needed before presenting his results. Loosely speaking, a chaotic transient behaves like a chaotic solution (Grebogi et al. 1983). A chaotic transient can occur in a continuum or a discrete dynamical system. The concern here is "**numerically induced chaotic transients**" or "**spurious chaotic transients**". One of the major characteristics of a numerically induced chaotic transient is that if one does not integrate the discretized equations long enough, the numerical solution has all the characteristics of a chaotic solution. The required number of integration steps might be extremely large before the numerical solution can get out of the chaotic transient mode. In addition, even without a numerically induced chaotic transient behavior, standard numerical methods usually experience a drastic reduction in step size and convergence rate near a bifurcation point (in this case the transition point) in addition to the bifurcation points due to the discretized parameters. See Section III for a discussion. Consequently, the possible numerically induced chaotic transient is especially worrisome in direct numerical simulations that are near the onset of turbulence. Away from the transition point, this type of numerical simulation is already very CPU intensive and the convergence rate is usually rather slow. Due to the limited computer resources, the numerical simulation can result in chaotic transients indistinguishable from sustained turbulence, yielding a spurious picture of the flow for a given Reynolds number. Thus, the danger of relying on numerical tests for the onset of turbulence is evident.

5.1. Chaotic Transients Near the Onset of Turbulence in Direct Numerical Simulations of Channel Flow

Numerical simulations of wall-bounded turbulent shear flows have proven to be a powerful tool for investigating both the physics and mathematics underpinning these practically important flows. Boundary layers and turbulence are inescapable in aeronautical applications, and simple flows over a flat plate or within a channel provide an accessible arena in which to understand turbulent dynamics and to test ideas for its modification and control that can benefit the performance of real aircraft.

Direct numerical simulations (DNS) of turbulent channel flow are the best developed of these techniques, with a better than 20 year history (Deardorff 1970, Schumann 1973, Moin & Kim 1982), and a relatively quick maturity (Kim et al. 1987) due to the favorable mapping of high accuracy spectral methods onto the geometry and known phenomenology of this flow. The physical situation is depicted in Fig. 5.1, where a flow is confined between planes at $y = \pm 1$ and is driven in the x -direction by a mean pressure gradient dp/dx . The flow is characterized by a Reynolds number $Re = U_\infty L/\nu$, where U_∞ is the mean centerline velocity, L is the channel half-height, and ν is the kinematic viscosity. Within the channel the flow satisfies the incompressible Navier-Stokes equations and the no-slip boundary conditions are applied at the walls. In the particular calculations shown here these equations have been manipulated into velocity-vorticity form, where one integrates equations for the wall-normal velocity v , and normal vorticity η and recovers the other two velocity components from the incompressibility condition and definition of η .

$$\frac{\partial}{\partial t} \Delta^2 v = h_v + \frac{1}{Re} \Delta^4 v \quad (5.1a)$$

$$\frac{\partial}{\partial t} \eta = h_\eta + \frac{1}{Re} \Delta^2 \eta \quad (5.1b)$$

$$f + \frac{\partial v}{\partial y} = 0 \quad (5.1c)$$

where

$$f = \frac{\partial u}{\partial x} + \frac{\partial w}{\partial z}, \quad \eta = \frac{\partial u}{\partial z} - \frac{\partial w}{\partial x} \quad (5.1d)$$

$$h_v = -\frac{\partial}{\partial y} \left(\frac{\partial H_1}{\partial x} + \frac{\partial H_3}{\partial z} \right) + \left(\frac{\partial^2}{\partial x^2} + \frac{\partial^2}{\partial z^2} \right) H_2 \quad (5.1e)$$

$$h_\eta = \frac{\partial H_1}{\partial z} - \frac{\partial H_3}{\partial x}. \quad (5.1f)$$

Here the H_i contain the nonlinear terms in the primitive form of the Navier-Stokes equations and the mean pressure gradient.

Two experimentally observed facts figure strongly in the choice of numerical method used to integrate the Navier-Stokes equations in this geometry: the velocity increases extremely rapidly normal to the wall, and turbulent channel flows are essentially homogeneous in planes parallel to the wall. The first requires a concentration of grid points near the wall, and the second suggests use of a doubly periodic domain in planes parallel to the wall. Happily, a high accuracy spectral representation of the velocity field $(\mathbf{u}, \mathbf{v}, \mathbf{w})$ meets these needs:

$$\vec{u} = \sum_l \sum_m \sum_n \vec{A}_{lmn}(t) T_l(\mathbf{y}) e^{im\alpha + in\beta z}, \quad (5.2)$$

where the $T_l(\mathbf{y})$ are Chebyshev polynomials. The numerical problem then becomes dependent on α and β in addition to Re . For time advance mixed explicit-implicit methods are used. The nonlinear terms in the equations are advanced using second-order Adams-Bashforth or a low storage, third-order Runge-Kutta scheme (Spalart et al. 1991), while the viscous terms are advanced by Crank-Nicholson. The algorithm based on this spectral spatial representation and mixed time advance has been tested and used extensively, demonstrating an ability not only to reproduce experimental results, but to go beyond them in elucidating flow features not easily investigated in experiments. This code, and ones similar, (Handler et al. 1989, Jung et al. 1992) are currently being used to investigate a variety of turbulence control ideas suitable for turbulent drag reduction and (conceivably) separation control.

One of the central problems in studies of wall bounded shear flows is the determination of when a steady laminar flow becomes unstable and transitions to turbulence. In dynamical systems' terms, the Navier-Stokes equations always have a fixed point solution for low enough Reynolds numbers, but for each flow geometry the Reynolds number at which this fixed point bifurcates needs to be determined. In channel flow the fixed point solution (a parabolic velocity profile across the channel, $\mathbf{u}(\mathbf{y}) = (1 - \mathbf{y}^2)$) becomes linearly unstable at $Re = 5,772$ (Orszag 1971). However, since turbulence appears in experiments at much lower Reynolds numbers, it was conjectured that this bifurcation must be subcritical. Subsequent numerical solution of the nonlinear stability equations (Herbert 1976, Ehrenstein & Koch 1991) demonstrated this to be true, showing that limit cycle solutions with amplitude ϵ branch back to lower Reynolds numbers before subsequently passing through a turning point and curving back toward higher Reynolds numbers. Thus for Reynolds numbers just above the turning point the flow equations have at least four solutions: the fixed point; two unstable limit cycles; and a chaotic solution (experimentally observed turbulence). Determining the location of the turning point in $(\alpha, \beta, \epsilon, Re)$ space is known as the minimum-critical-Reynolds-number problem, and its solution is by no means complete.

One way to investigate the turning point problem is to perform DNS of channel flow for conditions believed to be near this critical condition. Beginning with a known turbulent initial condition from higher Reynolds number, one integrates the flow solver in time at the target Reynolds number to determine whether the flow decays back to the fixed point or sustains itself as turbulence. Although this may not be the most efficient way to bracket the turning point, it has the advantage that the peculiar dynamics of the flow near the turning point, whether in

decay or sustained turbulence, are observable, and this yields information about the path along which flows become turbulent at these low Reynolds numbers.

Unfortunately the flow dynamics are very peculiar near the turning point, and extremely long chaotic transients are observed in the computations that make a fine determination of that point all but impossible by this method. This can be seen in Fig. 5.2, where a time history of the turbulent energy in a channel flow (energy above that in the laminar flow) is plotted for a Reynolds number of 2,191. To understand the time scale of the phenomenon some experimental facts need to be recalled. In typical experimental investigations of channel flow, the infinite transverse and streamwise extent of the ideal flow are approximated by studying flow in high aspect ratio (10-40) rectangular ducts that typically are 50-100 duct heights long. If times are non-dimensionalized by the centerline mean velocity U_∞ and the duct half height L , then statistics on turbulence are gathered by averaging hot-wire data over intervals $\Delta t U_\infty / L \sim 200$. In the simulations and figure the time scale is based on the friction velocity u_τ and L , where typically $15-20 u_\tau \sim U_\infty$. Thus averaging over intervals $\Delta t u_\tau / L \sim 10$ should and does yield stable flow statistics that compare well with experiments. This can be seen in Figs. 5.3-5.5, where the near-wall velocity profile, cross-channel turbulence intensities, and Reynolds and shear stress distribution for the $\Delta t u_\tau / L \sim 10$ interval near the end of the transient, delineated by the arrows in Fig. 5.2, are shown. In each case they correspond well to available experimental data. Yet look at the time scale of the transient; it spans $\Delta t u_\tau / L \sim 300$, thirty times longer than the time needed to obtain stable statistics that would convince most experimentalists that they are viewing a fully developed turbulent channel flow. This is further complicated by the wide variation of the transient length, dependent upon both the grid resolution (number of modes in the spectral representation) and the linearly stable time step of the integration. In fact, for fixed (α, β, Re) it is possible to obtain sustained turbulence for one time step, but see it rapidly decay to the laminar flow for another, lower value of the step.

Extended chaotic transients near bifurcation points are not an unknown phenomenon; the "meta-chaos" of the Lorenz system is but one of many known examples. However, the practicalities of numerical computation in fluid dynamics usually interfere with ones ability to discern whether a transient, or sustained turbulence, is being calculated. The computations required to obtain the transient plot in Fig. 5.2 needed 40 hours of single processor time on a Cray XMP, some ten years ago. Such a small amount of expended time was only possible because the spatial resolution of the calculation was relatively coarse ($32 \times 33 \times 32$), in keeping with the large scales of the phenomena expected at these flow conditions. Higher resolution calculations ($192 \times 129 \times 160$) (Kim et al. 1987) at greater Reynolds numbers typically have taken hundreds of hours (~ 250) to barely obtain the $\Delta t u_\tau / L = 10$ averaging interval that is so inadequate for detecting transients. Because such calculations are so time consuming, one typically chooses an integration time step that is a substantial fraction of the linear stability limit of the algorithm, so as to maximize the calculated "flow time" for expended CPU time. However, it is clear from these transient results that this practice has some dangers when close to critical points of the underlying continuous dynamical system. Thus it appears that just as pseudo-time integration to obtain steady solutions can result in spurious results, genuine time

integration can result in chaotic transients indistinguishable from sustained turbulence, also yielding a spurious picture of the flow for a given Reynolds number.

To conclude this section, here we give a feel for the number of integration steps required for the above numerical solution to get out of the chaotic transient mode. This transient calculation was performed using a time step of .0025. In these same units (time scaled by wall friction velocity u_τ and channel half height L) the transient calculation length was 409.6. Thus this calculation extended over 163,840 time steps.

In Keefe et al. (1992) the dynamics of the computation in terms of ‘‘dimension’’ and ‘‘Lyapunov exponent’’ calculations were performed at a higher Reynolds number $Re = 3200$. For this higher Reynolds number, a transient occurred using a smaller time step of 0.0015 and a transient calculation length of 644.52 or 429,680 time steps. To examine if chaos occurred, Keefe et al. then took a central portion of that calculation at around 45,600 time steps and computed the Lyapunov exponent hierarchy from it. See Keefe et al. for additional details.

5.2. Oscillations Induced by Numerical Viscosities in 1-D Euler Computations

5.2.1. Introduction

Earlier work has reported the difficulty of computing slowly moving shocks (Robert 1990, Woodward & Colella 1984), where first-order Godunov or Roe-type methods produce spurious long wave oscillations behind the shock and eventually ruin the downstream pattern. Here slowly moving means that the ratio of the shock speed to the maximum wave speed in the domain is much less than one. Several heuristic arguments, or improvements on the Riemann solver have been made in Arora & Roe (1996), Jin & Liu (1996), Liu (1995) and Woodward & Colella (1984). To investigate the dynamical behavior of shock-capturing methods for slowly moving shocks, we review the work of Jin and Liu (1996) using the traveling wave analysis and stability theory of discrete shocks. The goal is to carefully study this peculiar numerical phenomenon and to understand its formation and propagation, instead of solving this problem.

Recall that the definition of a discrete traveling wave solution Φ_j^n , an approximation of $U(x_j, t_n)$, $t_n = n\Delta t$, requires

$$\Phi_j^{nq} = \Phi_{j-np}^0, \quad (5.3)$$

where

$$s\Delta t/\Delta x = p/q, \quad (5.4)$$

with s the wave speed for some relative prime integers p and q . During a numerical calculation condition (5.4) may not hold. In other words, at different times the numerical viscous profiles correspond to different families of the traveling waves. It was shown by Jin and Liu that, at different time steps the numerical solutions correspond to different traveling wave profiles, unless (5.4) is met. The downstream oscillations are generated by such perturbations of the discrete traveling wave profile. The oscillations propagate along characteristics and behave

diffusively (decay in ℓ_2 and L_∞). The perturbing nature of the viscous shock (traveling wave) profile is the constant source for the generation of the downstream oscillations for all time.

In their numerical experiments they also observed the periodic structure of the perturbing viscous shock profile. The period is essentially the time for the shock to propagate one spatial grid cell.

In Section 5.2.2 a numerical example, using a Roe-type upwind scheme on a Riemann problem of the compressible Euler equations that admits slow shocks, is given. Among the numerical artifacts observed in this example are the momentum spikes at the shock, and the downstream oscillations. They are indeed numerical artifacts. The momentum spike is generated by the artificial numerical viscosity introduced in the continuity equation, which does not exist in the physical Navier-Stokes equations. The downstream oscillations are introduced by the dynamical behavior of the numerical viscous traveling wave profile. In Section 5.2.3 a traveling wave analysis on a ‘‘viscous isentropic Euler equations’’ formulation (Euler equations with a special linear viscosity term in both the continuity and momentum equations) is presented to show the existence of the momentum spike. This is compared with the momentum profile of the Navier-Stokes equations, which does not have the spike. In section 5.2.4 the dynamics of the downstream oscillations will be examined, and its relation with the stability and perturbation of the discrete shocks will be established. For details see Jin & Liu (1996).

5.2.2. Numerical Solutions of a Slowly Moving Shock

Consider the one-dimensional compressible Euler equations of gas dynamics,

$$\partial_t \rho + \partial_x m = 0, \quad (5.5a)$$

$$\partial_t m + \partial_x (\rho u^2 + p) = 0, \quad (5.5b)$$

$$\partial_t E + \partial_x [u(E + p)] = 0. \quad (5.5c)$$

Here ρ , u , m , p and E are respectively the density, velocity, momentum, pressure and total internal energy per unit volume with $m = \rho u$. For an ideal gas, the equation of state is given by

$$p = (\gamma - 1) \left(E - \frac{1}{2} \rho u^2 \right). \quad (5.6)$$

Let F be the flux function for (5.5) and let A denote the Jacobian matrix $\partial F(U)/\partial U$ with $U = (\rho, m, E)^T$. The Euler equations (5.5) are hyperbolic with eigenvalues

$$a^1 = u - c, \quad a^2 = u, \quad a^3 = u + c, \quad (5.7)$$

where $c = \sqrt{\gamma p / \rho}$ is the local speed of sound. The right eigenvectors of A form the matrix $R = (R^1, R^2, R^3)$ given by

$$R = \begin{bmatrix} 1 & 1 & 1 \\ u - c & u & u + c \\ H - uc & \frac{1}{2}u^2 & H + uc \end{bmatrix}, \quad (5.8)$$

with $H = \frac{c^2}{\gamma-1} + \frac{u^2}{2}$. The inverse of R defines the left eigenvectors $(L^1, L^2, L^3) = R^{-1}$ of A by

$$R^{-1} = \begin{bmatrix} \frac{1}{2}(b_1 + \frac{u}{c}) & \frac{1}{2}(-b_2 u - \frac{1}{c}) & \frac{1}{2}b_2 \\ 1 - b_1 & b_2 u & -b_2 \\ \frac{1}{2}(b_1 - \frac{u}{c}) & \frac{1}{2}(-b_2 u + \frac{1}{c}) & \frac{1}{2}b_2 \end{bmatrix}, \quad (5.9)$$

with

$$b_2 = \frac{\gamma-1}{c^2}, \quad b_1 = b_2 \frac{u^2}{2}. \quad (5.10)$$

Let $\hat{A}_{j+1/2}$ be the Roe matrix satisfying (Roe 1981)

$$F(U_{j+1}) - F(U_j) = \hat{A}_{j+1/2}(U_{j+1} - U_j). \quad (5.11)$$

By projecting $U_{j+1} - U_j$ onto $\{R_{j+1/2}\}$ one obtains the characteristic decomposition

$$U_{j+1} - U_j = \sum_{p=1}^3 \alpha_{j+1/2}^p R_{j+1/2}^p. \quad (5.12)$$

In this decomposition the local characteristic variables $\alpha_{j+1/2}^p$ can be obtained using Roe's average which perfectly resolves stationary discontinuities.

Let $\mathbf{x}_{j+1/2}$ be the grid points, $U_{j+1/2}$ be the pointwise value of U at $\mathbf{x} = \mathbf{x}_{j+1/2}$, and U_j be the cell center value of U at $\mathbf{x}_j = (\mathbf{x}_{j+1/2} + \mathbf{x}_{j-1/2})$. A first-order upwind, Roe-type scheme (Smoller 1983), hereafter called UW, will be used to illustrate the phenomenon, although this phenomenon occurs for basically all shock-capturing methods. The numerical flux in UW is defined by

$$F_{j+1/2} = \frac{1}{2} \left[F(U_j) + F(U_{j+1}) \right] - \frac{1}{2} \text{sgn}(\lambda_{j+1/2}^p) (\gamma_{j+1}^p - \gamma_j^p) R_{j+1/2}^p, \quad (5.13a)$$

where γ_j^p is the component of $F(U_j)$ in the p -th characteristic family,

$$F(U_j) = \sum_{p=1}^3 \gamma_j^p R_j^p. \quad (5.13b)$$

Example: A Riemann problem using the following initial data (Roberts 1990) will be solved. In this problem, there is a Mach-3 shock moving to the right with a shock speed $s = 0.1096$:

$$U_L = \begin{bmatrix} 3.86 \\ -3.1266 \\ 27.0913 \end{bmatrix} \quad \text{if } 0 \leq \mathbf{x} < 0.5; \quad U_R = \begin{bmatrix} 1 \\ -3.44 \\ 8.4168 \end{bmatrix} \quad \text{if } 0.5 \leq \mathbf{x} \leq 1. \quad (5.14)$$

Here $\gamma = 1.4$ and the results at $t = 0.95$ are displayed in Fig. 5.6. The computation is carried out in the domain $[0, 1]$ with $\Delta \mathbf{x} = 0.01$, $\Delta t = 0.001$. One can see that there is a momentum spike and the post-shock solution is oscillatory.

5.2.3. The Momentum Spikes

A traveling wave analysis on the ‘‘viscous Euler equations’’ shows precisely the formation of the momentum spike. Consider the following ‘‘special viscous isentropic Euler equations’’ for density ρ and momentum m :

$$\partial_t \rho + \partial_x m = \epsilon \partial_{xx} \rho, \quad (5.15a)$$

$$\partial_t m + \partial_x \left[\frac{m^2}{\rho} + p(\rho) \right] = \epsilon \partial_{xx} m. \quad (5.15b)$$

Here the pressure $p(\rho) = k\rho^\gamma$ for some constants k and γ . This hyperbolic system has two distinct eigenvalues $u \pm c$, where $u = m/\rho$ is the velocity and $c = \sqrt{\gamma k \rho^{\gamma-1}}$ is the sound speed. Although the true numerical viscosity is far more complicated than those appearing on the right-hand-side of (5.15), a study on (5.15) is sufficient for a full understanding of the numerical momentum spike.

The traveling wave solution to (5.15) is examined. Let $\xi = \frac{x-st}{\epsilon}$, where s is the shock speed. Then the traveling wave solution takes the form

$$\rho(x, t) = \phi(\xi), \quad m(x, t) = \psi(\xi) \quad (5.16)$$

with asymptotic states

$$\phi(\pm\infty) = \phi_\pm, \quad \psi(\pm\infty) = \psi_\pm. \quad (5.17)$$

The Rankine-Hugoniot jump conditions require

$$-s(\phi_+ - \phi_-) + (\psi_+ - \psi_-) = 0, \quad (5.18a)$$

$$-s(\psi_+ - \psi_-) + \left[\frac{\psi_+^2}{\phi_+} + p(\phi_+) - \frac{\psi_-^2}{\phi_-} - p(\phi_-) \right] = 0. \quad (5.18b)$$

First, the shock is assumed stationary ($s = 0$). It corresponds to the eigenvalue $u - c$. Then the jump condition (5.18) reduces to

$$\psi_+ = \psi_-, \quad \frac{\psi_+^2}{\phi_+} + p(\phi_+) = \frac{\psi_-^2}{\phi_-} + p(\phi_-), \quad (5.19)$$

and the Lax entropy condition gives

$$0 < u_- - c_- < u_- + c_-, \quad u_+ - c_+ < 0 < u_+ + c_+, \quad (5.20)$$

where $u_\pm = \psi_\pm/\phi_\pm$ and $c = \sqrt{k\gamma\phi^{\gamma-1}}$.

Applying the traveling wave solution (5.16) in (5.15) one gets the following ODEs:

$$\partial_\xi \phi = \psi - \psi_-, \quad (5.21a)$$

$$\partial_\xi \psi = \frac{\psi^2}{\phi} + p(\phi) - \frac{\psi_-^2}{\phi_-} - p(\phi_-). \quad (5.21b)$$

This system has two fixed points: $V_+ = (\phi_+, \psi_-)$ on the right and $V_- = (\phi_-, \psi_-)$ on the left in the phase plane of (ϕ, ψ) . It has two distinct eigenvalues, $\lambda_1 = u - c$ and $\lambda_2 = u + c$, with corresponding eigenvectors $R_1 = (1, u - c)^T$ and $R_2 = (1, u + c)^T$. By the entropy condition (5.20), V_+ is a saddle point with a stable manifold on R_1 , and V_- is a source. Thus a heteroclinic orbit O will connect V_- and V_+ in the direction of R_1 (Smoller 1983), as shown in Fig. 5.7. (In Fig. 5.7 R_1^\pm and R_2^\pm are the two eigenvectors at V_\pm respectively). The orbit O is smooth, and $\partial_\xi \phi$ is not identically zero if $\phi_- \neq \phi_+$. Thus (5.21a) implies that ψ is not a constant. Moreover, whenever $\phi(\xi)$ connects ϕ_- and ϕ_+ with a monotone profile, $\partial_\xi \phi$ becomes a spike. Thus $\psi = \partial_\xi \phi + \psi_-$ is a spike.

For a nonstationary shock, the traveling wave solution (5.16) applied to (5.15a) gives

$$\partial_\xi \phi = -s(\phi - \phi_-) + \psi - \psi_-, \quad (5.22)$$

or

$$\psi = s\phi + \partial_\xi \phi + (\psi_- - s\phi_-). \quad (5.23)$$

Hence ψ is a superposition of a monotone profile $s\phi$ with a spike corresponding to $\partial_\xi \phi$. When s is small (for a stationary or a slowly moving shock), the monotone profile $s\phi$ becomes small and the spike term $\partial_\xi \phi$ dominates. Thus the shock profile of ψ is a non-monotone spike. Therefore the spike is usually generated in a stationary or slowly moving shock, as shown in the earlier examples. For a strong shock the monotone profile $s\phi$ dominates so the shock profile of the momentum is monotone.

Since the more physical viscous shock profile is determined by that of the Navier-Stokes equations, the viscous profile of the isentropic Navier-Stokes equations is now studied and compare it with that of the viscous Euler equations (5.15). The isentropic Navier-Stokes equations are

$$\partial_t \rho + \partial_\bullet m = 0, \quad (5.24a)$$

$$\partial_t m + \partial_\bullet \left[\frac{m^2}{\rho} + p(\rho) \right] = \epsilon \partial_{\bullet\bullet} \left(\frac{m}{\rho} \right). \quad (5.24b)$$

Applying the traveling wave solution (5.16) in (5.24) and again assuming the shock speed $s = 0$, one obtains the following ODEs:

$$\psi \equiv \psi_-, \quad (5.25a)$$

$$\partial_\xi \left(\frac{\psi}{\phi} \right) = \frac{\psi^2}{\phi} + p(\phi) - \frac{\psi_-^2}{\phi_-} - p(\phi_-). \quad (5.25b)$$

Equation (5.25a) shows that ψ is a constant and thus contains no spike. Let $f(\phi) = \frac{\psi^2}{\phi} + p(\phi)$, then (5.25b) becomes

$$\partial_\xi \left(\frac{\psi}{\phi} \right) = f(\phi) - f(\phi_-). \quad (5.26)$$

Since $f(\phi)$ is a strict convex function and $f(\phi_-) = f(\phi_+)$, $f(\phi) - f(\phi_-)$ is always negative between ϕ_- and ϕ_+ . Therefore, $\partial_\xi(1/\phi)$ does not change sign by (5.26). This implies the monotonicity of $1/\phi$ or ϕ .

When $s \neq 0$, applying the traveling wave solution (5.16) in (5.24a) gives

$$\psi = s\phi + (\psi_- - s\phi_-). \quad (5.27)$$

Thus whenever ϕ is monotone so is ψ . This excludes the possibility of a momentum spike for a moving viscous shock in the Navier-Stokes equations.

In conclusion, even if the viscous profile of ϕ of the Navier-Stokes equations (5.24) could be similar to that of the viscous Euler equations (5.15), the profiles of ψ may be significantly different. Since the physically relevant solution of the Euler equations is considered to be the zero viscosity limit of the Navier-Stokes equations, the momentum spike appearing in the viscous Euler equations is totally nonphysical.

By examining the interrelation between the viscous Euler and the Navier-Stokes equation one can come up with a change of variables that recovers the Navier-Stokes equations in an asymptotic sense from the Euler equations. This also motivates a numerical change of variable from the cell-center or cell average momentum to the mass flux, which eliminates the momentum spike exactly. For details see (Jin & Liu 1996). However, what is more catastrophic is the downstream oscillations, which cannot be easily eliminated, as will be studied next.

5.2.4. The Downstream Oscillations

Note that almost all shock-capturing methods are in conservative form. Due to the conservation of momentum, the total mass of momentum carried by the spike profile should be compensated by an equal amount of momentum mass elsewhere. This explains the formation of the downstream waves.

Figure 5.8 shows the result of UW1 for the previous example after 5 time steps to illustrate the formation of the momentum spike and downstream wave. As the density is smeared, the momentum forms a spike and a downstream wave. The spike and the downstream wave carry the same mass so the total momentum is conserved.

In order to demonstrate that the downstream oscillations propagate along characteristics and are diffusive, the Roe decomposition (5.12) is used, where α^p represents the component of $U_{j+1} - U_j$ in the p -th characteristic family. The numerical ‘‘characteristic’’ variable is defined as

$$\beta_j^p = \sum_{i \leq j} \alpha_{i+1/2}^p \Delta x. \quad (5.28)$$

A distinction between the dispersive oscillations associated with center difference schemes and the downstream oscillations studied here is that the latter lie only in their own characteristic

family. For example a wave which appears in β^p does not appear in β^q for $p \neq q$. These can be seen in Fig. 5.9 where each wave moves away with the corresponding characteristic speed, and behaves diffusively (spread out and decay).

Figure 5.10 displays the time evolution of the momentum profile of the first-order Roe's scheme for the same example. One can see that the spike (viscous) profile keeps fluctuating in an $O(1)$ manner, causing the downstream oscillations for all time. The diffusive nature of the downstream oscillations is evident in the picture.

Figure 5.11 shows the peak of the momentum spike as a function of time. The fluctuating nature of the spike is evident. *The more the mass of the spike profile varies the more strongly the diffusion waves emerge for momentum conservation.* Interesting is that *the peaks are periodic, with the duration of each period agreeing with the time for the shock to move one grid point.* Consequently, the discrete shock profile is stable only modulo this period. However, within each period it is fluctuating, which becomes the source of the new downstream waves.

Recall that the definition of a discrete traveling wave solution Φ_j^n , an approximation of $U(x_j, t_n)$, $t_n = n\Delta t$, requires $\Phi_j^{nq} = \Phi_{j-np}^0$, where $s\Delta t/\Delta x = p/q$ for some relative prime integers p and q . The stability of such a discrete shock for the Lax-Friedrichs scheme was established by Jennings (1974) for scalar equations and by Majda and Ralston (1979) and Liu & Xin (1993) for nonlinear systems. The periodicity of the momentum peaks in Fig. 5.11 shows the stability of the discrete traveling wave solution Φ_j^n for these schemes' modulo the time for the shock to travel one grid point. This is because, when $s\Delta t \ll \Delta x$, there exists a sufficiently large q such that $|q(s\Delta t) - \Delta x| < s\Delta t$, or $|s\Delta t/\Delta x - 1/q| \leq 2/q^2$. However, within each period the numerical shock layer is unsteady and corresponds to different traveling wave profiles, which become the source of the new downstream waves in all time for these schemes.

A scheme that completely eliminates the downstream oscillations in later time should have a steady viscous profile beyond the initial formation of the spike; i.e., the momentum spike peak should remain a constant in later time. However, this is impossible as long as the shock is moving and it takes many times for the shock to move to the next cell.

The discrete shock profile perturbs even when the shock does not move slowly. Thus the downstream oscillations exist even for fast shocks. However, in the fast shock case the momentum profile is monotone and thus does not leave much room for the shock profile to perturb. In other words, each perturbation does not change the mass of the viscous profile much, and the downstream errors become negligible. For slow shocks the momentum profile has a spike, which increases the mass of the viscous profile and the relative mass change in each perturbation. Therefore, the downstream errors become more significant. This also illustrates why the downstream errors in the density are far less significant. Since the density is monotone, the relative change in the mass of the viscous profile is smaller than that of the momentum.

In summary, although each family of the downstream waves decay time-asymptotically, the perturbing spike or viscous profile is a constant source for the generation of new downstream

waves, causing the downstream noise for *all* time. Higher order methods use higher order interpolations, which amplify the noise and exhibit rich but spurious post-shock structures.

5.2.5. Discussions and Conclusions

As studied in (Jin & Liu 1996), similar behavior occurs in schemes that are of monotone, TVD or ENO type. Note that all these monotonicity theories are established only for scalar equations, or linear systems via the characteristic variables. For nonlinear systems there are no global characteristic variables. Thus these methods are usually extended to nonlinear systems using the idea for linear systems; i.e., via the so-called local characteristic decomposition (using the Roe matrix example). Since there is no theory for the monotonicity of these methods for nonlinear systems, it is not surprising to see the non-monotone behavior represented by the spike and the downstream oscillations reported here. As pointed out by Jin & Liu (1996), to fully solve this problem, instead of applying scalarly monotone, TVD or ENO scheme to nonlinear systems, one may need a method that is *systematically* ‘monotone, TVD or ENO’. One may also need to choose numerical viscosity properly so it mimics the physical viscosity of the Navier-Stokes equations. The ultimate goal is to have a scheme that not only provides a high resolution but, more importantly, has a more stable viscosity profile.

The novelty of the work of Jin and Liu is that they are the first to use the traveling wave analysis to prove the non-monotonicity of the solution for nonlinear systems, and to link the downstream oscillations to the stability of discrete traveling wave profile. To really understand the behavior of shock-capturing methods for nonlinear systems, and to ultimately design nonoscillatory schemes for nonlinear systems, good theories for both inviscid and viscous nonlinear systems need to be developed. This remains an open and challenging research subject for the future.

5.3. Spurious Vortices in Under-Resolved Incompressible Thin Shear Layer Flow Simulations

Brown & Minion (1995) performed a thorough study of a Godunov-projection method and a fourth-order central difference method for the two-dimensional incompressible Navier-Stokes equations as a function of the resolution of the computational mesh with the rest of the physical and discretized parameters fixed. In the authors’ opinion, this is a good example of isolating the cause of the spurious behavior. The physical problem is a doubly periodic double shear layer. The shear layers are perturbed slightly at the initial time, which causes the shear layer to roll up in time into large vortical structures. For a chosen shear layer width that is considered to be thin and a fixed perturbation size, they compared the solution for four different grid sizes (64×64 , 128×128 , 256×256 , 512×512) with a reference solution using a grid size of 1024×1024 . For the 256×256 grid, a spurious vortex was formed midway between the periodically repeating main vortex on each shear layer. The 128×128 solution showed three spurious vortices along the shear layer. The spurious vortex disappeared with a 512×512 mesh. They also disabled the limiters (a strictly upwind Fromm’s method), and found the

behavior to be similar. They also cited other work using Lax-Wendroff type and ENO schemes where similar behavior was observed. They concluded that the spurious vortex is the artifact of underresolution of the grid. Linking this behavior with a re-interpretation of their conclusion using nonlinear dynamics, we interpret their observation as follows. For the particular grid size and time step combination, stable spurious equilibrium points were introduced by the numerics into a portion of the flow field while the major portion of the flow field was predicted correctly. In other words, the spurious vortices are the solution of the discretized counterpart for that particular range of grid size and time step. The number of stable spurious vortices is a function of the grid size. As the grid spacing decreases, the spurious equilibriums gradually become unstable and the numerical solution mimics the true solution.

5.4. Convergence rate for systems of hyperbolic conservation laws

In Section 4.2.1 the system (4.7a), (4.7b) was solved with the initial data

$$u_0(x) = \begin{cases} 1 & x \leq 0 \\ -1 & x > 0 \end{cases}, \quad v_0(x) = 1. \quad (5.29)$$

The exact solution is then independent of time. In order to see the dynamical behavior of the error propagating from the shock, here a time dependent problem is solved instead. This can be accomplished by changing to a different initial data. Sjogreen (1996) use the initial data

$$u_0(x) = \begin{cases} 1 & x \leq 0 \\ -1 & x > 0 \end{cases} \quad v_0(x) = \sin \pi x \quad (5.30)$$

for the same system of partial differential equations (4.7). With these data, the exact solution is

$$u(x, t) = u_0(x) \quad v(x, t) = \sin \pi(x - t). \quad (5.31)$$

He solves the problem numerically on the interval $-1 \leq x \leq 1$, using 100 uniformly distributed grid points. The numerical method is again a fully second order accurate scheme of ENO type in space, and a second order accurate Runge-Kutta method in time. The exact value $v(-1, t) = \sin \pi(-1 - t)$ is given on the left boundary and second order accurate extrapolation is used at the boundary $x = 1$.

Figure 5.12 shows the u and v -components of the solution at the time 0.265958, computed on 100 grid points. There is an error in the v component, similar to what can be seen in Figure 4.2. However here it is harder to see it in the plot, since the sine wave solution forces a different scaling of the y -axis.

A better way of seeing the error is in Fig. 5.13, where the logarithm of the pointwise error in the v component is plotted against x . The three plots correspond to 30, 100, and 200 time steps respectively. A domain of first order grid convergence is propagating out from the shock, seen as a flat region of large error in the plots. The first order convergence in this region was, in this

case, obtained from numerical experiments, although analytical examples are also possible (see Engquist & Sjogreen (1995)).

VI. Concluding Remarks

The need for the study of dynamics of numerics is prompted by the fact that the type of problem studied using CFD has changed dramatically over the past decade. CFD is also undergoing an important transition and it is increasingly used in nontraditional areas. But even within its field, many algorithms widely used in practical CFD applications were originally designed for much simpler problems, such as perfect or ideal gas flows. As can be seen in the literature, a straightforward application of these numerical methods to high speed flows, nonequilibrium flows, advanced turbulence modeling or combustion related problems can lead to wrong results, slow convergence, or even nonconvergent solutions. The need for new algorithms and/or modification and improvement to existing numerical methods in order to deal with emerging disciplines is evident. We believe the nonlinear dynamical approach for CFD can contribute to the success of this goal. The first step toward achieving this goal is to understand the nonlinear behavior, limits and barriers, and to isolate spurious behavior of existing numerical schemes.

We have revealed some of the causes of spurious phenomena due to the numerics in an attempt to improve the understanding of the effects of numerical uncertainties in CFD. We illustrated with practical CFD examples that exhibit similar properties and qualitative behavior as elementary examples in which the full dynamical behavior of the numerics can be analyzed. We have also shown that guidelines developed using linearization methods are not always valid for nonlinear problems. Even well-informed use of conventional methods may lead to nonsense on unconventional problems. We have gained an improved understanding of long time behavior of nonlinear problems and nonlinear stability, convergence and reliability of time-marching approaches. We have learned that numerics can introduce and suppress chaos and can also introduce chaotic transients and the danger of relying on numerical tests (e.g., direct numerical simulation) for the onset of turbulence and chaos is evident. The nonlinear phenomenon and spurious behavior exhibited by the numerics in solving genuinely nonlinear problems reveal many of the limitations, challenges and barriers in CFD. We believe the knowledge gained so far has already provided some improved guidelines for overcoming the spurious behaviors without resorting entirely to the tuning of computational parameters. Since standard procedures such as using physical guidelines, grid refinement, halving of the time step, and using more than one scheme to assure the quality, reliability and the integrity of the numerical solution for stiff and strongly nonlinear problems are not foolproof and/or not always possible, the dynamical systems approach can be a viable complement. Before additional theories are established, we conclude that the safest route is to have some understanding of the dynamical behavior, limits and barriers of the numerical method being used.

As can be seen, recent advances in dynamics of numerics showed the advantage of adaptive step size error control for long time integrations of nonlinear ODEs. Although much research

is needed to construct suitable yet practical similar adaptive methods for PDEs, these early developments lead our way to future theories. There remains the challenge of constructing adaptive step size control methods that are suitable yet practical for time marching to the steady states for aeronautical CFD applications. Another even more challenging area is the quest for an adaptive numerical scheme that leads to guaranteed and rapid convergence to the correct steady-state numerical solutions. These two key challenges are particularly important for CFD. We conclude the paper with the following guidelines to minimize spurious dynamics in time-marching to the steady state.

Some Guidelines to Minimize Spurious Dynamics: Due to the spurious dynamics introduced by the numerics, one usually will not be able to map out the complete numerical basins of attraction and bifurcation diagrams for the entire problem in practical situations. Only in isolated situation with a particular physical problem and numerical method combination such as the one studied in Lafon & Yee (1991, 1992) are continuation methods able to locate all of the essential spurious branches of the bifurcation curves.

On the other hand, continuation methods are widely used in dynamical systems when one wants to understand certain properties of key branches of the bifurcation curve, especially if one knows (or can ascertain by other means) a starting solution on that particular branch. For example, in the Taylor-Couette flow problem, extensive use is made of continuation methods to map out the critical Reynolds number when the flow behavior undergoes drastic changes in flow patterns, since in this case we know how the flow behaves for the low Reynolds number case. Another example is in Bailey and Beam (1991) who used it to study the hysteresis behavior of the flow of an airfoil in terms of angles of attack for the steady PDEs. In this case, the flow behavior is readily obtained for low angles of attack (before hysteresis). Most of the use of the continuation method so far is focused on elliptic PDEs or steady PDEs. These studies seldom address the possibilities of spurious dynamics due to the numerics, especially for IBVPs using time-marching approaches. It is remarked that a shortcoming in association with solving the steady PDEs is that a small radius of convergence or nonconvergence of the numerical solution is often encountered even with the aid of multigrid, preconditioners, and/or relaxation methods, especially when the PDEs are of the mixed type (e.g., the steady inviscid supersonic flow over a blunt body). In addition, the solutions obtained do not distinguish whether the steady states are stable or not.

Besides the study in Lafon & Yee (1991, 1992), here we propose a further step of applying this technique to the discretized counterparts of the time-dependent PDEs in order to avoid spurious asymptotes due to unknown initial data. The idea relies on the knowledge of a known or a reliable numerical solution on the correct (non-spurious) branch of the bifurcation curve as a function of the physical parameter of interest. The logic is that if one starts on the correct branch, one avoids getting trapped on any of the spurious branches. Also the issue of unknown initial data related to time-marching approaches is avoided or can be minimized. Details of the approach and numerical examples will be reported in a forthcoming paper. Here we will give a short narrative summary of the procedure.

In many fluid problems where the solution behavior is well known for certain values of the physical parameters, but unknown for other values. For these other values of the parameters, the problem might become very stiff and/or strongly nonlinear, making the available numerical schemes (or the scheme in use) intractable. In this situation, continuation methods in bifurcation theory can become very useful. If possible, one should start with the physical parameter of a known or reliable steady state (e.g., flow behavior is usually known for low angles of attack but not for high angles of attack). One can then use a continuation method such as the pseudo arclength continuation method of Keller (1977) (or the recent development in this area) to solve for the bifurcation curve as a function of the physical parameter. The equations used are the discretized counterpart of the steady PDEs or the time-dependent PDEs. If time-marching approaches are used, a reliable steady-state numerical solution (as a starting value on the correct branch of the bifurcation curve for a particular value of the physical parameter) is assumed. This starting steady-state numerical solution is assumed to have the proper time step and initial data combination and to have the grid spacing fine enough to resolve the flow feature. The continuation method will produce a continuous spectrum of the numerical solutions as the underlying physical parameter is varied until it arrives at a critical value p_c such that it either experiences a bifurcation point or fails to converge. Since we started on the correct branch of the bifurcation curve, the solution obtained before that p_c should be more reliable than if one starts with the physical parameter in question and tries to stretch the limitation of the scheme. Note that by starting a reliable solution on the correct branch of the bifurcation curve, the dependence of the numerical solution on the initial data associated with time-marching methods can be avoided.

Finally, when one is not sure of the numerical solution, the continuation method can be used to double check the numerical solution. This approach can even reveal the true limitations of the existing scheme. In other words, the approach can reveal the critical physical parameter for which the numerical method breaks down. On the other hand, if one wants to find out the largest possible time step that one can use for a particular problem and physical parameter, one can also use continuation methods to trace out the bifurcation curve as a function of the time step. In this case, one can start with a small time step with the correct steady state and observe the critical time step as it undergoes instability or bifurcation.

Acknowledgments

The authors wish to thank their collaborators David Griffiths, Andre Lafon and Andrew Stuart for contributing to their earlier work. The contributions of Sections 4.2 and 5.4 by Bjorn Sjogreen of the Uppsala University, Section 5.1 by Laurence Keefe of Nielsen Engineering, and Section 5.2 by Shi Jin of Georgia Institute of Technology are gratefully acknowledged. Special thanks to Tom Coakley, Terry Holst and Marcel Vinokur for their critical review of the manuscript.

References

- Adams, E. (1990), "Periodic Solutions: Enclosure, Verification, and Applications," *Computer Arithmetic and Self-Validating Numerical Methods*, Academic Press, pp. 199-245.
- Arora, M. and Roe, P.L. (1996), "On post-shock oscillations due to shock capturing schemes in unsteady flows," *J. Comp. Phys.*, to appear.
- Arriola, L.M. (1993), private communication
- Aves, M.A., Griffiths, D.F. and Higham, D.J. (1995), "Does Error Control Suppress Spuriousity?" To appear in *SIAM J. Num. Analy.*
- Bailey, H.E. and Beam, R.M. (1991), "Newton's Method Applied to Finite-Difference Approximations for the Steady-State Compressible Navier-Stokes Equations," *J. Comput. Phys.*, Vol. 93, PP. 108-127.
- Beam, R.M. and Bailey, H.E. (1988), "Direct Solver for Navier-Stokes Equations," *Proceedings of International Conference on Computational Engineering Science*, Atlanta, GA.
- Beam, R.M. and Warming, R.F. (1978), An implicit Factored Scheme for the Compressible Navier-Stokes Equations, *AIAA J.*, Vol. 16, pp. 293-402.
- Beam, R.M., Warming, R.F. and H.C. Yee (1982), "Stability Analysis for Numerical Boundary Conditions and Implicit Difference Approximations of Hyperbolic Equations," *J. Comp. Physics*, Vol. 48, pp. 200-222.
- Beyn, W.J. and Doedel, E.J. (1981) "Stability and Multiplicity of Solutions to Discretizations of Nonlinear Ordinary Differential Equations," *SIAM J. Sci. Statist. Comput.*, Vol. 2, pp. 107-120.
- Beyn, W.-J. and Lorenz, J. (1982), "Spurious Solutions for Discrete Superlinear Boundary Value Problems," *Computing*, Vol. 28, pp. 43-51.
- Beyn, W.-J. (1987), "On the Numerical Approximation of Phase Portraits Near Stationary Points," *SIAM J. Numer. Anal.*, Vol. 24, pp. 1095-1113.
- Brezzi, F., Ushike S. and Fujii, H. (1984), "Real and Ghost Bifurcation Dynamics in Difference Schemes for Ordinary Differential Equations," *Numerical Methods for Bifurcation Problems*, T. Kupper, H.D. Mittleman and H. Weber eds., Birkhauser-Verlag, Boston.
- Briley, W.R. and McDonald, H. (1977), "Solution of the Multidimensional Compressible Navier-Stokes Equations by a Generalized Implicit Method," *J. Comput. Phys.*, Vol. 24, pp. 372-397.
- Brown, D.L. and Minion, M.L. (1995), "Performance of Under-resolved Two-Dimensional Incompressible Flow Simulations," *J. Comput. Phys.*, Vol. 122, pp. 165-183.
- Budd, C., Huang, W. and Russell, R.D. (1995a), "Moving Mesh Methods for Problems with Blow-Up," *SIAM J. Sci. Stat. Comp.*, to appear.
- Budd, C.J., Stuart, A.M., Koomullil, G.P. and Yee, H.C. (1995b), "Numerical Solution

Behavior of Model Convection-Diffusion BVP with Grid Adaptation,' in preparation.

Burton, P.A. and Sweby, P.K. (1995), "A Dynamical Approach Study of Some Explicit and Implicit TVD Schemes and Their Convergence to Steady-State Solutions," Numerical Analysis Report 5/95, 1995, Department of Mathematics, University of Reading, England.

Butcher, J.C. (1987), *Numerical Analysis of Ordinary Differential Equations*, John Wiley & Son, Chichester.

Casper, J. and Carpenter, M. (1995), "Computational Considerations for the Simulation of Shock-Induced Sound," submitted to SIAM J. Sci. Comput., Oct. 1995.

Chow, S.-N., Hale, J.K. (1982), *Methods of Bifurcation Theory*, Springer-Verlag, New York.

Colella, P., Majda, A. and Roytburd, V. (1986), "Theoretical and Numerical Structure for Reacting Shock Waves," SIAM J. Sci. Stat. Comput., Vol. 7, pp. 1059-1080.

Corless, R.M. (1994a), "Error Backward," *Contemp. Math.* Vol. 172, pp. 31-62.

Corless, R.M. (1994b), "What Good Are Numerical Simulations of Chaotic Dynamical Systems?" *Computers Math. Applic.* Vol. 28, PP. 107-121.

Cosner, R.R. (1995), "CFD Validation Requirements for Technology Transition," AIAA 95-2227, 26th AIAA Fluid Dynamics Conference, June 19-22, 1995, San Diego, CA.

Crocco, L. (1965), "A Suggestion for the Numerical Solution of the Steady Navier-Stokes Equations," *AIAA J.*, Vol 3, pp. 1824-1832.

Dahlquist, G., Edsberg, L. and Skolleremo, G. (1982), "Are the numerical methods and software satisfactory for chemical kinetics?" *Numerical Integration of DE and Large Linear Systems*, J. Hinze, ed., Springer-Verlag, pp. 146-164.

Davoudzadeh, F., McDonald, H. and Thompson, B.E. (1995), "Accuracy Evaluation of Unsteady CFD Numerical Schemes by Vortex Preservation," *Computers & Fluids*, Vol. 24, pp. 883-895.

Deardorff, J. (1970), "A numerical study of three-dimensional turbulent channel flow at large Reynolds number," *J. Fluid Mech.* 41, p453-480.

Demuren, A.O. and Wilson, R.V. (1994), "Estimating Uncertainty in Computations of Two-Dimensional Separated Flows," *Transactions of ASME*, Vol. 116, pp. 216-220.

Devaney, R.L. (1987), *An Introduction to Chaotic Dynamical Systems*, Addison Wesley, New York.

Dieci, L. and Estep, D. (1991), "Some Stability Aspects of Schemes for the Adaptive Integration of Stiff Initial Value Problems," *SIAM J. Sci. Stat. Comput.*, Vol. 12, pp. 1284-1303.

Doedel, E. (1986), "AUTO: Software for Continuation and Bifurcation Problems in Ordinary Differential Equations," *Cal. Tech. Report*, Pasadena, Calif.

Doedel, E.J. and Beyn, W.-J. (1981), "Stability and Multiplicity of Solutions to Discretizations of Nonlinear Ordinary Differential Equations, SIAM J. Sci. Stat. Comp. 2, pp 107-120.

Donat, R. (1994), "Studies on Error Propagation for Certain Nonlinear Approximations to Hyperbolic Equations: Discontinuities in Derivatives," SIAM J. Numer. Anal., Vol. 31, pp. 655-679.

Ehrenstein, U. and Koch, W. (1991), "Nonlinear bifurcation study of plane Poiseuille flow," J. Fluid Mech., Vol. 228, pp. 111-148.

Embid, P., Goodman, J. and Majda, A. (1984), "Multiple Steady States for 1-D Transonic Flow," SIAM J. Sci. Stat. Comput., Vol. 5, pp. 21-41.

Engquist, B. and Sjogreen, B. (1995), "High Order Shock Capturing Methods," *CFD Reviews*, Hafez & Oshima, Eds., John Wiley, New York, pp. 210-233.

Engquist, B. and Sjogreen, B. (1996), "Numerical convergence rate in the presence of shocks," to appear.

Feigenbaum, M.J. (1978) "Quantitative Universality for a Class of Nonlinear Transformations," J. Stat. Phys., Vol. 19, pp. 25-52.

Ferziger, J.H. (1989) "Estimation and Reduction of Numerical Error," Forum on Methods of Estimating Uncertainty Limits in Fluid Flow Computations, ASME Winter Annual Meeting, San Francisco, Dec. 1989.

Friedman, M. (1995), "On Computing Connecting Orbits," presented at the Conference on Dynamical Numerical Analysis, Georgia Institute of Technology, Atlanta, Georgia, Dec. 14-16, 1995.

Gear, C.W. (1971), *Numerical Initial Value Problems in Ordinary Differential Equations*, Prentice-Hall.

Globus, A., Levit, C. and Lasinski, T. (1991), "A Tool for Visualizing the Topology of Three-Dimensional Vector Fields," NAS Applied Research Branch Report RNR-91-017, NASA Ames Research Center.

Godunov, S.K. (1959), "A finite difference method for the numerical computation of discontinuous solutions of the equations to fluid dynamics," Mat. Sb. Vol. 47, pp. 271-290.

Gresho, P. (1996), *Incompressible Flow and the Finite Element Method, Vol. 1*, John Wiley and Sons, Chichester, to appear 1996.

Grebogi, C., Ott, E. and Yorke, J.A. (1983), "Crises, Sudden Changes in Chaotic Attractors, and Transient Chaos," Physica 7D, pp. 181-200.

Grebogi, C., Ott, E. and Yorke, J.A. (1987), Science, Vol. 238, pp. 632-638.

Griffiths, D.F. and Mitchell, A.R. (1988), "Stable Periodic Solutions of a Nonlinear Partial Difference Equation in Reaction Diffusion," Report NA/113, Jan. 1988, Dept. Math. and

Comput. Science, University of Dundee, Scotland U.K.

Griffiths, D.F., Sweby, P.K. and Yee, H.C. (1992a), "On Spurious Asymptotes Numerical Solutions of Explicit Runge-Kutta Schemes," *IMA J. Numer. Anal.* 12, pp. 319-338.

Griffiths, D.F., Stuart, A.M. and Yee, H.C. (1992b), "Numerical Wave Propagation in Hyperbolic Problems with Nonlinear Source Terms," *SIAM J. of Numer. Analy.*, Vol. 29, pp. 1244-1260.

Guckenheimer, J. and Holmes, P. (1983), *Nonlinear Oscillations, Dynamical Systems, and Bifurcations of Vector Fields*, Springer-Verlag, New York.

Gustafsson, B. (1991), "The Euler and Navier-Stokes Equations: Wellposedness, Stability and Composite Grids," von Karman Institute for Fluid Dynamics Lectures Series 1991-01, Feb. 18-22, 1991, Rhode-St-Genese, Belgium.

Gustafsson, B., Kreiss, H.O. and Olinger, J. (1995), *Time Dependent Problems and Difference Methods*, John Wiley and Sons, New York.

Hagstrom, T. and Keller, H.B. (1986), "The Numerical Calculation of travelling Wave Solutions of Nonlinear Parabolic Equations," *SIAM J. Sci. Stat. Comput.*, Vol. 7.

Hale, J. and Kocak, H. (1991), *Dynamics and Bifurcations*, Springer-Verlag, New York.

Hale, J.K. (1994), "Numerical Dynamics," *AMS Contemporary Mathematics*, Vol. 172, Providence, Rhode Island.

Hairer, E., Iserles, A. and Sanz-Serna, J.M. (1989), "Equilibria of Runge-Kutta Methods," *Numer. Math.*, Vol. 58, pp. 243-254.

Handler, P.A., Hendricks, E.W. and Leighton, R.I., (1989), *NRL Memorandum Report 6410*, 1989.

Harten, A., Hyman, J.M. and Lax, P.D. (1976), "On Finite-Difference Approximations and Entropy Conditions for Shocks," *Comm. Pure Appl. Math.*, Vol. 29, pp. 297-322.

Harten, A. (1983), "A High Resolution Scheme for Computation of Weak Solutions of Hyperbolic Conservation Laws," *J. Comp. Phys.*, Vol. 49, pp. 357-393.

Harten, A. (1984), "On a Class of High Resolution Total-Variation-Stable Finite-Difference Schemes," *SIAM J. Num. Anal.*, Vol. 21, pp. 1-23.

Harten, A. and Osher, S. (1987), "Uniformly High-Order Accurate Nonoscillatory Schemes I," *SIAM J. Num. Analy.* Vol. 24, pp. 279-309.

Harten, A., Osher, S., Engquist, B. and Chakravarthy, S. (1986), "Some Results on Uniformly High Order Accurate Essentially Non-oscillatory Schemes," *ICASE Report 86-18*, Mar. 1986.

Harten, A. (1986), "On High-Order Accurate Interpolation for Non-Oscillatory Shock-Capturing Schemes," *The IMA Volumes in Mathematics and its Applications*, Vol. 2, Springer-Verlag, pp. 71-106.

Henon, M. (1976), "A Two Dimensional Mapping with a Strange Attractor," *Commun. Math. Phys.*, Vol. 50, pp. 69-77.

Herbert, Th. (1976), *Lecture Notes in Physics 59*, Springer-Verlag, p235.

Higham, D.J. and Stuart, A.M. (1995), "Analysis of the Dynamics of Local Error Control via a Piecewise Continuous Residual," to appear.

Hoppensteadt, F.C. (1993), *Analysis and Simulation of Chaotic Systems*, Springer-Verlag, New York.

Hsu, C.S. and Yee, H.C. (1975), "Behavior of Dynamical Systems Governed by a Simple Nonlinear Difference Equation," *J. Appl. Mech.*, Vol. 44, pp. 870-876.

Hsu, C.S. (1987), *Cell-to-Cell Mapping*, Springer-Verlag, New York.

Humphries, A.R. (1992) Spurious Solutions of Numerical Methods for Initial Value Problems, *IMA J. Num. Anal.*, Vol. 12.

Hung, C.M., Sung, C.H. and Chen, C.L. (1991), "Computation of Saddle Point of Attachment," AIAA-91-1713, AIAA 22nd Fluid Dynamics, Plasma Dynamics and Lasers Conference, Honolulu, Hawaii.

IMSL Math Library, Fortran Subroutines for Mathematical Applications, 1 (1989).

Iserles, A. (1988), "Stability and Dynamics of Numerical Methods for Nonlinear Ordinary differential Equations," DAMTP 1988/NA1, University of Cambridge, Cambridge England.

Iserles, A., Peplow, A.T. and Stuart, A.M. (1990) A Unified Approach to Spurious Solutions Introduced by Time Discretisation, Part I: Basic Theory, DAMTP 1990/NA4, Numerical Analysis Reports, University of Cambridge.

Jackson, E.A. (1989), *Perspectives of Nonlinear Dynamics*, Vol. I, Cambridge University Press, New York.

Jameson, A. (1991), "Airfoils Admitting Nonunique Solutions to the Euler Equations," AIAA-91-1625.

Jennings, G. (1974), "Discrete shocks," *Comm. Pure Appl. Math.* 27, pp. 25-37.

Jin, S. and Liu, J.-G. (1996), "The effects of numerical viscosities, I: the slowly moving shocks," *J. Comp. Phys.*, to appear.

Johnson, C. (1995), "On Computability and Error Control in CFD," *Inter. J. Num. Meth. in Fluids*, Vol. 20, pp. 777-788.

Johnson, C., Rannacher, R. and Boman, M. (1995), "Numerics and Hydrodynamics Stability: Toward Error Control in Computational Fluid Dynamics," *SIAM J. Numer. Analy.*, Vol. 32, pp. 1058-1079.

Jung, W.J., Mangiavacchi, N. and Ahkavan, R. (1992), "Suppression of turbulence in wall bounded flow by high frequency spanwise oscillations," *Phys. Fluids A*, Vol. 4, pp. 1605-1607.

Keefe, L., Moin, P. and Kim, J. (1992), "The Dimension of Attractors Underlying Periodic Turbulent Poiseuille Flow," *J. Fluid Mech.*, Vol. 242, pp. 1-29.

Keefe, L. (1996), unpublished; private communication.

Keener, J.P. (1987), *Pitman Research Notes 157, Ordinary and Partial Differential Equations*, edited by B.D. Sleeman and R.J. Jarvis, Longman Sci. Tech., Harlow, p. 95-112.

Keller, H.B. (1977), "Numerical Solution of Bifurcation and Nonlinear Eigenvalue Problems," *Applications of Bifurcation Theory*, P.H. Rabinowitz, ed., Academic Press, pp. 359-384.

Kellogg, R.B., Shubin, G.R. and Stephens, A.B. (1980), "Uniqueness and the Cell Reynolds Number," *SIAM J. Numer. Anal.* Vol. 17, pp. 733-739.

Kim, J., Moin, P. and Moser, R. (1987), "Turbulence statistics in fully developed channel flow at low Reynolds number," *J. Fluid Mech.*, Vol. 177, pp. 133-166.

Klopper, G. and Yee, H.C. (1988), "Viscous Hypersonic Shock on Shock Interaction on Blunt Cowl Lips," AIAA-88-0233, AIAA 26th Aerospace Sciences Meeting, Jan. 11-14, 1988, Reno, Nevada, paper accepted by AIAA J.

Kreiss, H-O. and Lundqvist, E. (1968), "On Difference Approximations with Wrong Boundary Values," *Math. Comp.*, Vol. 22, pp. 1-12.

Kubicek, M. and Marek, M. (1983), *Computational Methods in Bifurcation Theory and Dissipative Structures*, Springer-Verlag, New York.

Lafon, A. and Yee, H.C. (1991), "Dynamical Approach Study of Spurious Steady-State Numerical Solutions for Nonlinear Differential Equations, Part III: The Effects of Nonlinear Source Terms in Reaction-Convection Equations," NASA Technical Memorandum 103877, July 1991; to appear, *Intern. J. of CFD*, 1996.

Lafon, A. and Yee, H.C. (1992), "Dynamical Approach Study of Spurious Steady-State Numerical Solutions of Nonlinear Differential Equations, Part IV: Stability vs. Numerical Treatment of Nonlinear Source Terms," ONERA-CERT Technical Report DERAT 45/5005.38, to appear in *Intern. J. CFD*, 1996

Lambert, J.D. (1973), *Computational Methods in Ordinary Differential Equations*, John Wiley, New York.

Langford, W.F. and Iooss, G. (1980), "Interactions of Hopf and Pitchfork Bifurcations," *ISNM 54, Bifurcation Problems and Their Numerical Solution*, Workshop on Bifurcation Problems and Their Numerical Solution, Dortmund, ed. H.D. Mittelman and H. Weber, Birkhauser Verlag, Basel, pp. 103-134.

Lerat, A. and Sides, J. (1988), "Efficient Solution of the Steady Euler Equations with a Centered Implicit Method," *Numerical Methods for Fluid Dynamics III*, K.W. Morton and M.J. Baines Eds., Clarendon Press, Oxford, pp. 65-86

LeRoux, A.Y. (1977) "A Numerical Conception of Entropy for Quasi-Linear Equations," *Math. Comput.*, Vol. 31, pp. 848-872.

LeVeque, R.J. and Yee, H.C. (1990), "A Study of Numerical Methods for Hyperbolic Conservation Laws with Stiff Source Terms," J. Comput. Phys., Vol. 86, pp. 187-210.

Lin, H.-C. (1995), "Dissipation additions to flux-difference splitting," J. Comp. Phys., Vol. 117, pp. 20-27.

Liu, J.-G. and Xin, Z.P. (1993) "Nonlinear stability of discrete shocks for systems of conservation laws," Arch. Rat'l Mech. Anal., Vol. 125, pp. 217--256.

Lorenz, E.N. (1989) "Computational Chaos -- A Prelude to Computational Instability," Physica D, Vol. 35, pp. 299-317.

MacCormack, R.W. (1969), "The Effect of Viscosity in Hypervelocity Impact Cratering," AIAA Paper No. 69-354, Cincinnati, Ohio, 1969.

Majda, A. and Ralston, J. (1979), "Discrete shock profiles for systems of conservation laws," Comm. Pure Appl. Math., Vol. 32, pp. 445-483.

Majda, A. and Osher, S. (1979), "Numerical Viscosity and the Entropy Condition," Commun. Pure Appl. Math., Vol. 32, pp. 797-838.

MAPLE (algebraic manipulation package), University of Waterloo, Canada, 1988.

Marvin, J.G., and Holst, T.L. (1990), "CFD Validation for Aerodynamic Flows -- Challenge for the 90's," AIAA-90-2995, 8th AIAA Applied Aerodynamics Conference, Portland OR, Aug. 1990.

Marvin, J.G. (1993), "Dryden Lectureship in Research, A Perspective on CFD Validation," AIAA-93-0002, 31st AIAA Aerospace Sciences Meeting, Reno, NV, Jan. 1993.

Mehta, U. (1995), "Guide to Credible Computational Fluid Dynamics Simulations," AIAA-95-2225, 26th AIAA Fluid Dynamics Conference, June 19-22, 1995, San Diego, CA.

Melnik, R.E., Siclari, M.J., Barber, T. and Verhoff, A. (1994), "A Process for Industry Certification of Physical Simulation Codes," AIAA-94-2235, 25th AIAA Fluid Dynamics Conference, June 20-23, 1994, Colorado Springs, CO.

Mitchell, A.R. (1976), *Computational Methods in Partial Differential Equations*, Wiley and Son, New York.

Mitchell, A.R. and Griffiths, D.F. (1985), "Beyond the Linearized Stability Limit in Non Linear Problems," Report NA/88 July 1985, Department of Mathematical Sciences, University of Dundee, Scotland U.K.

Mitchell, A.R. and Bruch, J.C., Jr. (1985), "A Numerical Study of Chaos in a Reaction-Diffusion Equation," Numerical Methods for PDEs, Vol. 1, pp. 13-23.

Mitchell, A.R., Stein, G. and Maritz, M. (1988) "Periodic Structure Beyond a Hopf Bifurcation," Comm. Appl. Num. Meth., Vol. 4, pp. 263-272.

Mitchell, A.R. and Schoombie, S.W. (1989), "Nonlinear Diffusion and Stable Period 2 Solutions of a Discrete Reaction-Diffusion Model," J. Comp. Appl. Math., Vol 25, pp.

363-372.

Moin, P., and Kim, J. (1982), "Numerical investigation of turbulent channel flow," *J. Fluid Mech.*, Vol. 118, pp. 341-378.

Moore, D.R., Weiss, N.O. and Wilkins, J.M. (1990), "The Reliability of Numerical Experiments: Transitions to Chaos in Thermosolutal Convection," *Nonlinearity*, Vol. 3, pp. 997-1014.

Moretti, G. and Abbett, M., (1966), "A Time-Dependent Computational Method for Blunt Body Flows," *AIAA Journal*, Vol. 4, pp. 2136-2141.

Mulard, V. and Moules, G. (1991), "Non-equilibrium Viscous Flow calculations in Hypersonic Nozzles," *Proceedings of the Workshop on Hypersonic Flows for Reentry Problems, Part II, Antibes, France, 15-19 April 1991.*

Mulder, W.A. and van Leer, B. (1984) "Experiments with Implicit Upwind Methods for the Euler Equations," *J. Comput. Phys.*, Vol. 59, pp. 232-246.

Neil, B. (1994), "An Investigation of the Dynamics of Several Equidistribution Schemes," M.Sc. Dissertation, Department of Mathematics, The University of Reading, England.

Orszag, S. (1971), "Accurate solution of the Orr-Sommerfeld stability equation," *J. Fluid Mech.*, Vol. 50, pp. 689-703.

Panov, A.M. (1956), "Behavior of the Trajectories of a System of Finite Difference Equations in the Neighbourhood of a Singular Point," *Uch. Zap. Ural. Gos. Univ. vyp.*, Vol. 19, pp. 89-99.

Park, C. (1985), "On Convergence of Chemically Reacting Flows," *AIAA Paper 85-0247, AIAA 23rd Aerospace Sciences Meeting, Jan 14-17 1985, Reno, Nevada.*

Peitgen, H.-O., Saupe, D. and Schmitt, K. (1981), "Nonlinear Elliptic Boundary Value Problems versus Their Finite Difference Approximations: Numerically Irrelevant Solutions," *J. Reine Angew. Mathematik*, Vol. 322, pp. 74-117.

Perron, O. (1929), "Uber Stabilitat und Asymptotisches Uberhalten de Losungen eines Systems endlicher Differenzgleichungen," *J. Reine Angew. Math.*, Vol. 161, pp. 41-64.

Phillips, N.A. (1959), "An Example of Nonlinear Computational Instability," *The Atmosphere and the Sea in Motion*, B. Bolin ed., Rockefeller Institute, New York.

Poliashenko, M. and Aidun, C.K. (1995), "Computational Dynamics of Ordinary Differential Equations," *Intern. J. Bifurcation and Chaos*, Vol. 5, pp. 159-174.

Proceedings of the IMA conference on the Dynamics of Numerics and Numerics of Dynamics, July 31 - August 2, 1990, University of Bristol, Bristol, England.

Pruffer, M. (1985), "Turbulence in Multistep Methods for Initial Value Problems," *SIAM J. Appl. Math.* Vol. 45, pp. 32-69.

Quirk, J.J. (1994), "A contribution to the great Riemann solver debate," *Int'l J. Num. Meth. Fluids*, Vol. 18, pp. 555-574.

Read, P.L. and Thomas, N.P.J. (1995), "An Evaluation of Semi-Lagrangian Advection Schemes in Simulations of Rotating, Stratified Flows in the Laboratory," Submitted to *Quart. J. R. Met. Soc.* May 1995.

Ren, Y. and Russell, R.D. (1992), "Moving Mesh Techniques Based Upon Equidistribution and Their Stability," *SIAM J. Sci. Stat. Comput.*, Vol. 13, pp. 1265-1286.

Richtmyer, R.D. and Morton, K.W. (1967), *Difference Methods for Initial-Value Problems*, Interscience-Wiley, New York.

Roberts, T.W. (1990), "The behavior of flux difference splitting schemes near slowly moving shock waves," *J. Comp. Phys.*, Vol. 90, pp. 141-160.

Roe, P.L. (1981), "Approximate Riemann solvers, parameter vectors, and difference schemes," *J. Comp. Phys.*, Vol. 43, pp. 357-372.

Saad, Y. (1994), "Preconditioning Krylov Subspace Methods for CFD Applications," *Proceedings of the International Workshop on Solution Techniques for Large-Scale CFD Problems*, Habashi, W.G. Editor, Montreal, Canada, Sept. 26-28, 1994.

Salas, M. D., Abarbanel, S. and Gottlieb, D. (1986), "Multiple Steady States for Characteristic Initial Value Problems. *J. App. Numer. Math.*," Vol. 2, pp. 193-210.

Sanz-Serna, J.M. and Vellido, F. (1985), "Nonlinear Instability, the Dynamic Approach," in *Proceedings Dundee*, G.A. Watson and D.F. Griffiths, eds., Pitman, London.

Sanz-Serna, J.M. (1985), "Studies in Numerical Nonlinear Instability I: Why do leapfrog schemes go unstable?," *SIAM J. Sci. Stat. Comput.* Vol. 6, pp. 923-938.

Sanz-Serna, J.M. (1990) "Numerical Ordinary Differential Equations vs. Dynamical Systems," *Applied Math. Comput. Report 1990/3*, Universidad de Valladolid.

Schreiber, R. and Keller, H.B. (1983), "Spurious Solution in Driven Cavity Calculations," *J. Comput. Phys.*, Vol. 49, pp. 310-333.

Schumann, U. (1973) "Ein Verfahren zur direkten numerischen Simulation turbulenter Stromungen in Platten- und Ringspaltkanalen und uber seine Anwendung zur Untersuchung von Tubulenzmodellen," *Dissertation, University of Karlsruhe*. NASA TTF 15391, 1973.

Seydel, R. (1988), *From Equilibrium to Chaos*, Elsevier, New York.

Shu, C.-W. and Osher, S. (1989), "Efficient implementation of essentially non-oscillatory shock-capturing schemes, II," *J. Comp. Phys.*, Vol. 83, pp. 32-78.

Shubin, G.R., Stephens, A.B. and Glaz, H.M. (1981), "Steady Shock Tracking and Newton's Method Applied to One-Dimensional Duct Flow," *J. Comput. Phys.*, Vol. 39, pp. 364-374.

Sleeman, B.D., Griffiths, D.F., Mitchell, A.R. and Smith, P.D. (1988), "Stable Periodic Solutions in Nonlinear Difference Equations," *SIAM J. Sci. Stat. Comput.*, Vol. 9, pp.

543-557.

Sjogreen, B. (1996), private communication.

Spalart, P.R., Moser, R.D. and Rogers, M.M. (1991), "Spectral methods for the Navier-Stokes equations with one infinite and two periodic directions," *J. Comp. Phys.*, Vol. 96, p297.

Smoller, J. (1983), *Shock Waves and Reaction-Diffusion Equations*, Springer-Verlag, New York.

Steger, J. (1978), "Implicit Finite-Difference Simulation of Flow about Arbitrary Two-Dimensional Geometries," *AIAA J.*, Vol. 16, pp. 679-686.

Stephens, A.B. and Shubin, G.R. (1981) "Multiple Solutions and Bifurcation of Finite Difference Approximations to Some Steady Problems of Fluid Dynamics," *SIAM J. Sci. Statist Comput.*, Vol. 2, pp. 404-415.

Stewart, I. (1990), "Bifurcation Theory Old and New," *Proceedings of IMA Conferences on Dynamics of Numerics and Numerics of Dynamics*, Bristol, July 31 - Aug. 2, 1990.

Stuart, A.M. (1989), "Linear Instability Implies Spurious Periodic Solutions," *IMA J. Num. Anal.*, Vol. 9, pp. 465-486.

Stuart, A.M. (1994), "Numerical Analysis of Dynamical Systems," *Acta Numerica*, Cambridge University Press.

Stuart, A.M. (1995), "Probabilistic and Deterministic Convergence Proofs for Software for Initial Value Problems," to appear.

Sweby, P.K. (1984), "High Resolution Schemes using Flux Limiters for Hyperbolic Conservation Laws," *SIAM J. Numer. Anal.* Vol. 21, pp. 995-1011.

Sweby, P.K., Yee, H.C. and Griffiths, D.F. (1990), "On Spurious Steady-State Solutions of Explicit Runge-Kutta Schemes," University of Reading, Department of Mathematics, Numerical Analysis Report 3/90, also NASA TM 102819, March 1990.

Sweby, P.K. and Yee, H.C. (1991), "On Spurious Asymptotic Numerical Solutions of 2×2 Systems of ODEs," University of Reading, Department of Mathematics, Numerical analysis Report 7/91.

Sweby, P.K. and Yee, H.C. (1994), "On the Dynamics of Some Grid Adaptation Schemes," *Proceedings of the 4th International Conference on Numerical Grid Generation in CFD and Related Fields*, University College of Swansea, UK, also RIACS Technical Report 94.02, Feb. 1994.

Sweby, P.K., Lafon, A. and Yee, H.C. (1995), "On the Dynamics of Computing a Chemically Relaxed Nonequilibrium Flow," presented at the ICFD Conference on Numerical Methods for Fluid Dynamics, April 3-6, 1995, Oxford, UK.

Thompson, J.M.T. and Stewart, H.B. (1986), *Nonlinear Dynamics and Chaos*, John Wiley, New York.

Turkel, E. (1993), "Review of Preconditioning Methods for Fluid Dynamics," *App. Numer. Math.*, Vol. 12, pp. 257-284.

Uchibori, Y. and Sobey, I.J. (1992), "Dependence on Numerical Algorithm of Bifurcation Structure for Flow Through a Symmetric Expansion," Oxford University Computing Laboratory Report # 92/14, Oxford, England.

Ushiki, S. (1982), "Central Difference Scheme and Chaos," *Physica 4D*, pp. 407-424.

Vadillo, F. and Sanz-Serna, J.M. (1986), "Studies in Numerical Nonlinear Instability II: A New Look at $u_t + uu_x = 0$," *J. Comp. Phys.*, Vol. 66, pp. 225-238.

Von Karman Institute for Fluid Dynamics Lecture Series 1994-07 (1994), *Spatio-Temporal Instabilities of Aerodynamics and Hydrodynamics Flows*, May 30 - June 2, 1994, Rhode Saint Genise, Belgium.

Ware, J. and Berzins, M. (1995), "Adaptive Finite Volume Methods for Time-Dependent PDEs," in *Modeling, Mesh Generation, and Adaptive Numerical Methods for Partial Differential Equations*, Babuska et al., Eds., pp. 415-430.

Wesseling, P. (1992), *An Introduction to Multigrid Methods*, John Wiley & Sons, New York.

Wiggins, S. (1990), *Introduction to Applied Nonlinear Dynamical Systems and Chaos*, Springer-Verlag, New York.

Woodward, P. and Colella, P. (1984), "The numerical simulation of two-dimensional fluid flow with strong shocks," *J. Comp. Phys.*, Vol. 54, pp. 115-173.

Workshop on Chaotic Numerics (1994), Kloeden & Palmer Eds., *AMS Contemporary Mathematics Vol. 172*, Providence, Rhode Island.

Workshop on Hypersonics (1991), *Proceedings of the Workshop on Hypersonic Flows for Reentry Problems, Part II*, Antibes, France, 15-19 April 1991.

Yanenko, N.N. (1971), *The Method of Fractional Steps*, Springer-Verlag, New York.

Yee, H.C., (1981), "Numerical Approximation of Boundary Conditions with Applications to Inviscid Equations of Gas Dynamics," NASA TM-81265, March 1981.

Yee, H.C., Warming, R.F. and Harten, A. (1985), "Implicit Total Variation Diminishing (TVD) Schemes for Steady-State Calculations," *J. Comput. Phys.*, Vol. 57, pp. 327-360.

Yee, H.C. (1986) "Linearized Form of Implicit TVD Schemes for Multidimensional Euler and Navier-Stokes Equations," *Computers and Mathematics with Applications*, Vol. 12A, pp. 413-432, 1986.

Yee, H.C. and Harten, A. (1987), "Implicit TVD Schemes for Hyperbolic Conservation Laws in Curvilinear Coordinates," AIAA Paper No. 85-1513, *Proceedings of the AIAA 7th CFD Conference*, Cinn., Ohio, July, 1985, also *AIAA J.*, Vol. 25, pp. 266-274.

Yee, H.C. (1989), "A Class of High-Resolution Explicit and Implicit Shock-Capturing Methods," VKI Lecture Series 1989-04 March 6-10, 1989, also NASA TM-101088, Feb. 1989.

Yee, H.C., Klopfer, G.H. and Montagne, J.-L. (1990), "High-Resolution Shock-Capturing Schemes for Inviscid and Viscous Hypersonic Flows," *J. Comput. Phys.*, Vol. 88, pp. 31-61.

Yee, H.C., Sweby, P.K. and Griffiths, D.F. (1991), "Dynamical Approach Study of Spurious Steady-State Numerical Solutions for Nonlinear Differential Equations, Part I: The Dynamics of Time Discretizations and Its Implications for Algorithm Development in Computational Fluid Dynamics," NASA TM-102820, April 1990, also *J. Comput. Phys.*, Vol. 97, pp. 249-310.

Yee, H.C. and Sweby, P.K. (1994), "Global Asymptotic Behavior of Iterative Implicit Schemes," RIACS Technical Report 93.11, December 1993, NASA Ames Research Center, also *Intern. J. Bifurcation & Chaos*, Vol. 4, pp. 1579-1611.

Yee, H.C. and Sweby, P.K. (1995a), "Dynamical Approach Study of Spurious Steady-State Numerical Solutions for Nonlinear Differential Equations, Part II: Global Asymptotic Behavior of Time Discretizations," RNR-92-008, March 1992, NASA Ames Research Center; also *Intern. J. of CFD*, Vol. 4, pp. 219-283.

Yee, H.C. and Sweby, P.K. (1995b), "On Super-Stable Implicit Methods and Time-Marching Approaches," RIACS Technical Report 95.12, NASA Ames Research Center, July 1995; also, *Proceedings of the Conference on Numerical Methods for Euler and Navier-Stokes Equations*, Sept. 14-16, 1995, University of Montreal, Canada.

Yee, H.C. and Sweby, P.K. (1996), "Some Aspects of Numerical Uncertainties in Time Marching to Steady-State Computations," AIAA-96-2052, 27th AIAA Fluid Dynamics Conference, June 18-20, 1996, New Orleans, LA.

Scheme	Fixed points	Stable range
Explicit Euler	1	$0 < r < 2$
Modified Euler	1	$0 < r < 2$
	$1 + 2/r$	$0 < r < -1 + \sqrt{5} \approx 1.236$
	$2/r$	$2 < r < 1 + \sqrt{5} \approx 3.236$
Improved Euler	1	$0 < r < 2$
	$\frac{[2 + r \pm \sqrt{r^2 - 4}]}{2r}$	$2 < r < \sqrt{8} \approx 2.828$
Heun	1	$0 < r < 1 + (\sqrt{17} + 4)^{1/3} - (\sqrt{17} + 4)^{-1/3} \approx 2.513$
	*	$4.9137 < r < 4.9552$
	*	$6.4799 < r < 6.4853$
	*	$6.74405 < r < 6.74575$
R-K4	1	$0 < r < \frac{4}{3} + (\frac{172}{27} + \frac{4}{3}\sqrt{29})^{1/3} + (\frac{172}{27} - \frac{4}{3}\sqrt{29})^{1/3} \approx 2.785$
	*	$2.785 < r < 3.4156$
	*	$2.746 < r < 3.456$
	*	

Table 3.1. Fixed points of Runge-Kutta methods for $du/dt = \alpha u(1 - u)$.

Scheme	Fixed points	Stable range
Explicit Euler	$\frac{1}{2}$	$0 < r < 8$
Modified Euler	$\frac{1}{2}$	$0 < r < 8$
	$\frac{1}{4}[1 + \sqrt{1 - 32/r}]$	$32 < r < 32.014067$
	$\frac{1}{2}[1 \pm \sqrt{1 - 8/r}]$	$8 < r < 4(1 + \sqrt{3}) \approx 10.928$
	$\frac{1}{4}[3 - \sqrt{1 - 32/r}]$	$32 < r < 32.014067$
Improved Euler	$\frac{1}{2}$	$0 < r < 8$
	$\frac{1 \pm \sqrt{1 - 8/r}}{2}$	$8 < r < 12$
	$\frac{1}{2} - \frac{\sqrt{1 - 12/r}}{4} \pm \frac{\sqrt{1 + 4/r}}{4}$	$12 < r < 4(1 + \sqrt{6}) \approx 13.798$
	$\frac{1}{2} + \frac{\sqrt{1 - 12/r}}{4} \pm \frac{\sqrt{1 + 4/r}}{4}$	$12 < r < 4(1 + \sqrt{6}) \approx 13.798$
Heun	$\frac{1}{2}$	$0 < r < 4(1 + (\sqrt{17} + 4)^{1/3} - (\sqrt{17} + 4)^{-1/3}) \approx 10.051$
R-K4	$\frac{1}{2}$	$0 < r < \frac{16}{3} + 4(\frac{172}{27} + \frac{4}{3}\sqrt{29})^{1/3} + 4(\frac{172}{27} - \frac{4}{3}\sqrt{29})^{1/3} \approx 11.14$

Table 3.2. Fixed points of Runge-Kutta methods for $du/dt = \alpha u(1 - u)(0.5 - u)$.

S(u)	(3.11)	(3.17)	(3.18)	(3.19)	(3.21)
$u(1-u)$	0	2	2	6	14
$u(\frac{1}{2}-u)(1-u)$	0	6	6	24	78

Table 3.3. The number of spurious fixed points of Runge-Kutta methods for (3.7a) and (3.23).

Equation	Period 2 orbits	Stable range
$u' = \alpha u(1-u)$	$\frac{r+2 \pm \sqrt{r^2-4}}{2r}$	$2 < r < \sqrt{6} \approx 2.4495$
$u' = \alpha u(1-u)(\frac{1}{2}-u)$	$\frac{1 \pm \sqrt{1-8/r}}{2}$	$8 < r < 12$
	$\frac{1}{2} - \frac{\sqrt{1-12/r}}{4} \pm \frac{\sqrt{1+4/r}}{4}$	$12 < r < 14$
	$\frac{1}{2} + \frac{\sqrt{1-12/r}}{4} \pm \frac{\sqrt{1+4/r}}{4}$	$12 < r < 14$

Table 3.4. Period 2 fixed points of the explicit Euler method.

scheme	c_i	c_j
E-O	0.65	0.9
minmod	0.5	0.75
superbee	—	0.7
van Leer	0.6	0.7
van Albada	0.6	0.7

Table 4.1. Convergence regions for the explicit schemes.

scheme	converges to x_1	converges to x_2
E-O	$c < 11$	$c \geq 22.5$
minmod	$c < 11$	$c \geq 21.5$
superbee	$c < 11$	—
van Leer	—	—
van Albada	$c < 11$	$c \geq 22.5$

Table 4.2. Convergence regions for the implicit schemes.

scheme	at stable shock			at unstable shock		
	X	Y	stable	X	Y	stable
explicit E-O	0.36	-0.47	$\Delta t < 0.057$	0.40	-0.32	—
				0.52	0.26	$\Delta t < 0.1043$
				-0.29	-0.53	$\Delta t < 0.1031$
implicit E-O	0.37	-0.48	$\forall \Delta t$	0.40	-0.32	$\Delta t > 1.0585$
				0.52	0.26	$\forall \Delta t$
				-0.29	-0.53	$\forall \Delta t$

Table 4.3. Analytical fixed points of the reduced system.

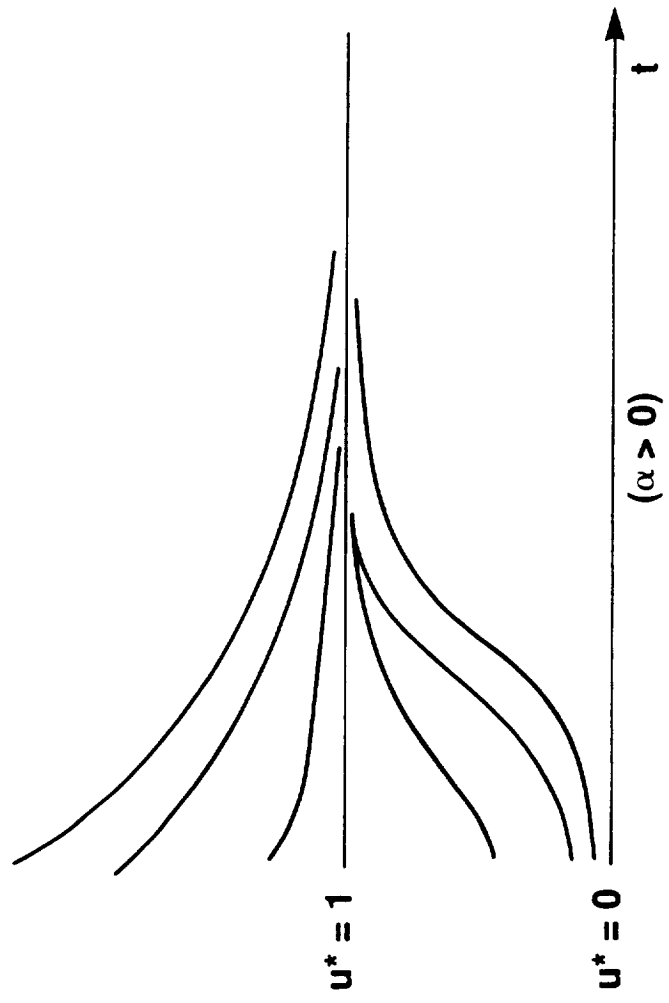


Fig. 3.1. Asymptotic solution behavior of the logistic ODE ($\alpha > 0$).

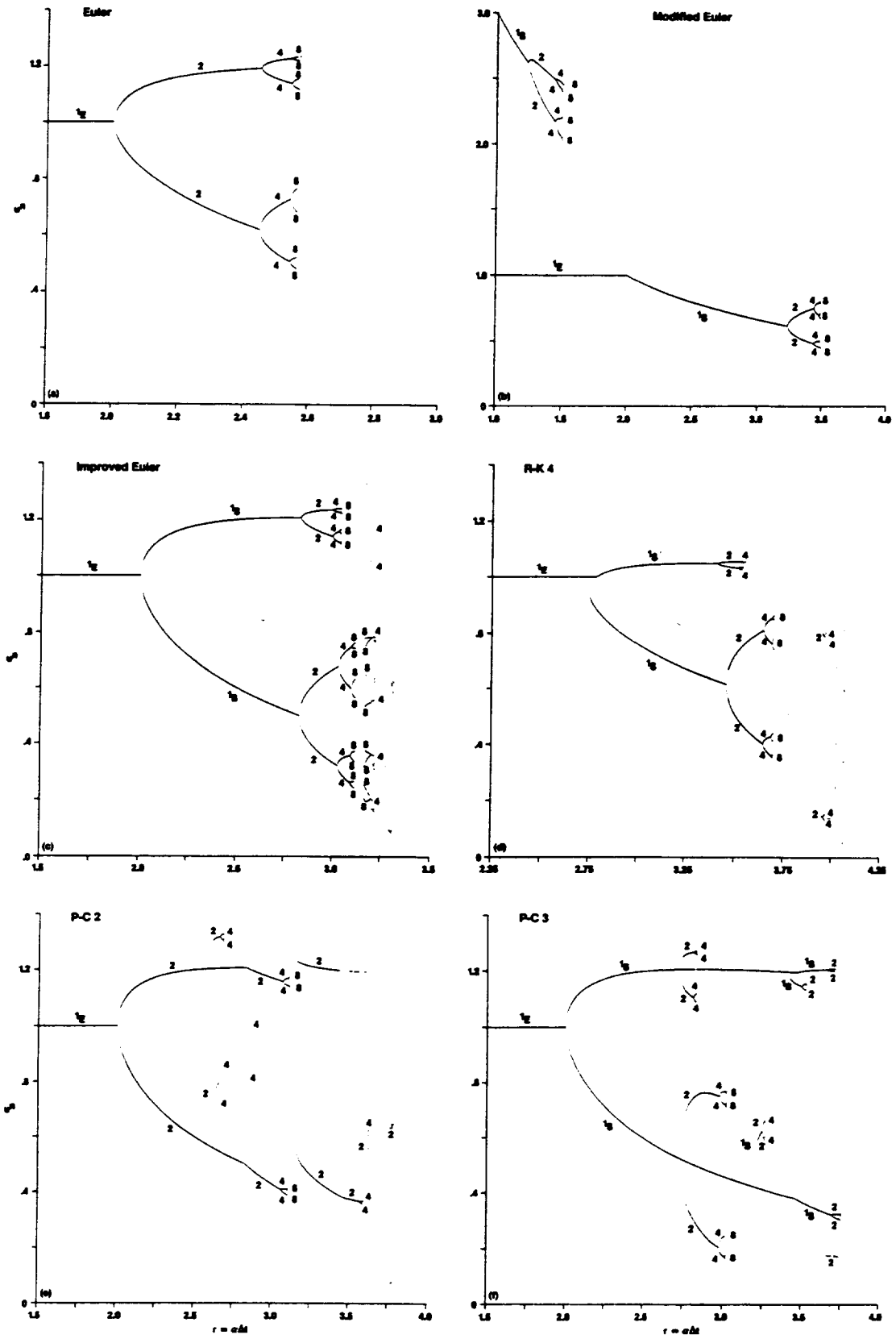


Fig. 3.2. Fixed point diagrams of periods 1, 2, 4, 8 for the logistic ODE ($\alpha > 0$).

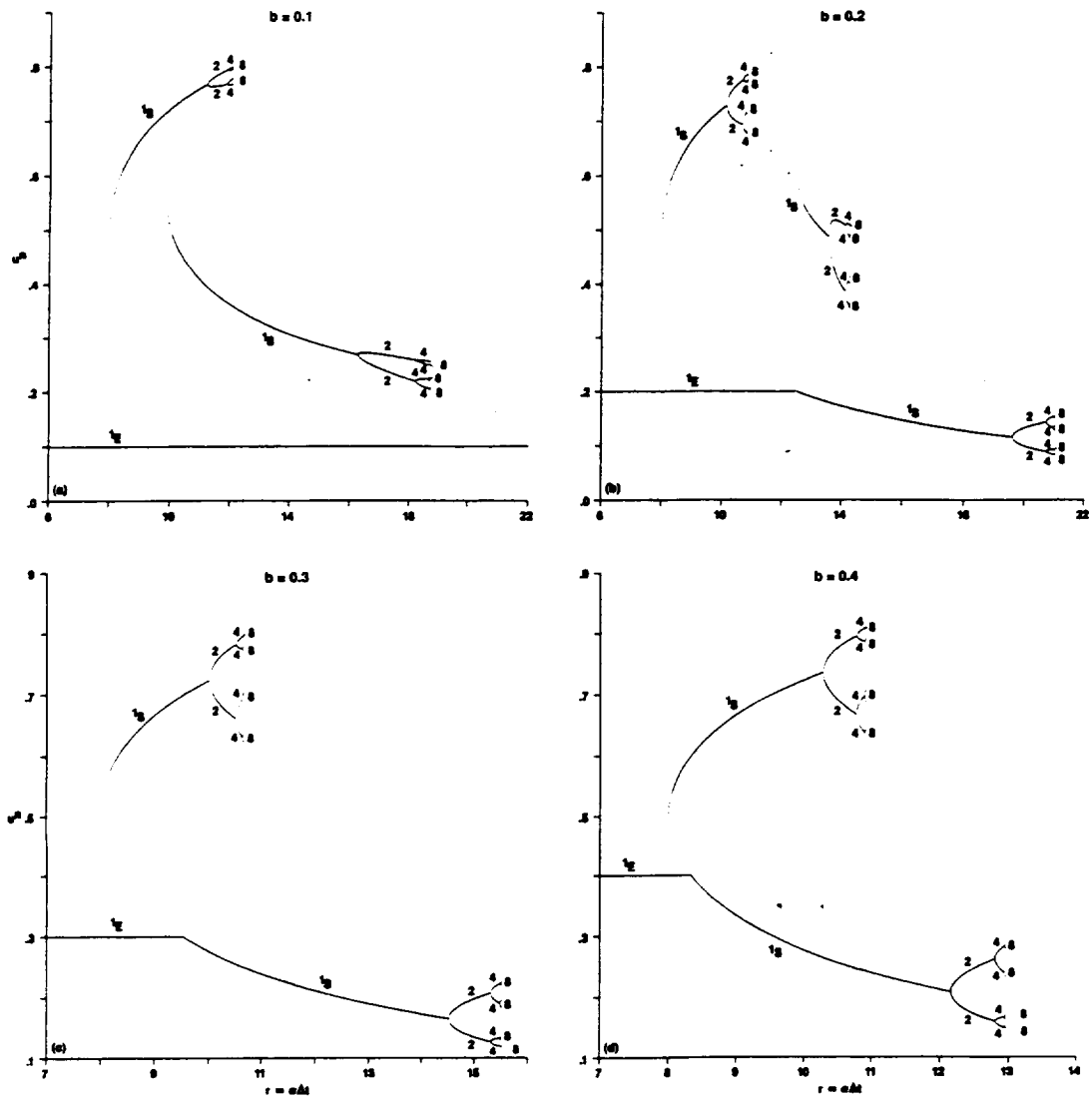
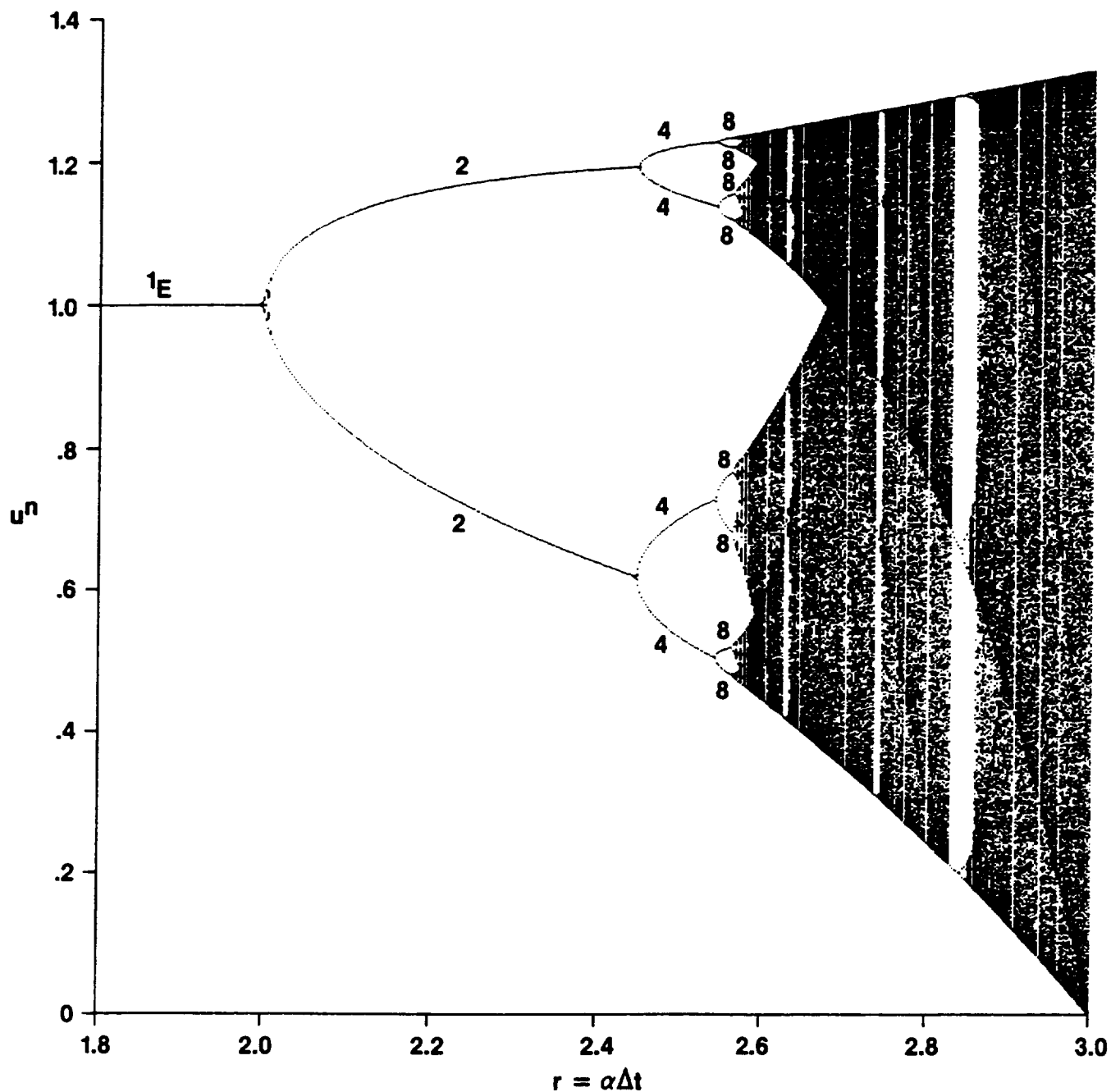


Fig. 3.3. Stable fixed points of periods 1, 2, 4, 8 of the modified Euler method for the ODE $du/dt = \alpha u(1-u)(b-u)$.



**DIAGRAM LOOKS THE SAME REGARDLESS OF I.C. FOR ALL $u^0 > 0$
 CHAOS WINDOWS NEAR: 2.627, 2.634, 2.738, 2.828, BELOW 3**

Fig. 3.4. Bifurcation diagram of the explicit Euler method for the logistic ODE ($\alpha > 0$).

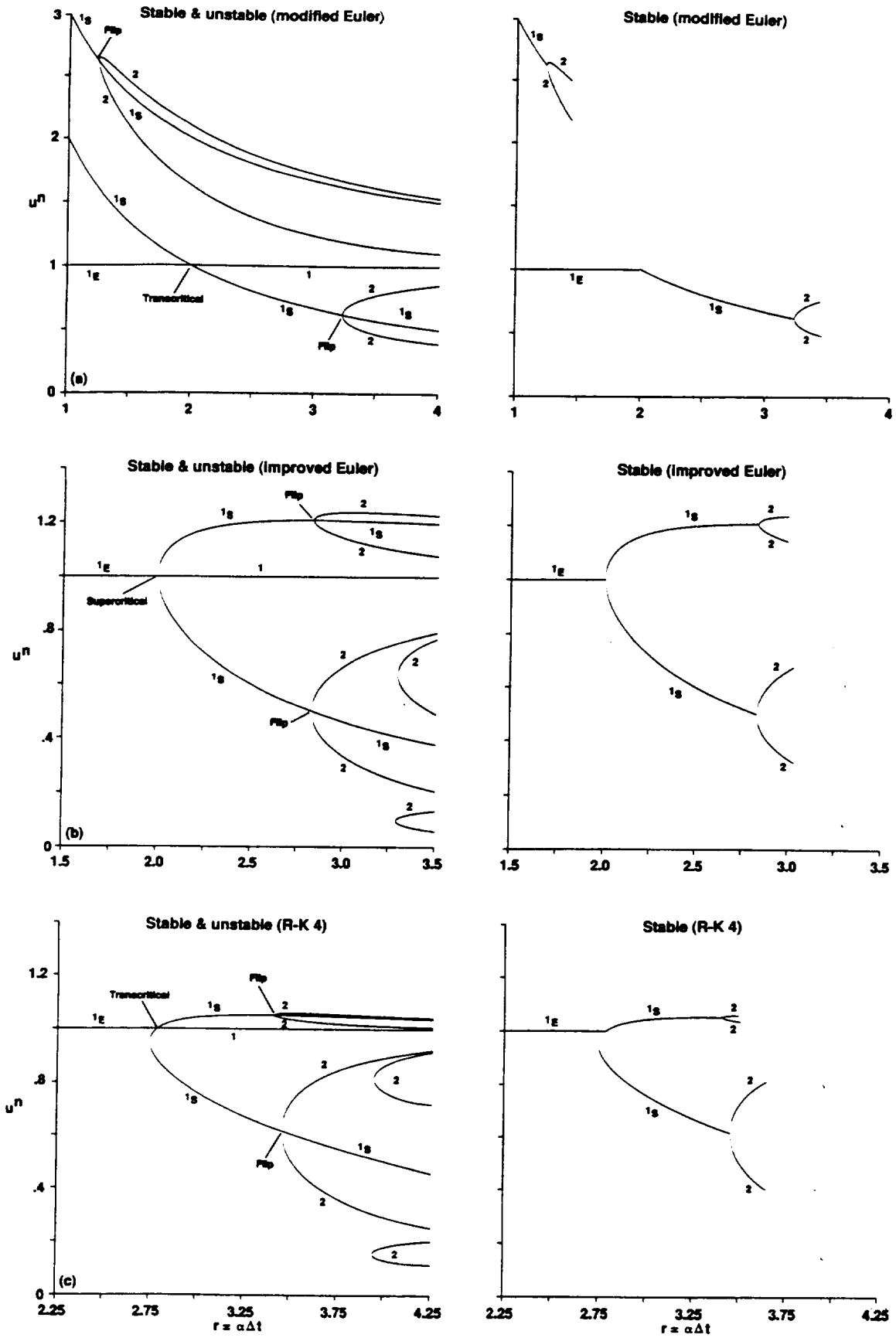


Fig. 3.5. Stable and unstable fixed points of periods 1,2 for the logistic ODE ($\alpha > 0$).

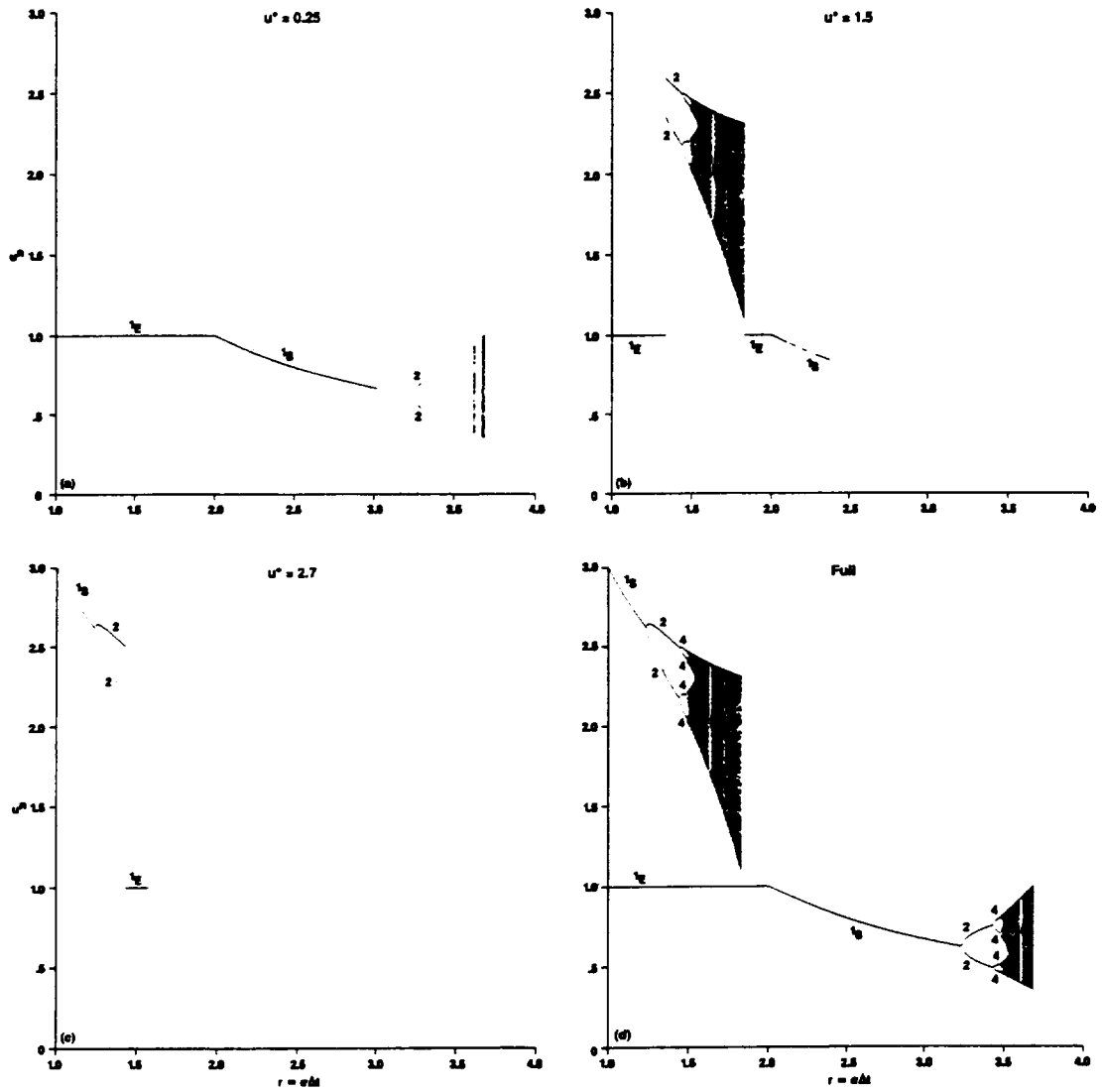


Fig. 3.6. Bifurcation diagrams of the modified Euler method for the logistic ODE ($\alpha > 0$).

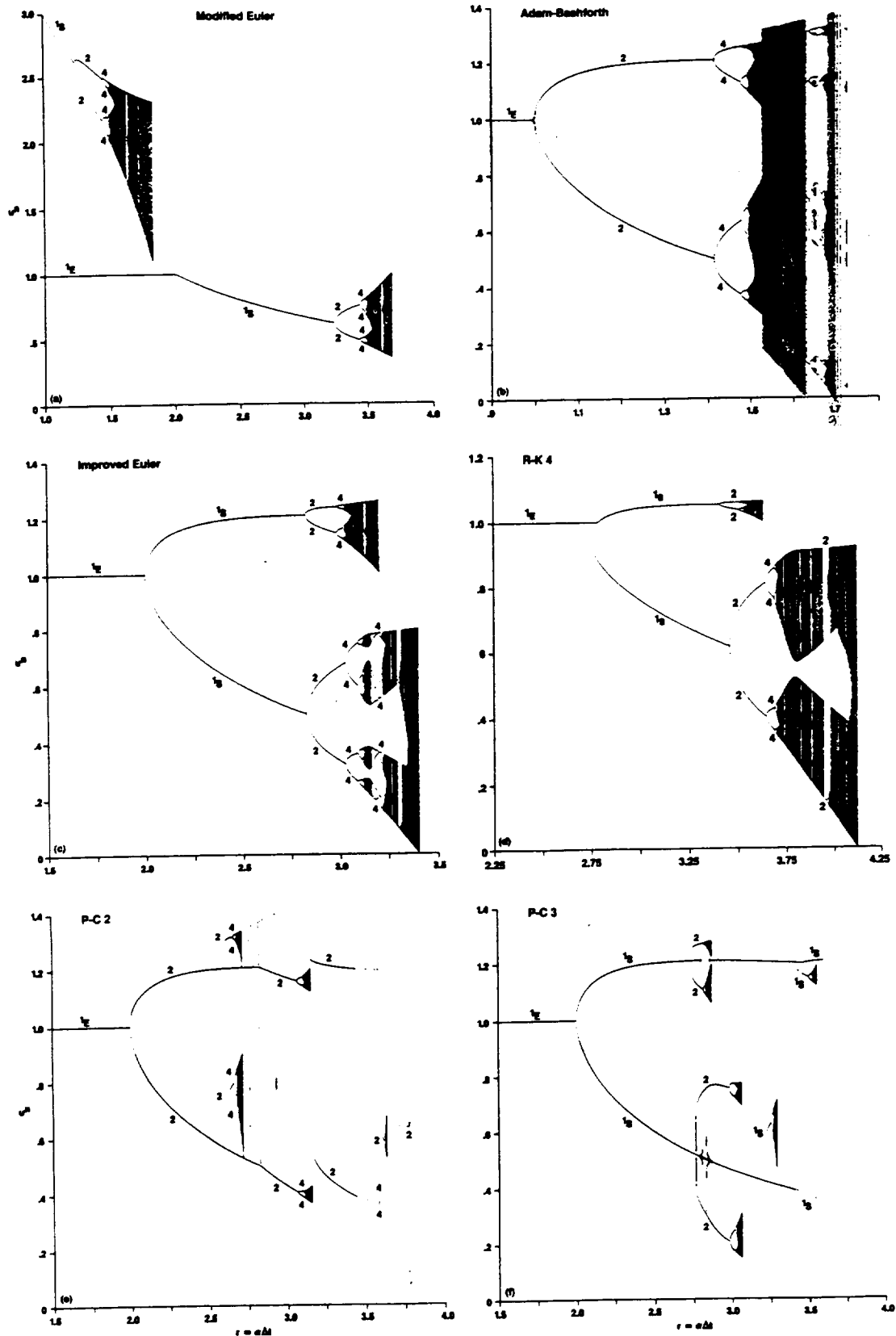


Fig. 3.7. Stable and unstable fixed points of periods 1,2 for the logistic ODE ($\alpha > 0$).

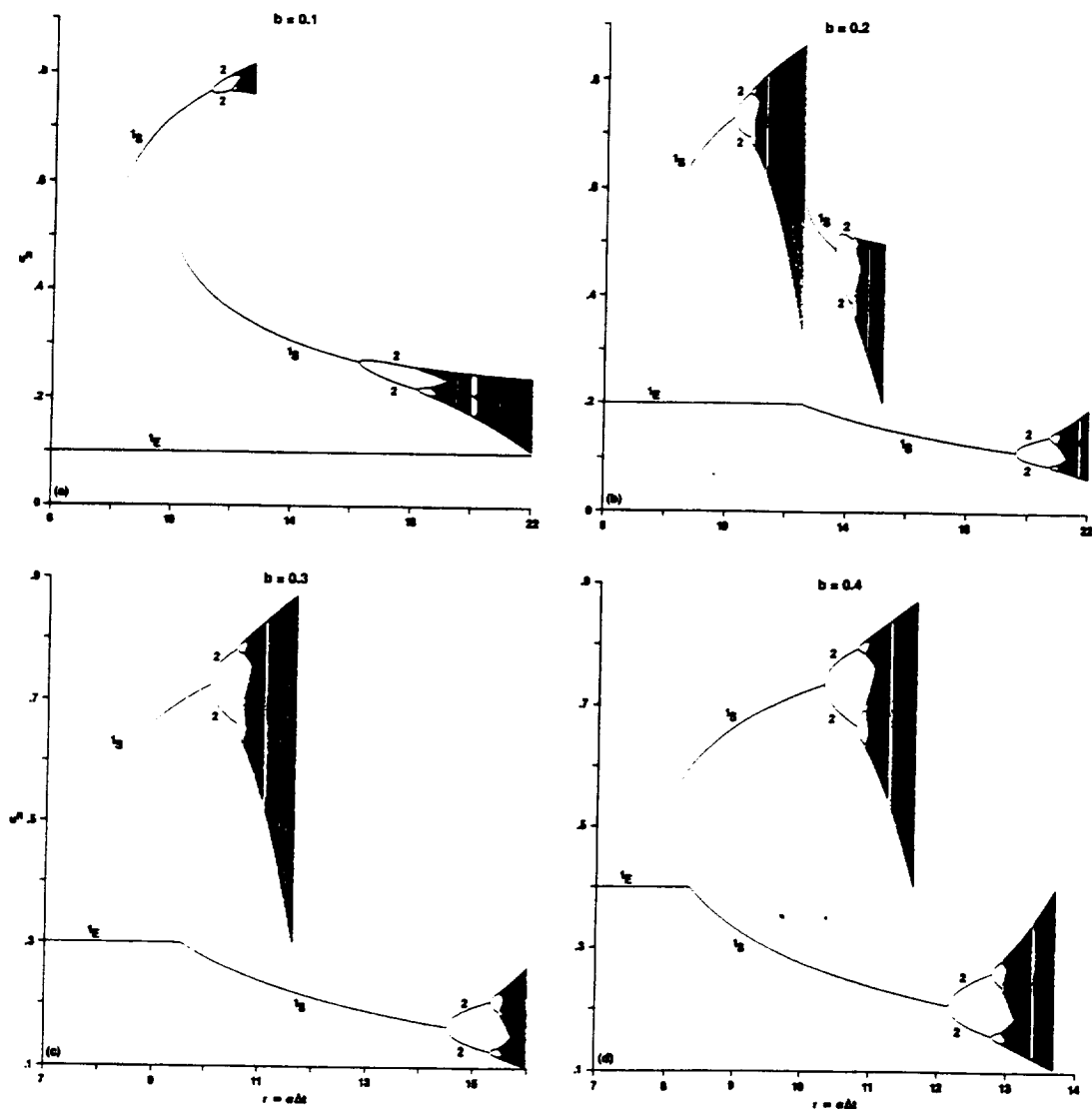


Fig. 3.8. "Full" Bifurcation diagrams for the modified Euler method for the ODE $du/dt = \alpha u(1-u)(b-u)$.

Bifurcation Diagrams & Basins of Attraction

$u' = au(1-u)$

Modified Euler

Improved Euler



Kutta

R-K4



Fig. 3.9.

Bifurcation Diagrams & Basins of Attraction

$$u' = au(1-u)$$

Linearized Implicit Euler

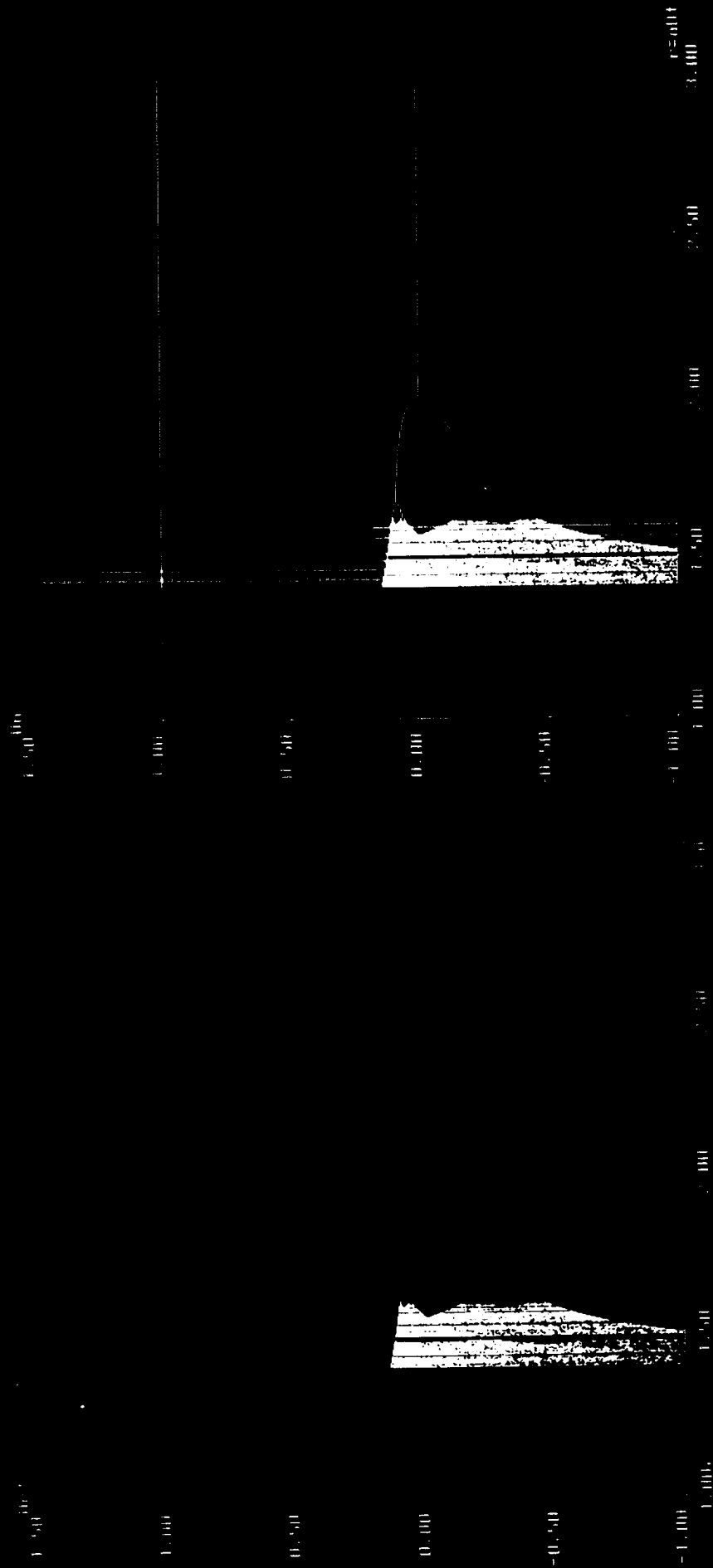


Fig. 3.10.

Bifurcation Diagrams & Basins of Attraction

$$u' = au(1-u)$$

Implicit Euler

Newton

Mod. Newton

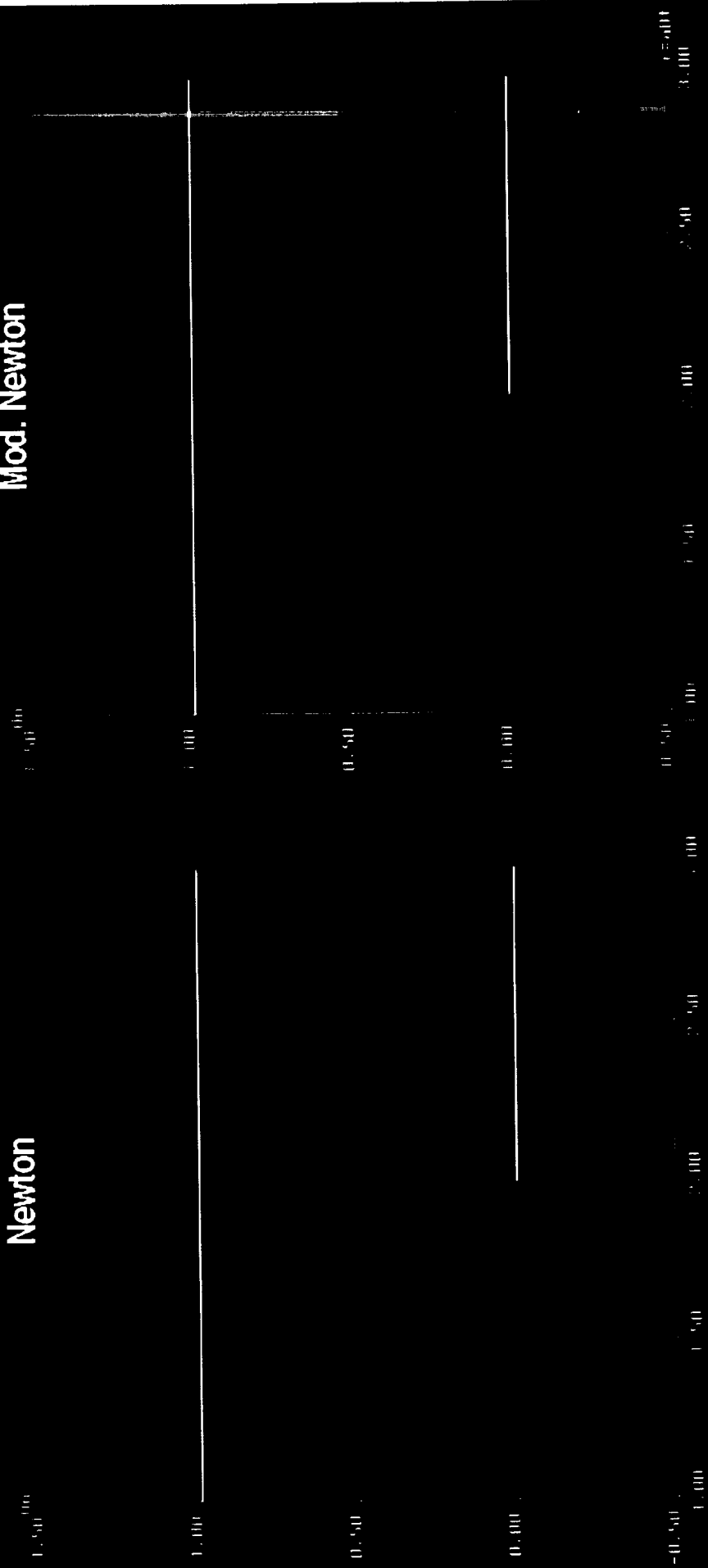


Fig. 3.11.

Bifurcation Diagrams & Basins of Attraction

$$u' = a u (1-u)$$

Linearized Trapezoidal

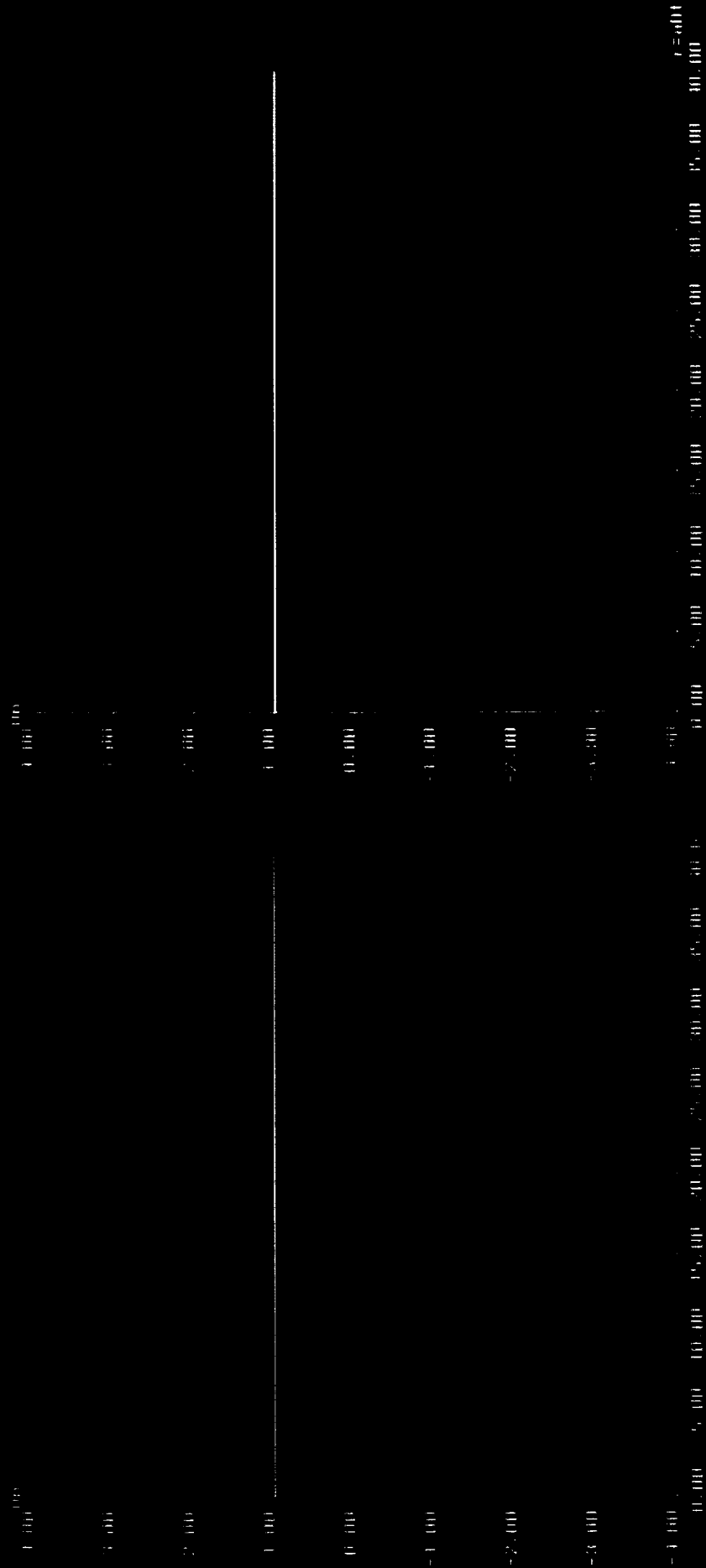


Fig. 3.12.

Bifurcation Diagrams & Basins of Attraction

$$u' = a u (1-u)$$

Trapezoidal

Newton

Mod. Newton

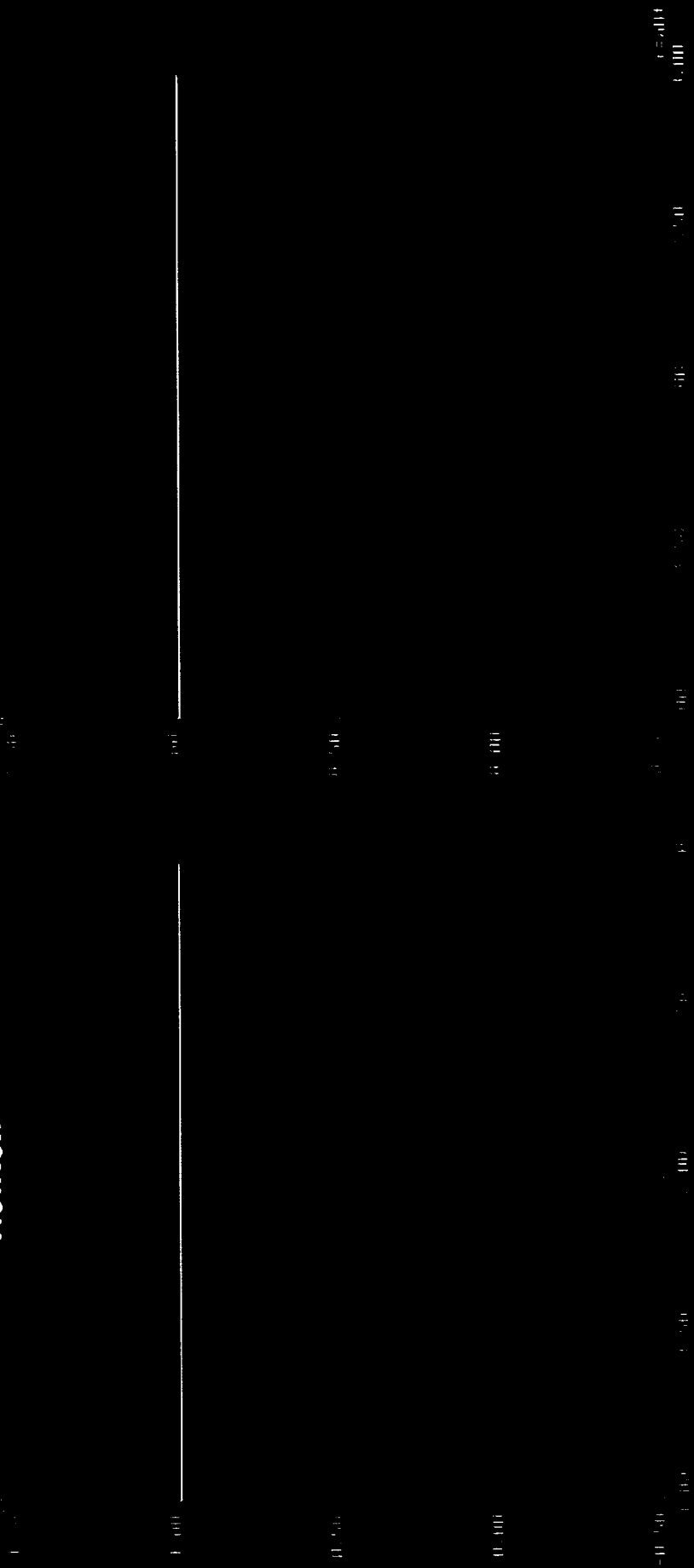


Fig. 3.13.

Bifurcation Diagrams & Basins of Attraction

$$u' = a u (1-u)$$

Linearized 3-level BDF

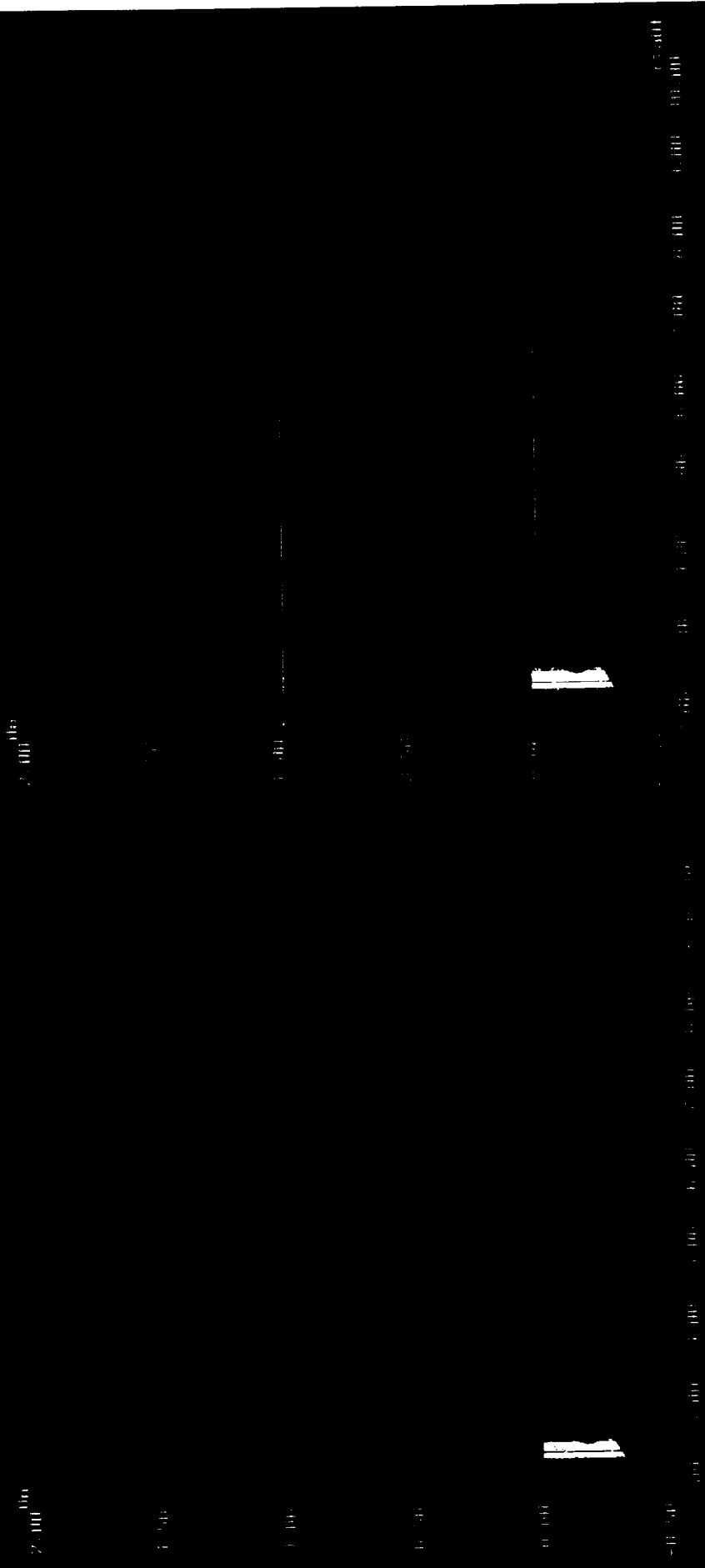


Fig. 3.14.

Bifurcation Diagrams & Basins of Attraction

$$u' = a u (1-u)$$

3-level BDF

Newton

Mod. Newton

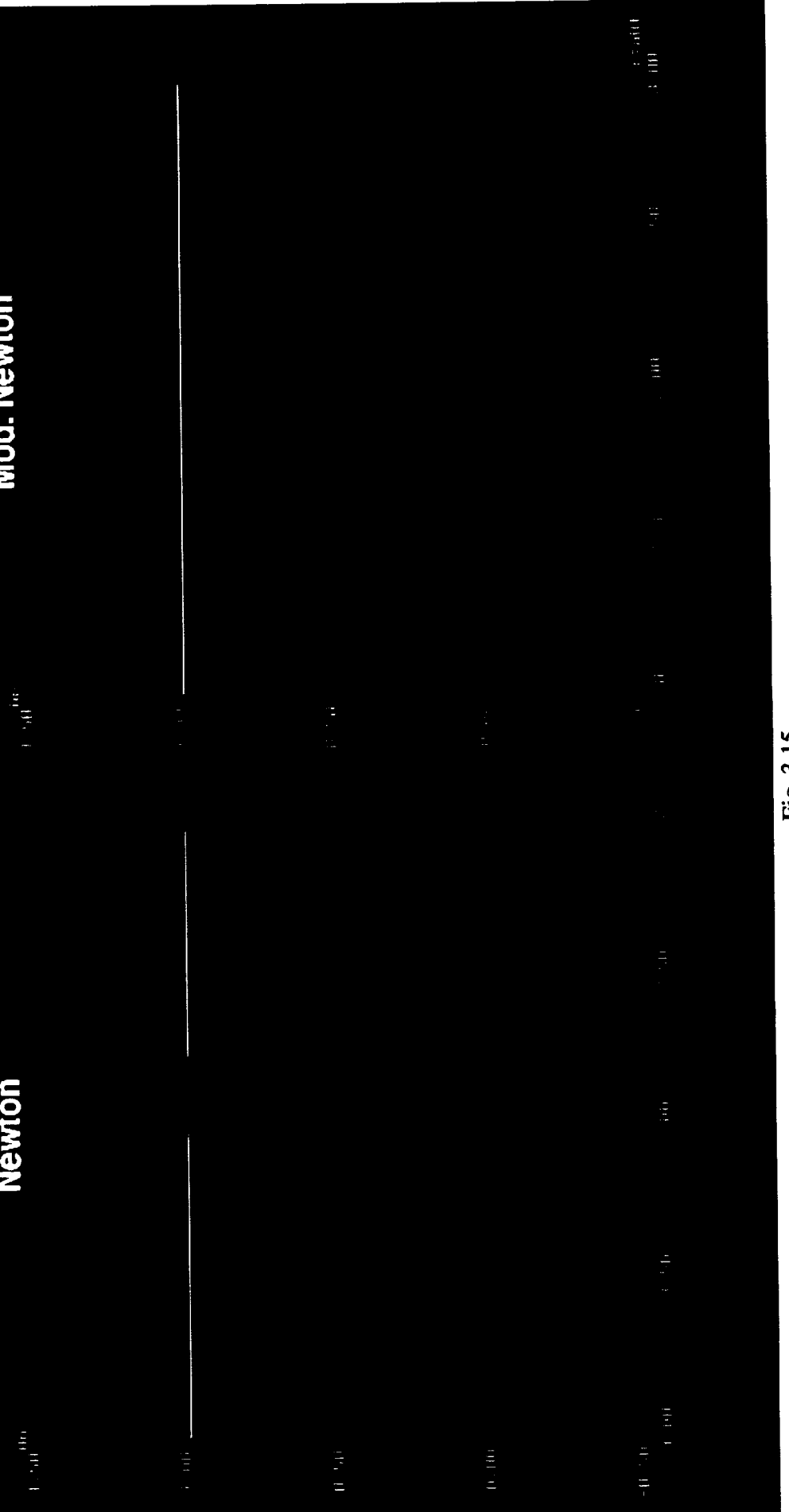


Fig. 3.15.

Bifurcation Diagrams & Basins of Attraction

$$u' = a u (1-u)$$

Semi-Imp.-Pred. Method

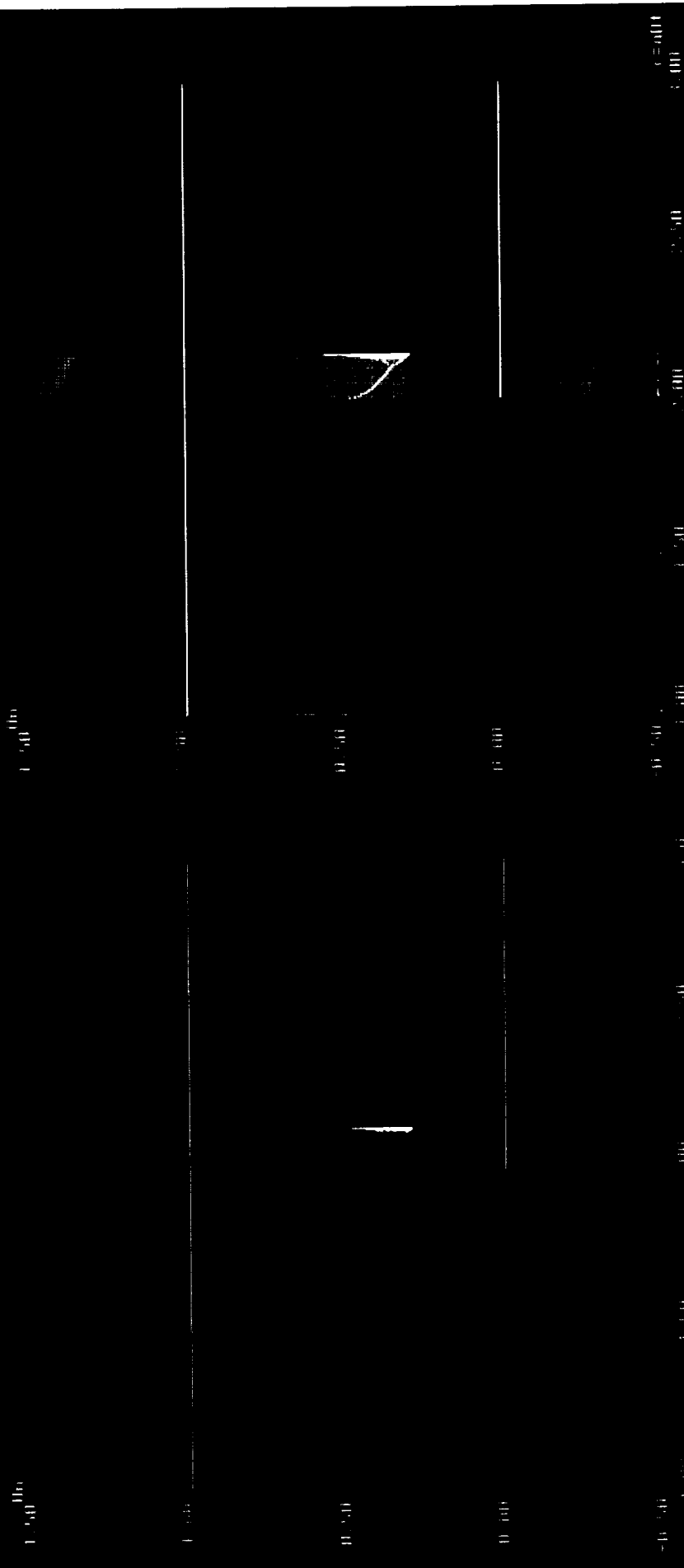
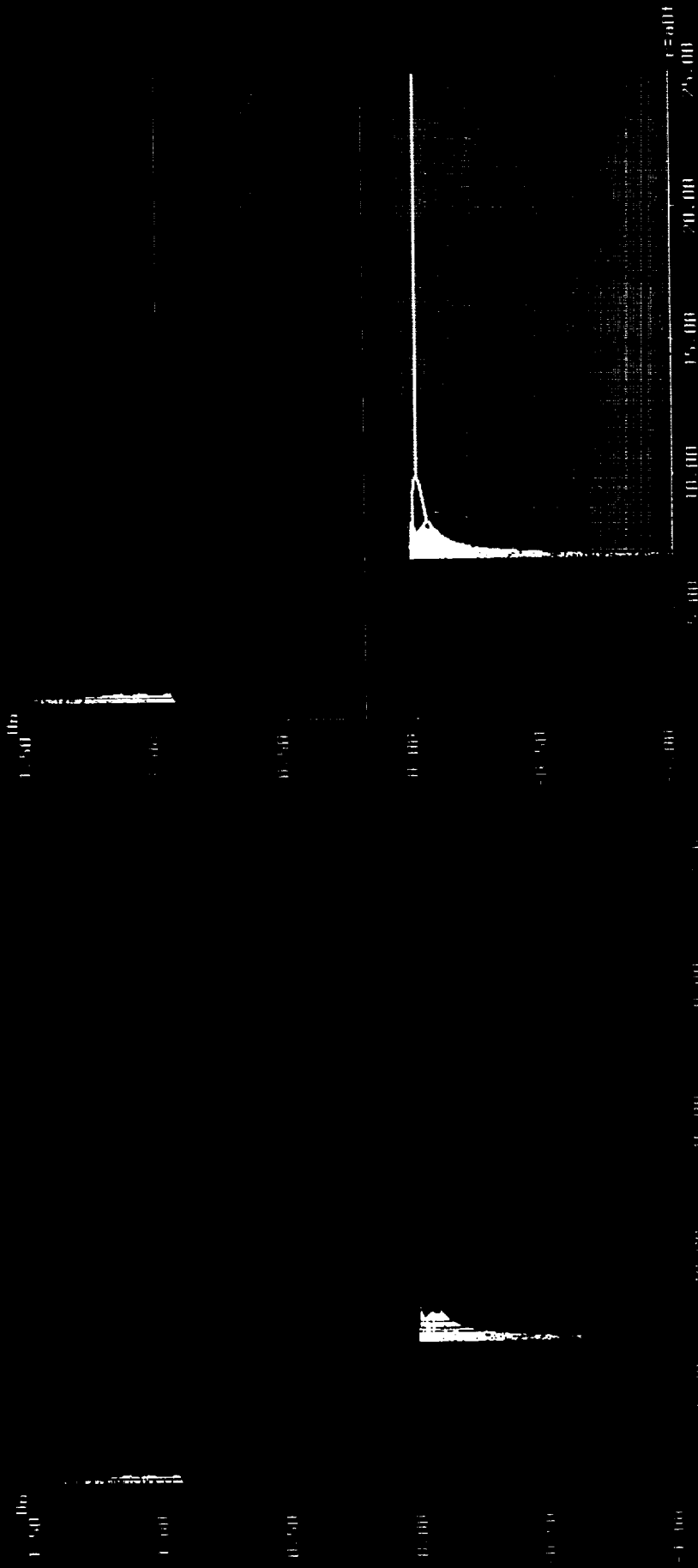


Fig. 3.16.

Bifurcation Diagrams & Basins of Attraction

$$u' = a u (1 - u) \quad (0.2 - u)$$

Linearized Implicit Euler



Bifurcation Diagrams & Basins of Attraction

$$u' = a u (1 - u) (0.2 - u)$$

Linearized Trapezoidal

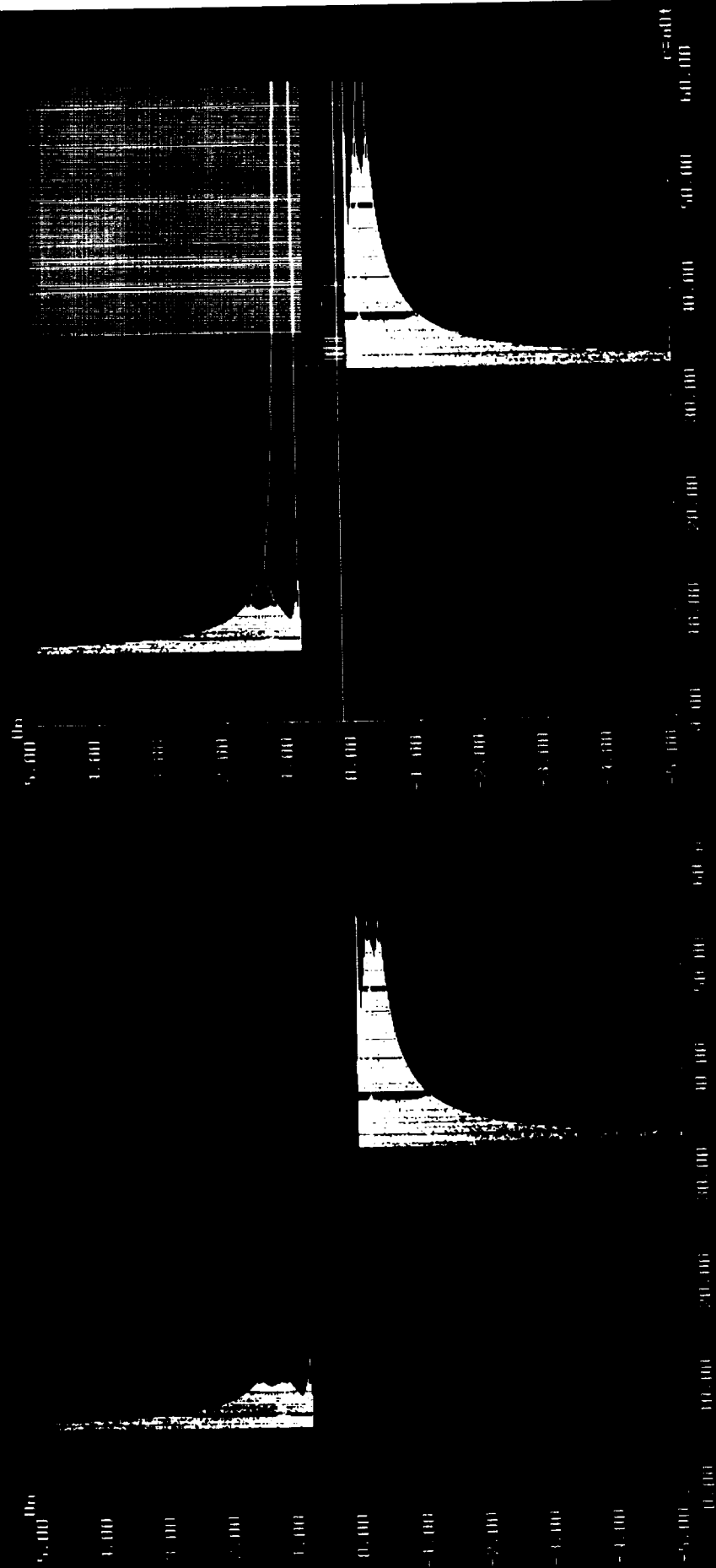


Fig. 3.18.

Bifurcation Diagrams & Basins of Attraction

$$u' = a u (1 - u) (0.2 - u)$$

Linearized 3-level BDF

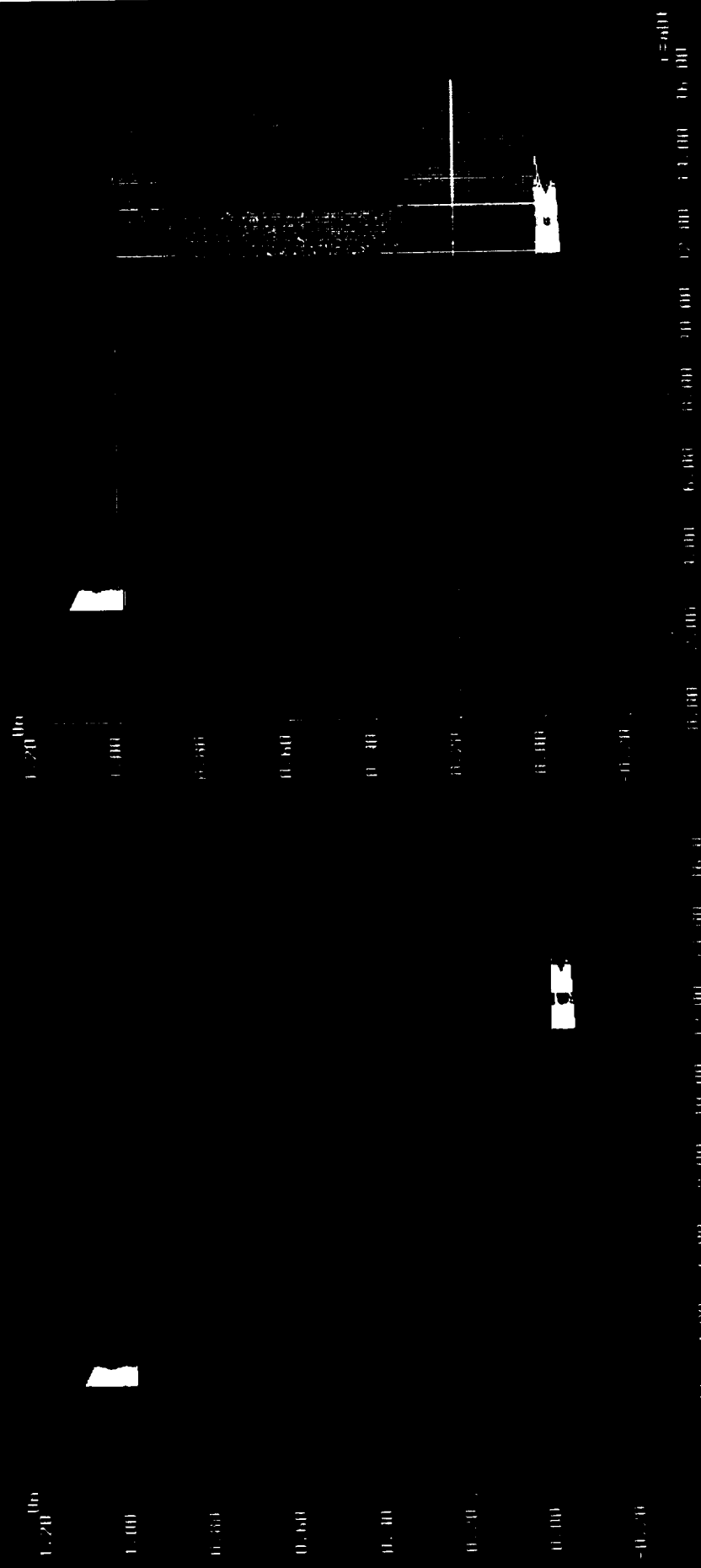


Fig. 3.19.

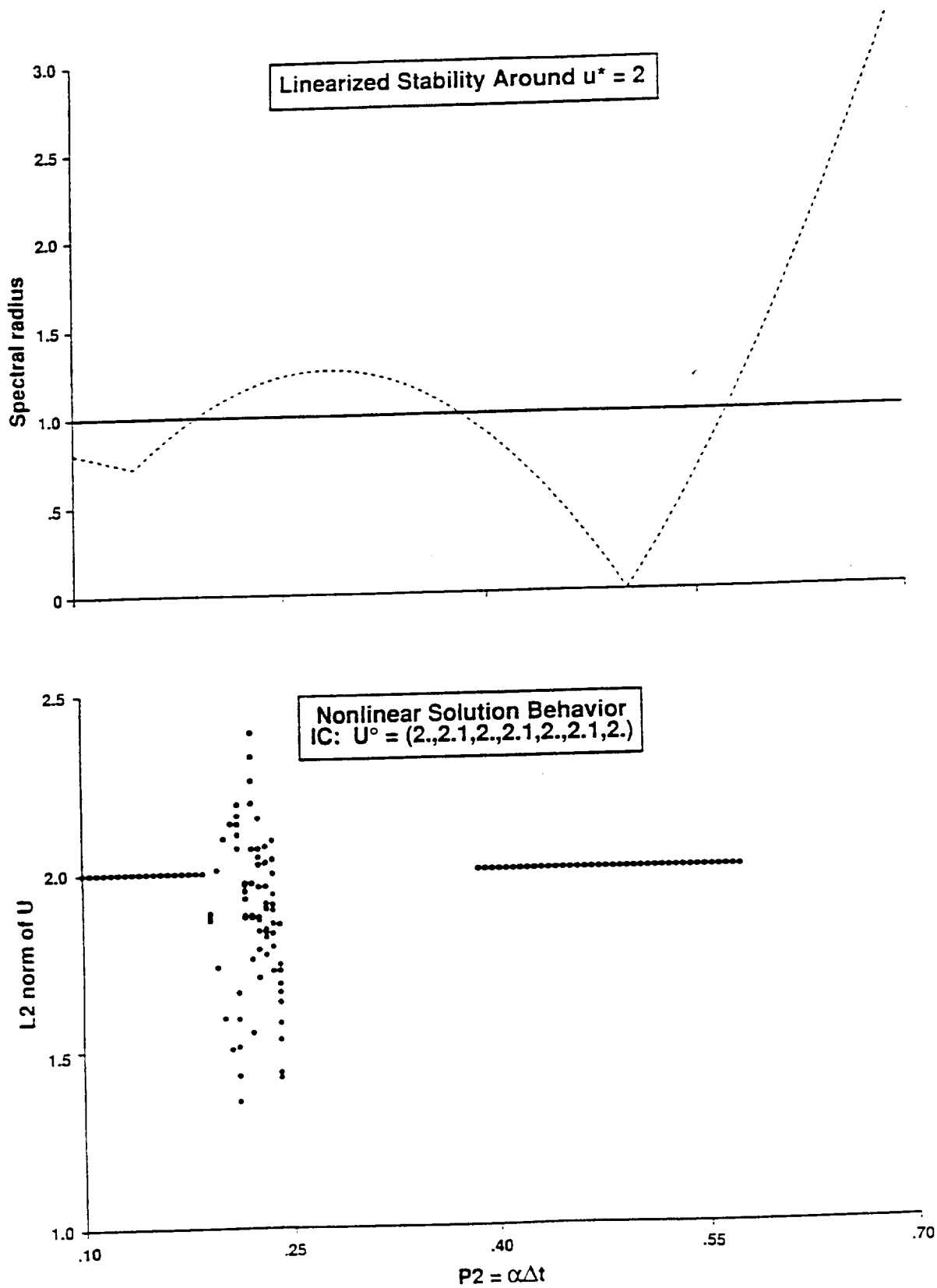


Fig. 3.20. Comparison for discretization UP1UI/EE and $p_1 = 7$ of (a) linearized stability analysis (around $u^* = 2$) and (b) nonlinear solution behavior with initial data U^o (\bullet : steady-state solution and other asymptotic solution, blank space : divergent solution).

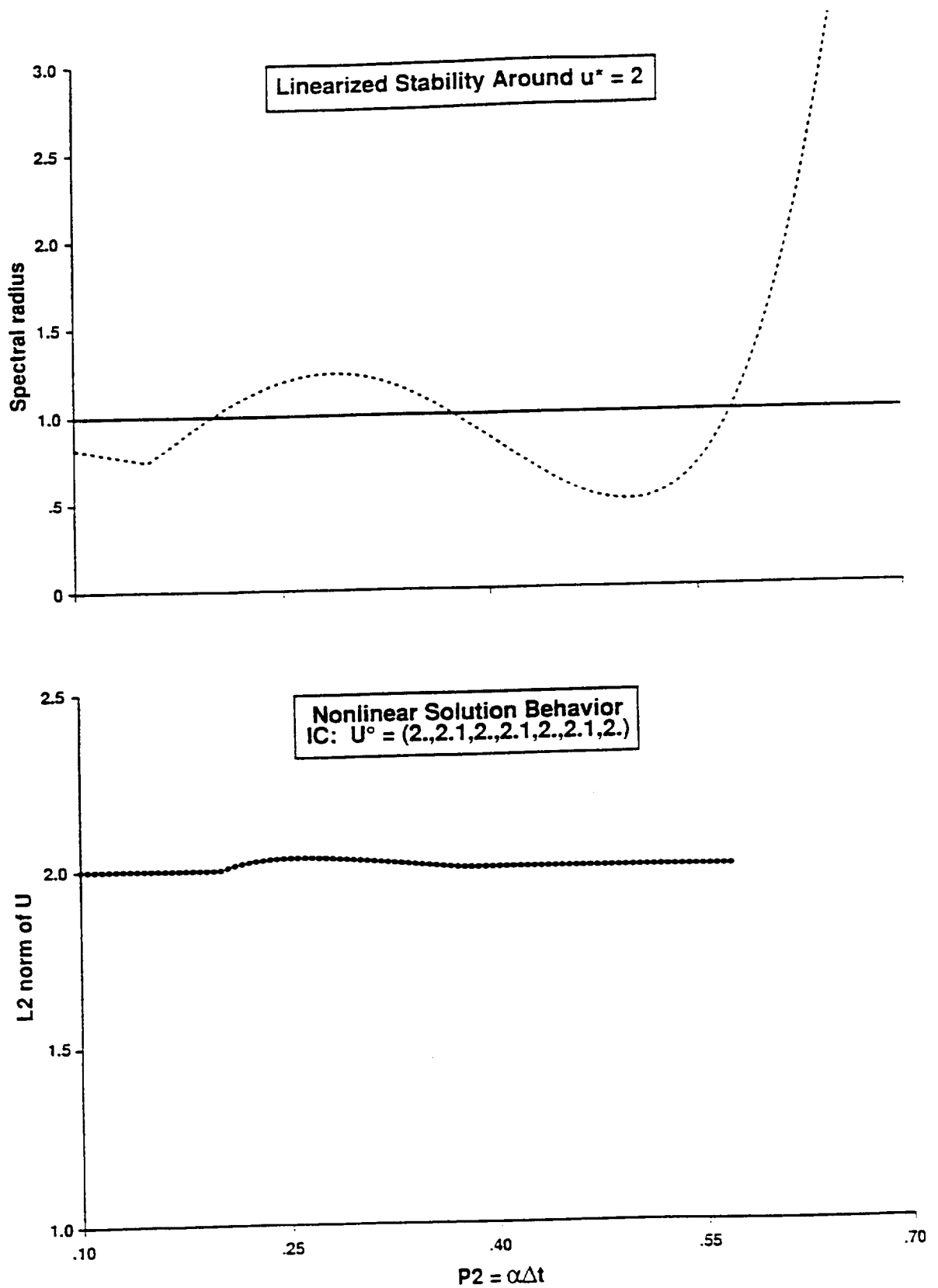


Fig. 3.21. Comparison for discretization UP1UI/ME and $p_1 = 7$ of (a) linearized stability analysis (around $u^* = 2$) and (b) nonlinear solution behavior with initial data U^o (• : steady-state solution and other asymptotic solution, blank space : divergent solution).

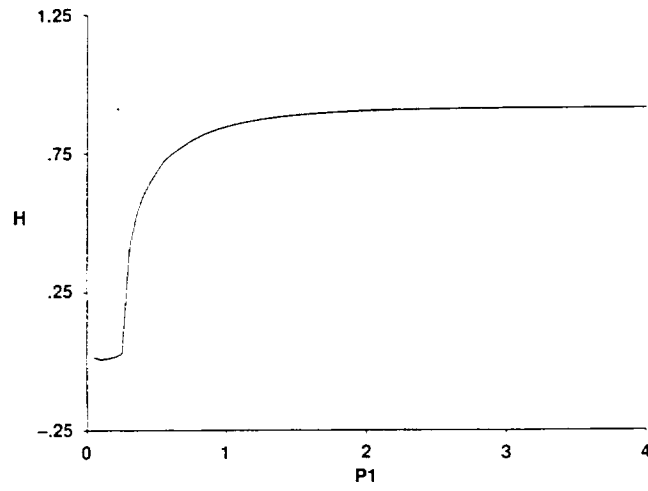


Fig. 3.22. Average wave speed W versus p_1 of the numerical solution with explicit Euler time discretization and spatial discretization UP1PW.

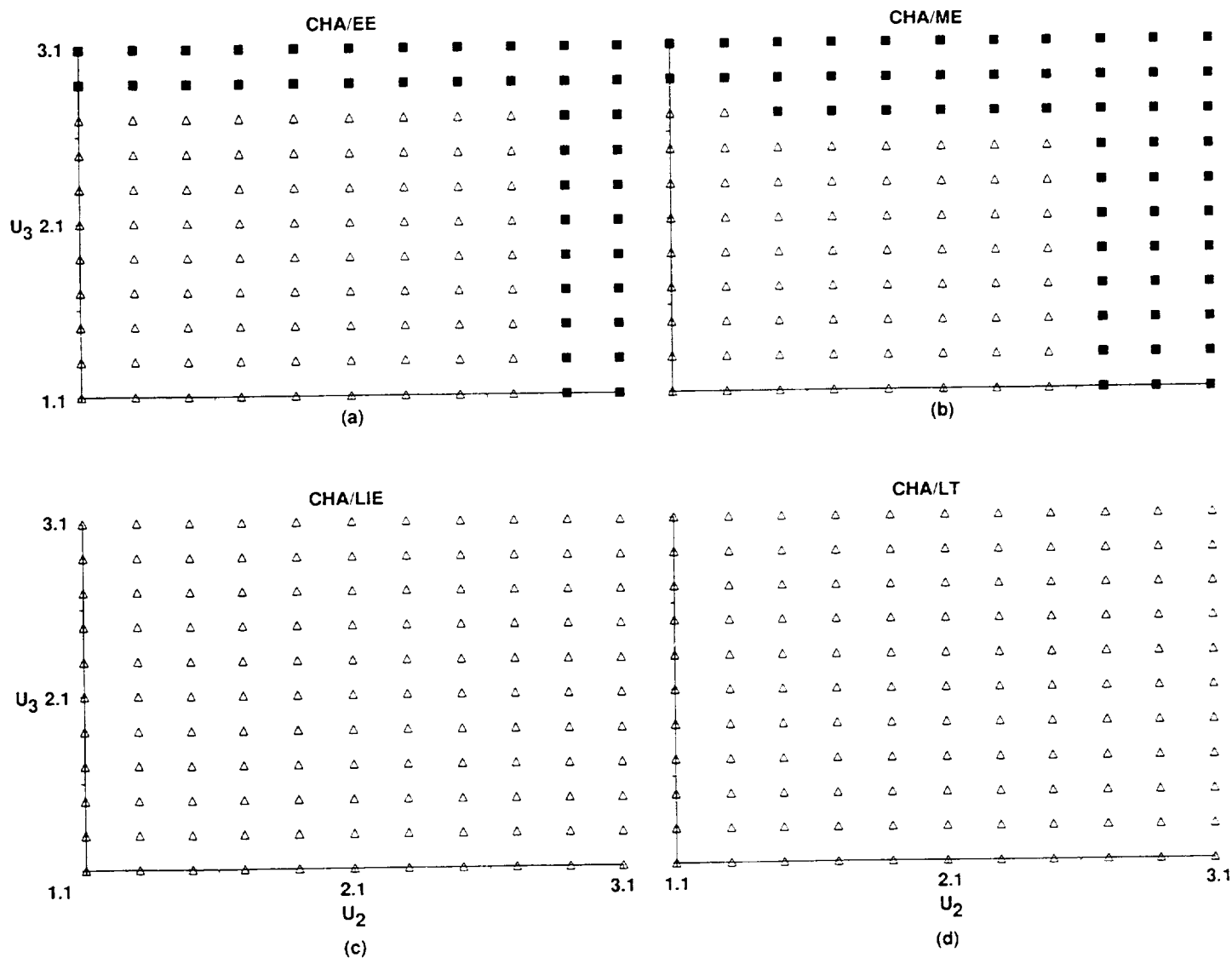


Fig. 3.23. Numerical basin of attraction for discretizations (a) CHA/EE, (b) CHA/ME, (c) CHA/LIE and (d) CHA/LT with $J = 4$, $p_1 = 0.1$ and $p_2 = 0.5$ (Δ : exact steady-state solution, \blacksquare : spurious steady-state solution, \bullet : other spurious asymptotic solution, blank space: divergent solution).

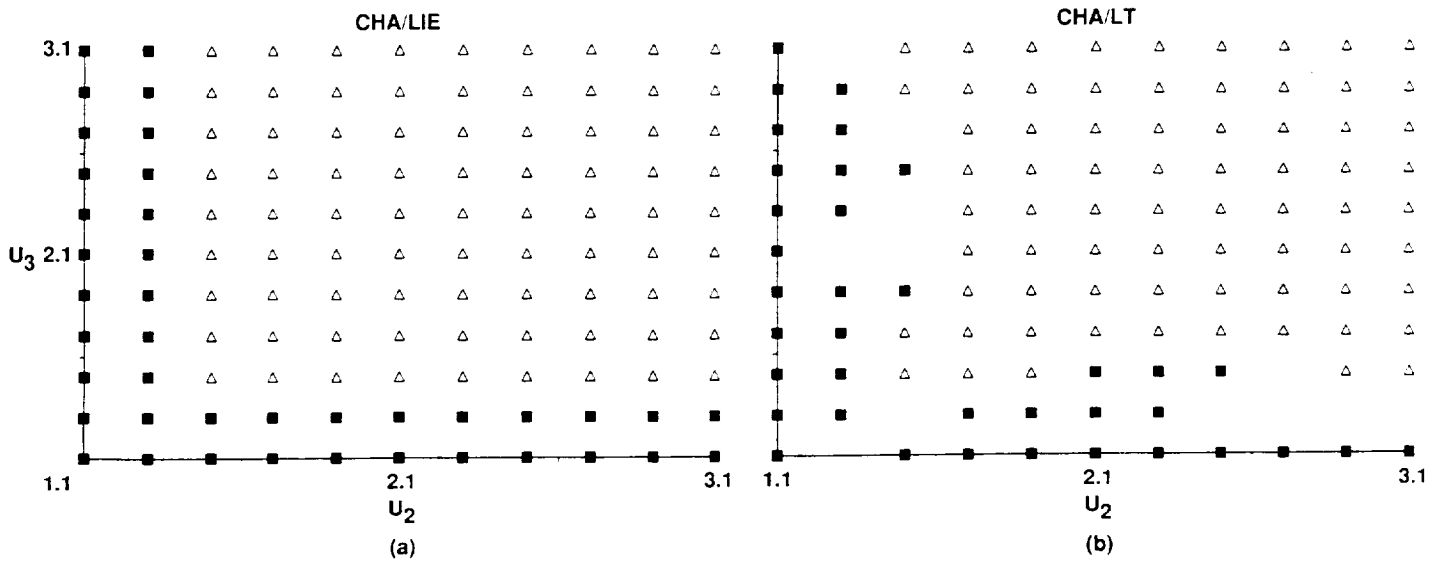


Fig. 3.24. Numerical basin of attraction for discretizations (a) CHA/LIE and (b) CHA/LT with $J = 4$, $p_1 = 0.1$ and $p_2 = 3$ (CFL = 0.3) (Δ : exact steady-state solution, \blacksquare : spurious steady-state solution, \bullet : other spurious asymptotic solution, blank space: divergent solution).

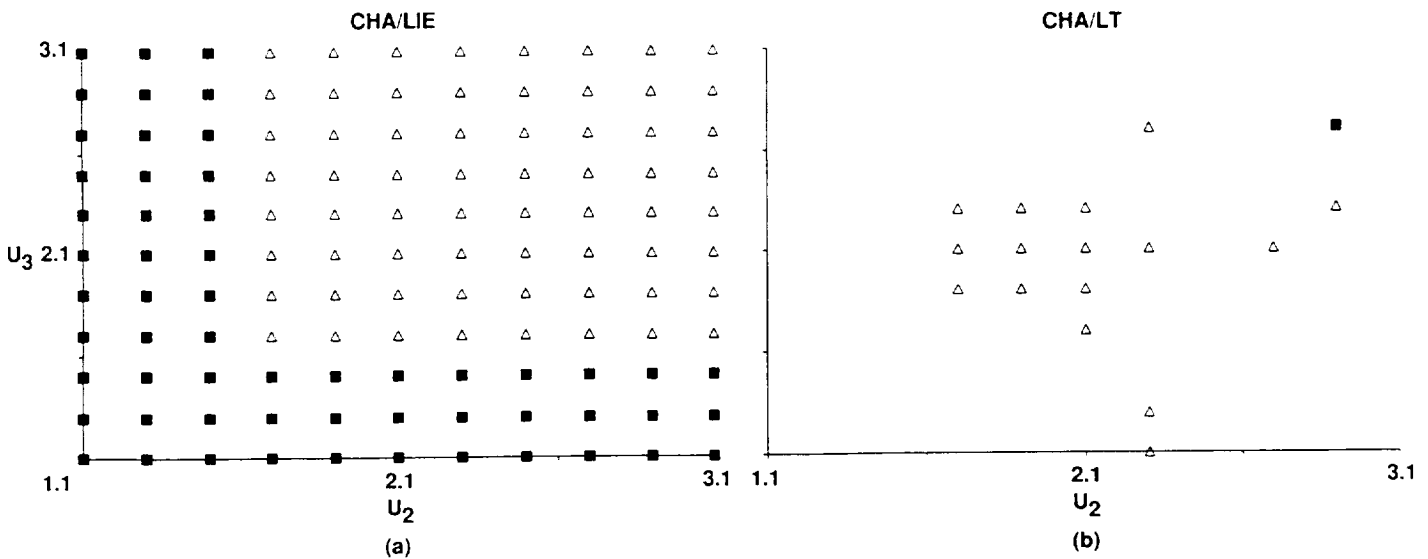


Fig. 3.25. Numerical basin of attraction for discretizations (a) CHA/LIE and (b) CHA/LT with $J = 4$, $p_1 = 0.1$ and $p_2 = 10$ (CFL = 1) (Δ : exact steady-state solution, \blacksquare : spurious steady-state solution, \bullet : other spurious asymptotic solution, blank space: divergent solution).

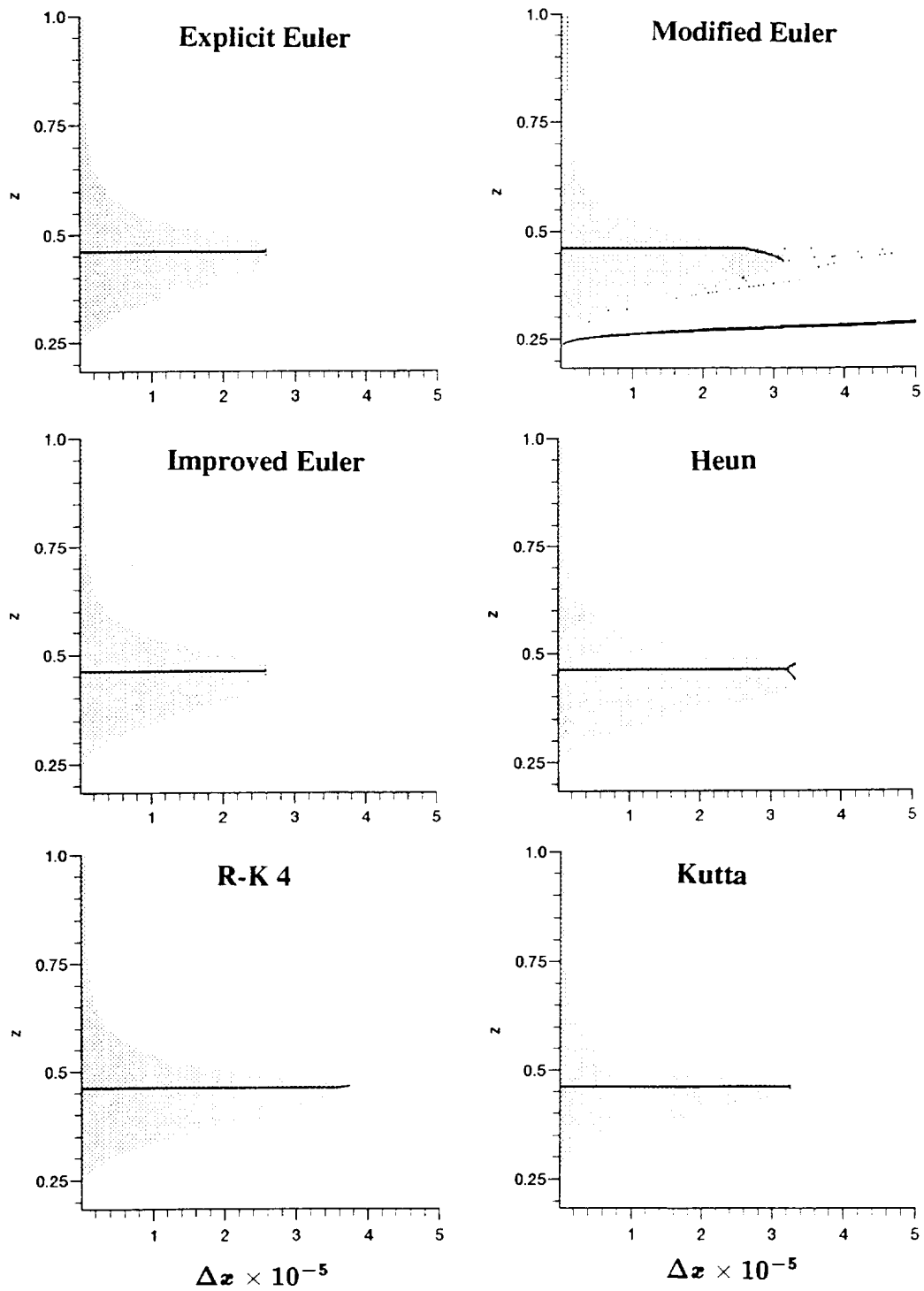


Fig. 4.1. Bifurcation diagrams of fixed points of the three-species reacting flow model.

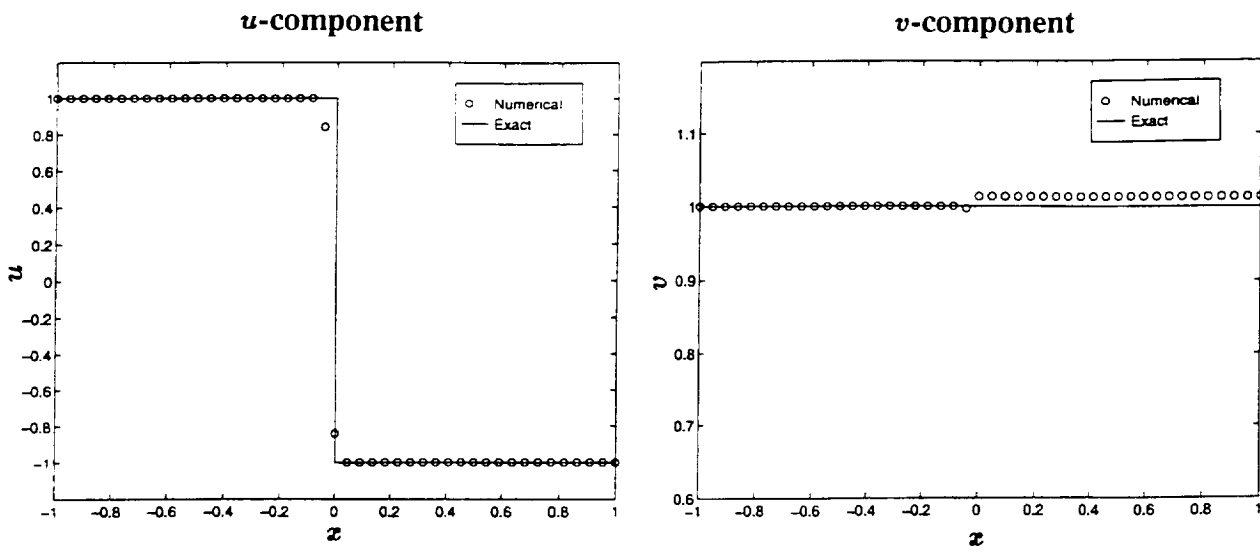


Fig. 4.2. The u - and v -components of (4.7) for a second-order ENO scheme.

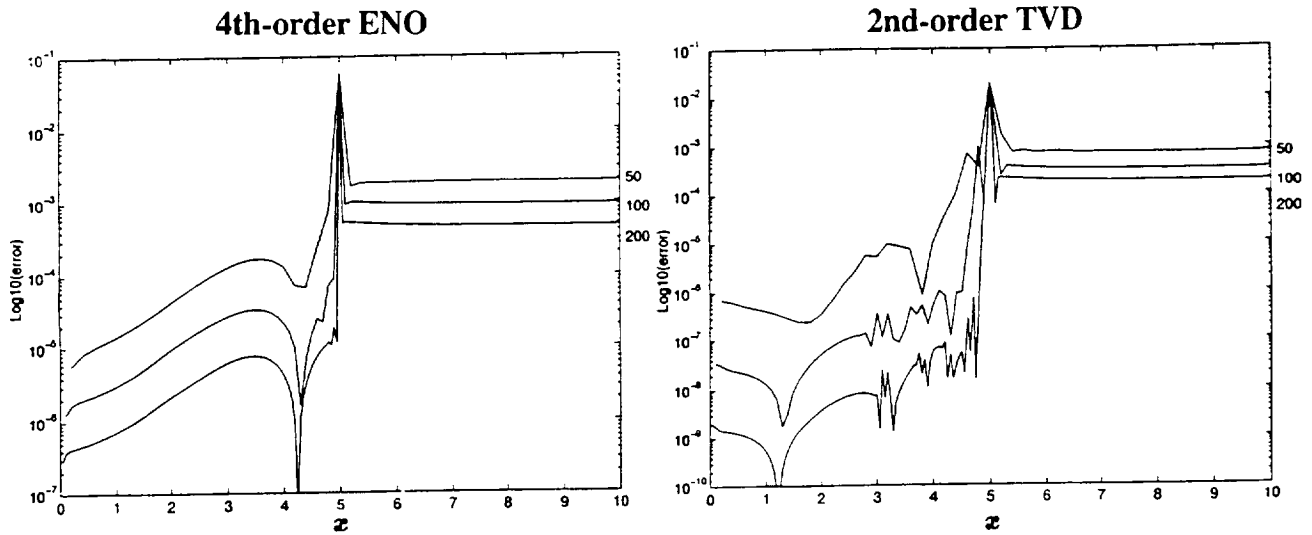


Fig. 4.3. Error in momentum of (4.7) for a fourth-order ENO (left) and a second-order TVD (right) scheme.

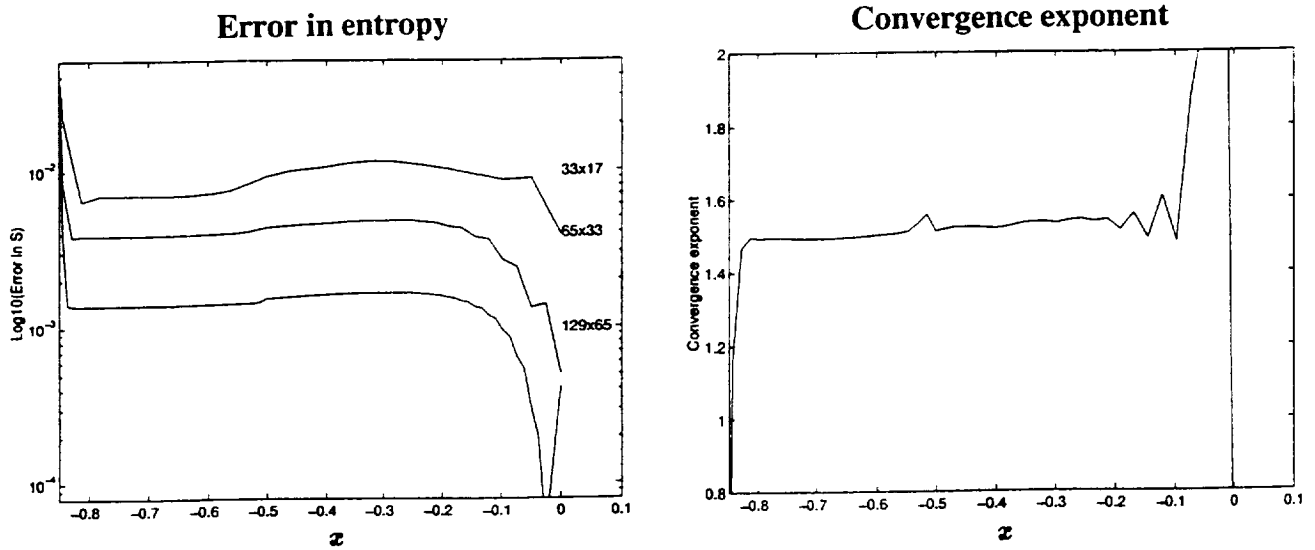


Fig. 4.4. Error in entropy (left) and convergence exponent (right) of (4.7) for a second-order UNO scheme.

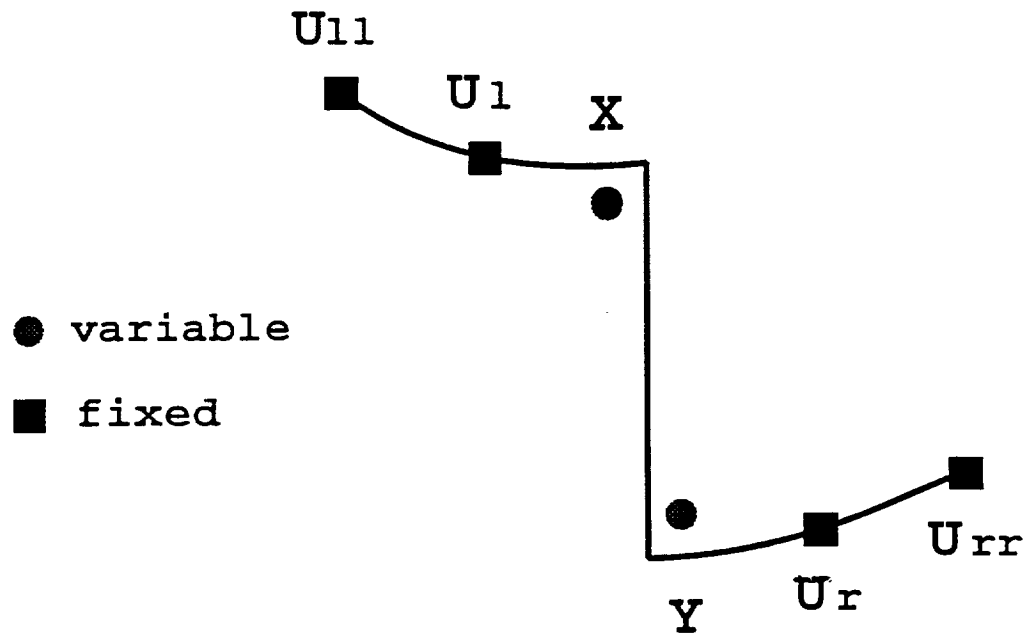


Fig. 4.5. Grid points of the reduced Embid et al. problem.

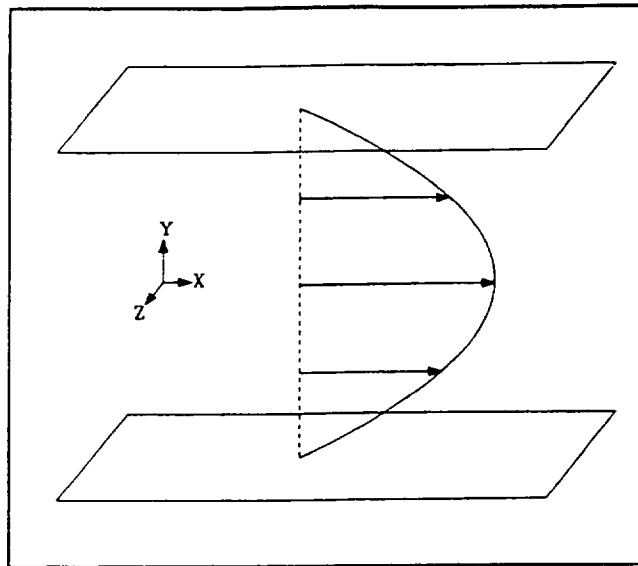


Fig. 5.1. Geometry of Poiseuille flow in a rectangular channel

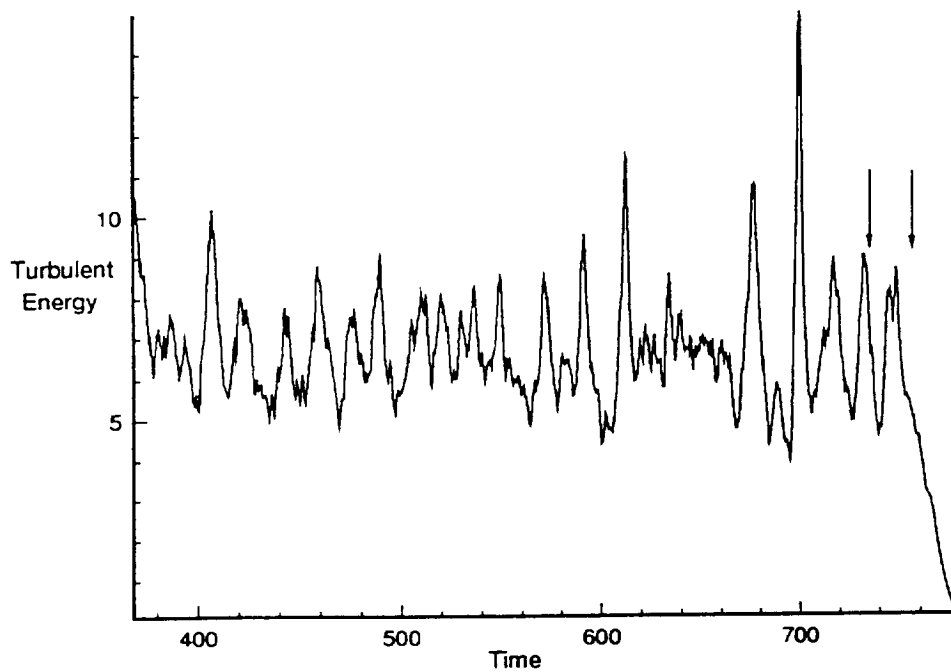


Fig. 5.2. Time history of the turbulent energy, showing extended chaotic transient before laminarization.

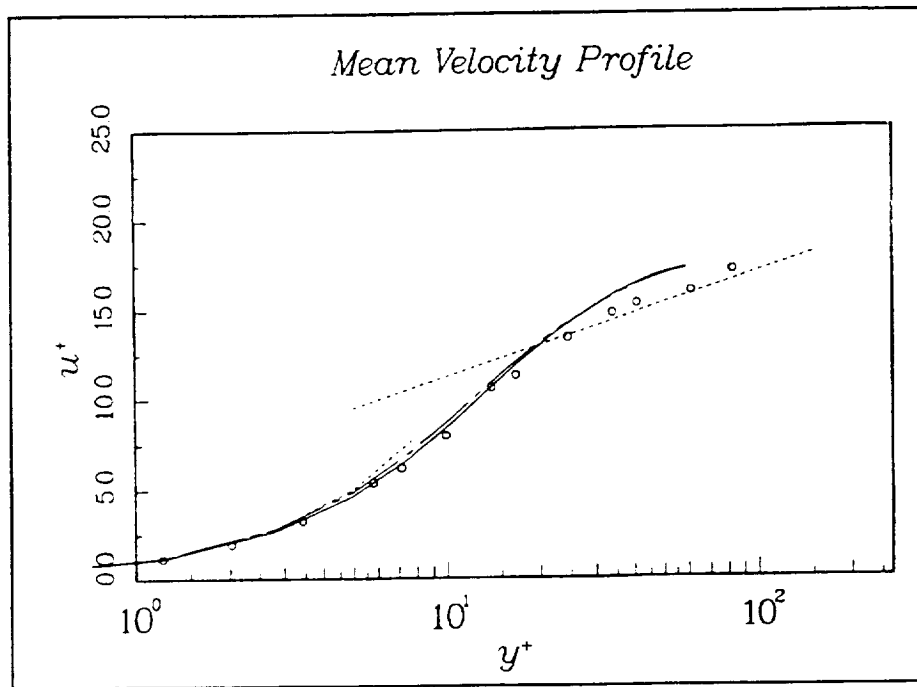


Fig 5.3. Near wall mean-velocity profiles. ○: "corrected" data of Eckelmann (1974); — : lower wall; - - - : upper wall; - - - - : "law of the wall" : $u^+ = y^+$, $u^+ = 2.5 \ln(y^+) + 5.5$

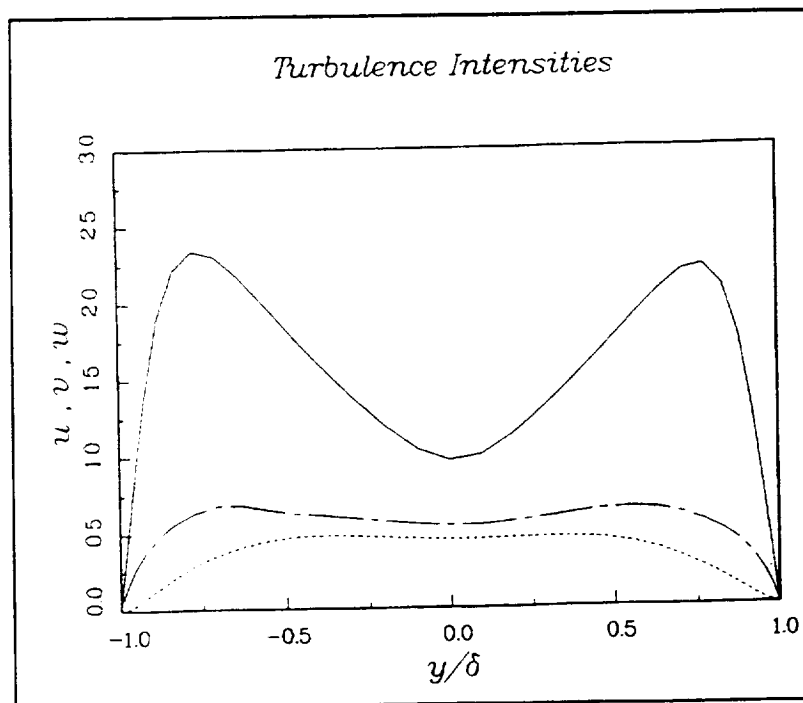


Fig. 5.4. Root-mean-square velocity fluctuations normalized by wall shear velocity. —, u_{rms} ; - - -, v_{rms} ; - · - ·, w_{rms} . Cross-channel coordinate normalized by $\delta = 2L$.

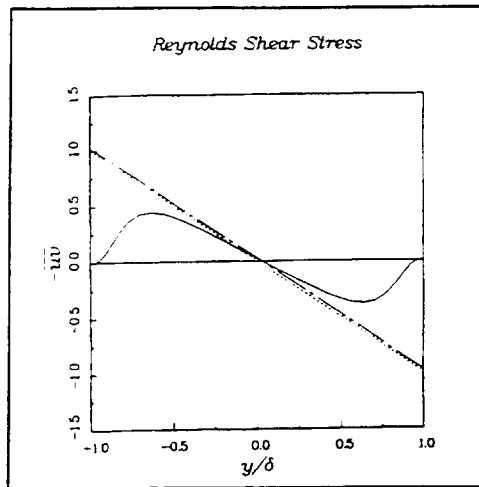


Fig. 5.5. Reynolds shear stress normalized by wall shear velocity. —, $-\overline{uv}$; - - - -, $-\overline{uv} + (1/Re)\partial\bar{u}/\partial y$; · · · ·, Total shear stress for fully developed channel

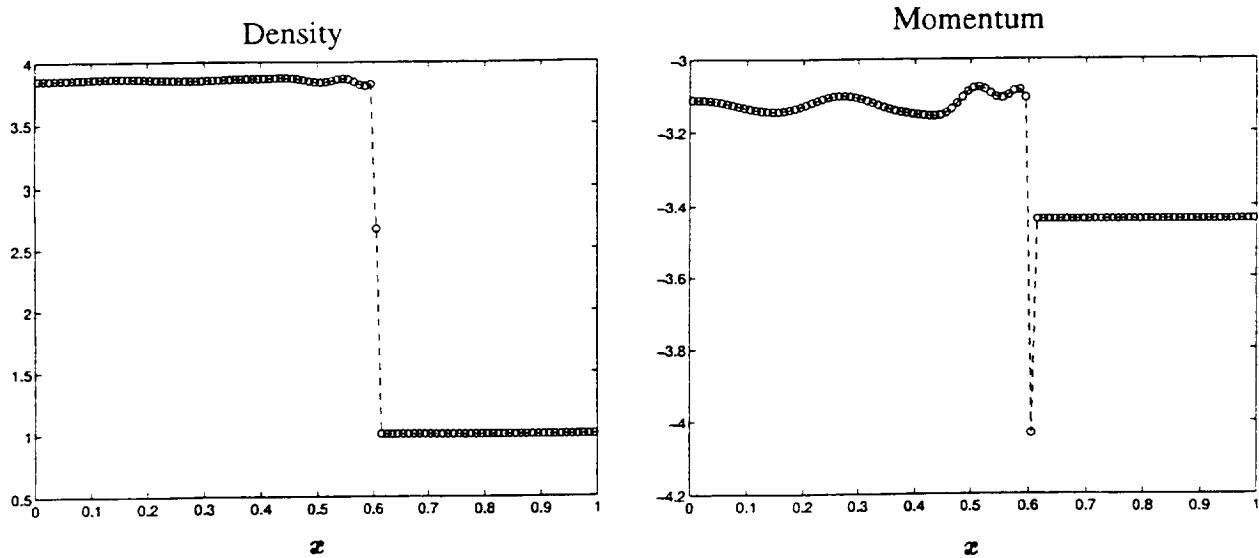


Fig. 5.6. A slowly moving shock at $t = 0.95$ computed by UW1 using $\Delta z = 0.01$ and $\Delta t = 0.001$.

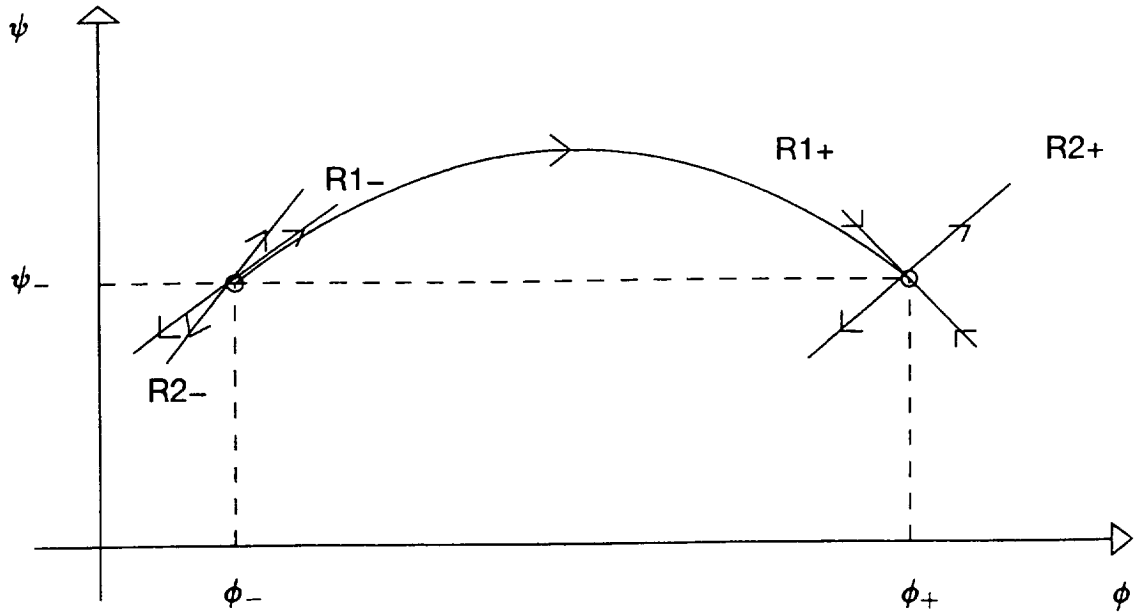


Fig. 5.7. A sketch of the phase portrait of Eqs.(5.21).

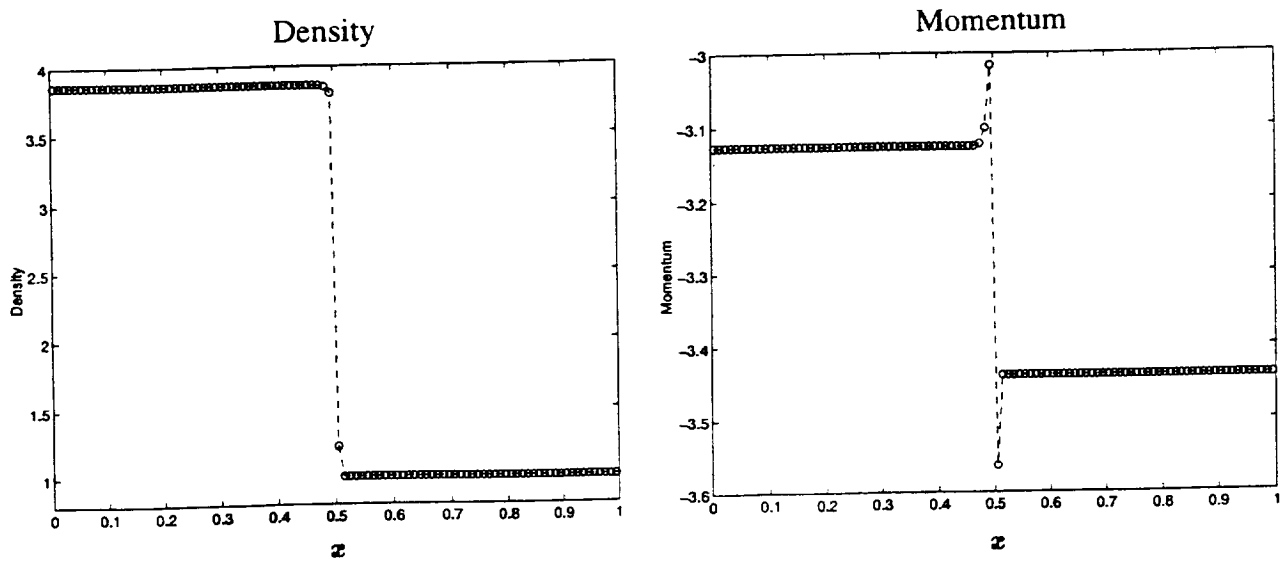


Fig. 5.8. The formation of the momentum spike and the downstream wave in the UW1 calculation after 5 time steps.

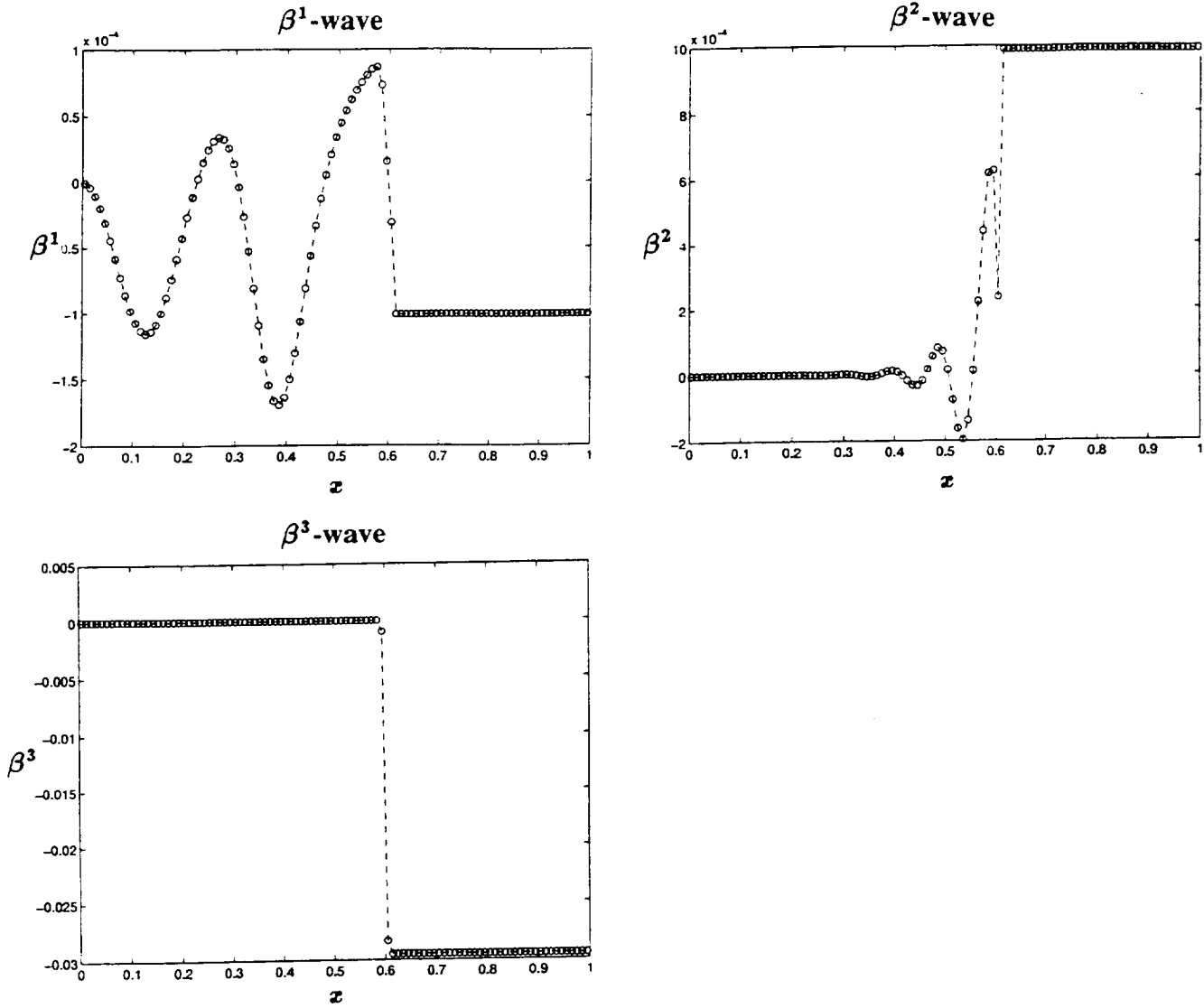


Fig. 5.9. The downstream waves in “characteristic” variables. Note that each wave belongs only to one characteristic family and diffuses.

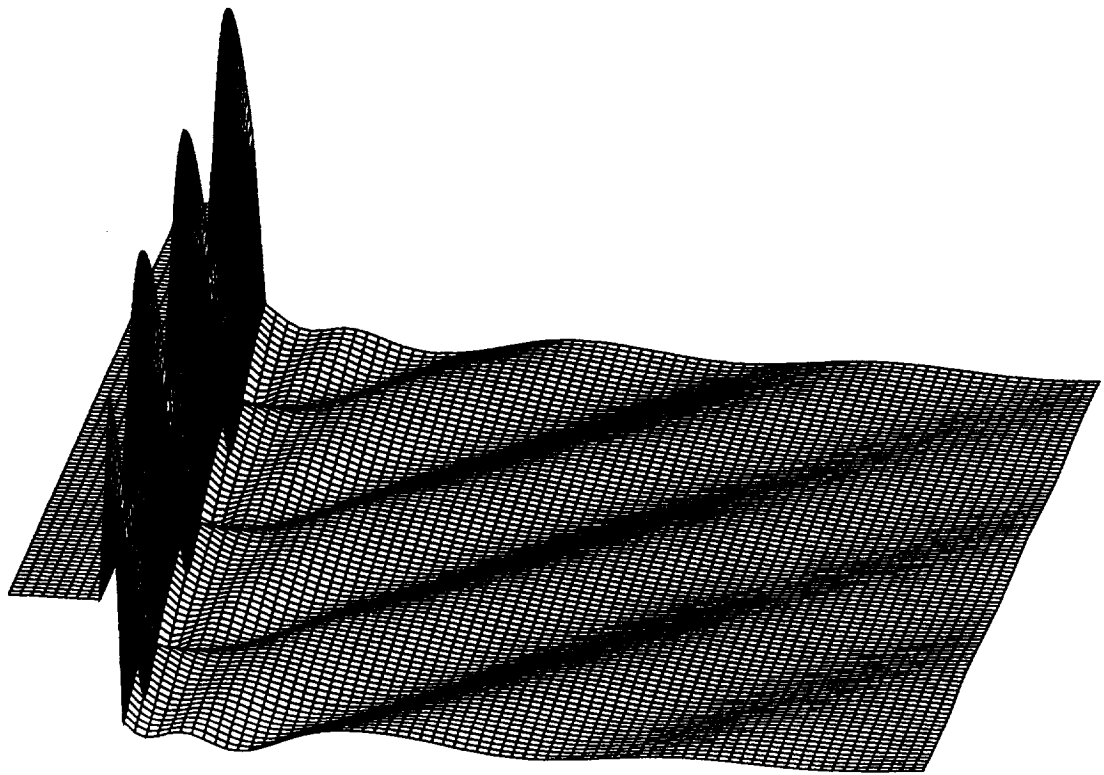


Fig. 5.10. Time evolution of the momentum spike and the downstream waves by the Roe's 1st-order upwind scheme for $t \in [0.5, 0.8]$. For better visualization these graphs are displayed upside down. The diffusive nature of the downstream pattern is apparent.

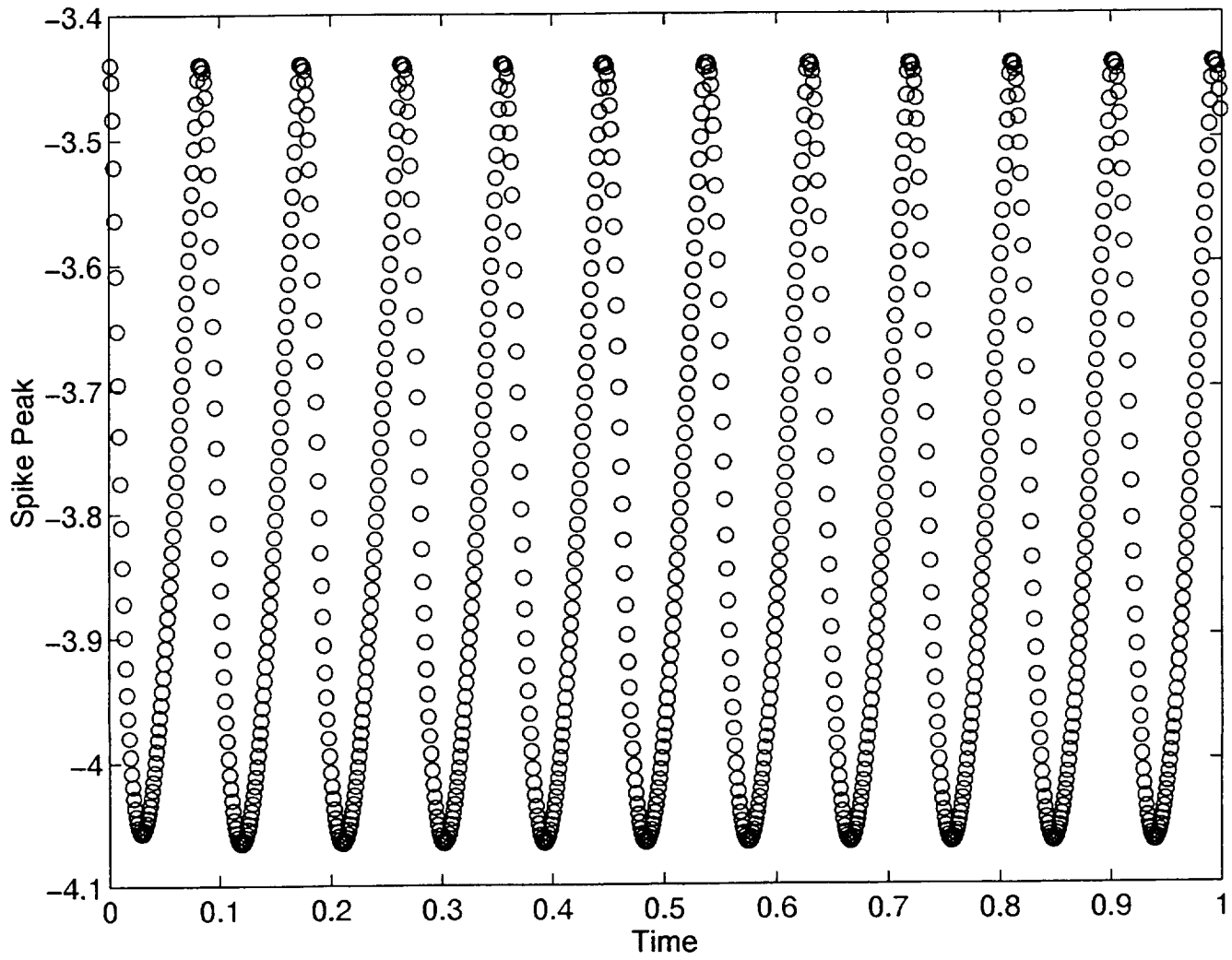


Fig. 5.11. Time evolution of the peak of the momentum spike by the Roe's 1st-order upwind scheme

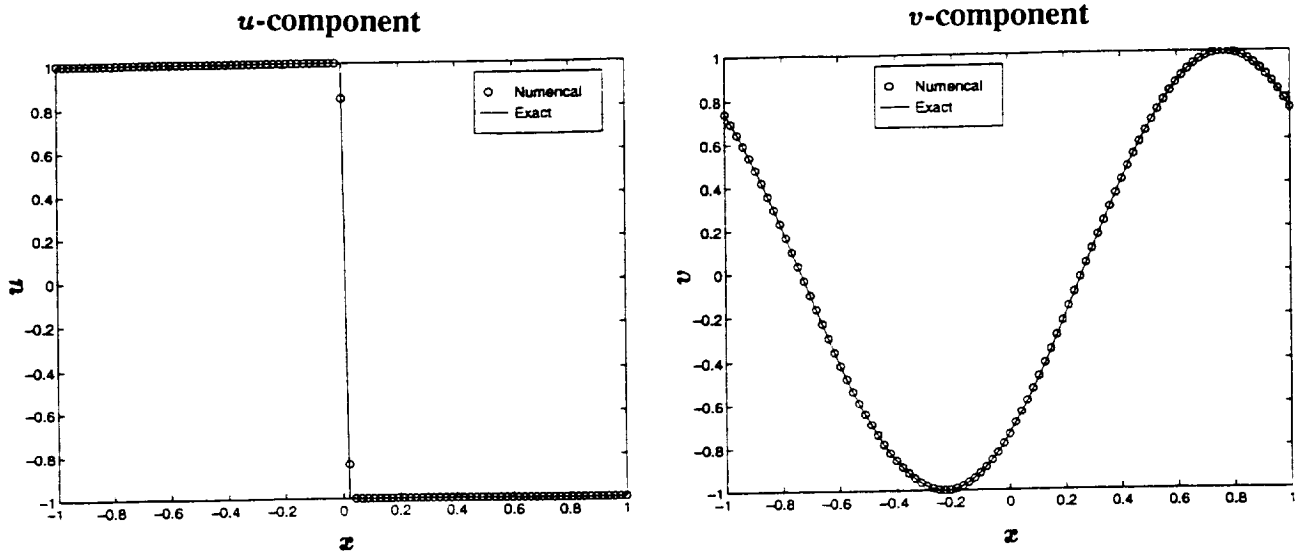


Fig. 5.12. The u and v -components of the solution of (4.7) and (5.30) at time 0.265958 for a 2nd-order ENO scheme with 100 grid points.

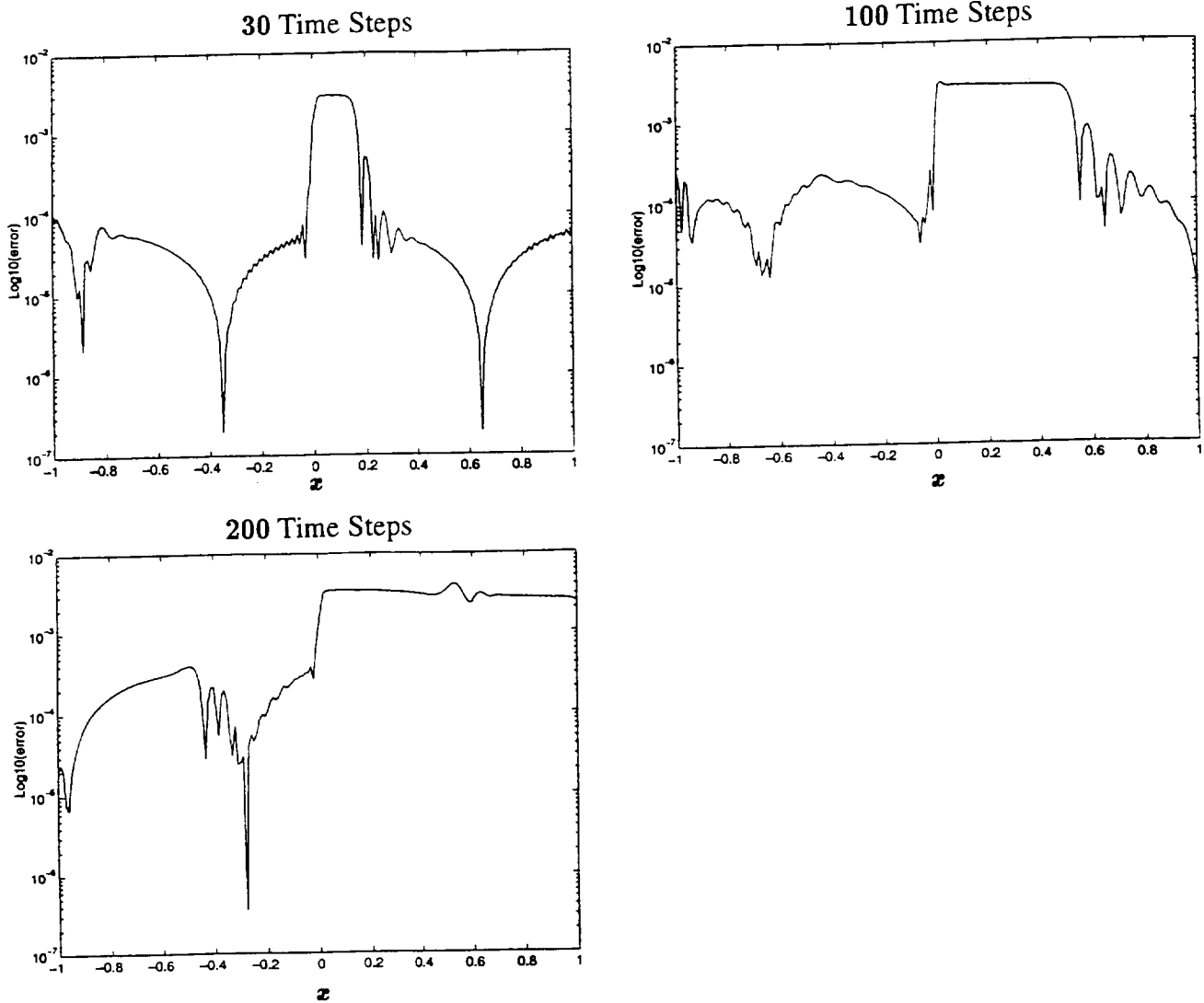


Fig. 5.13. Logarithm of the error in the v -component of (4.7) and (5.30) for a 2nd-order ENO scheme at 30, 100 and 200 time steps.

REPORT DOCUMENTATION PAGE

Form Approved
OMB No. 0704-0188

Public reporting burden for this collection of information is estimated to average 1 hour per response, including the time for reviewing instructions, searching existing data sources, gathering and maintaining the data needed, and completing and reviewing the collection of information. Send comments regarding this burden estimate or any other aspect of this collection of information, including suggestions for reducing this burden, to Washington Headquarters Services, Directorate for Information Operations and Reports, 1215 Jefferson Davis Highway, Suite 1204, Arlington, VA 22202-4302, and to the Office of Management and Budget, Paperwork Reduction Project (0704-0188), Washington, DC 20503.

1. AGENCY USE ONLY (Leave blank)	2. REPORT DATE April 1996	3. REPORT TYPE AND DATES COVERED Technical Memorandum	
4. TITLE AND SUBTITLE Nonlinear Dynamics & Numerical Uncertainties in CFD			5. FUNDING NUMBERS 505-59-53
6. AUTHOR(S) H. C. Yee and P. K. Sweby			
7. PERFORMING ORGANIZATION NAME(S) AND ADDRESS(ES) Ames Research Center Moffett Field, CA 94035-1000			8. PERFORMING ORGANIZATION REPORT NUMBER A-961743
9. SPONSORING/MONITORING AGENCY NAME(S) AND ADDRESS(ES) National Aeronautics and Space Administration Washington, DC 20546-0001			10. SPONSORING/MONITORING AGENCY REPORT NUMBER NASA TM-110398
11. SUPPLEMENTARY NOTES Point of Contact: H. C. Yee, Ames Research Center, MS 202A-1, Moffett Field, CA 94035-1000; (415) 604-4769			
12a. DISTRIBUTION/AVAILABILITY STATEMENT Unclassified — Unlimited Subject Category 64			12b. DISTRIBUTION CODE
13. ABSTRACT (Maximum 200 words) The application of nonlinear dynamics to improve the understanding of numerical uncertainties in computational fluid dynamics (CFD) is reviewed. Elementary examples in the use of dynamics to explain the nonlinear phenomena and spurious behavior that occur in numerics are given. The role of dynamics in the understanding of long time behavior of numerical integrations and the nonlinear stability, convergence, and reliability of using time-marching approaches for obtaining steady-state numerical solutions in CFD is explained. The study is complemented with spurious behavior observed in CFD computations.			
14. SUBJECT TERMS Spurious numerical solutions, Numerical uncertainties, Computational Fluid Dynamics (CFD), Dynamics of numerics, Spurious steady states, Spurious fixed points, Finite difference methods			15. NUMBER OF PAGES 133
			16. PRICE CODE A07
17. SECURITY CLASSIFICATION OF REPORT Unclassified	18. SECURITY CLASSIFICATION OF THIS PAGE Unclassified	19. SECURITY CLASSIFICATION OF ABSTRACT	20. LIMITATION OF ABSTRACT